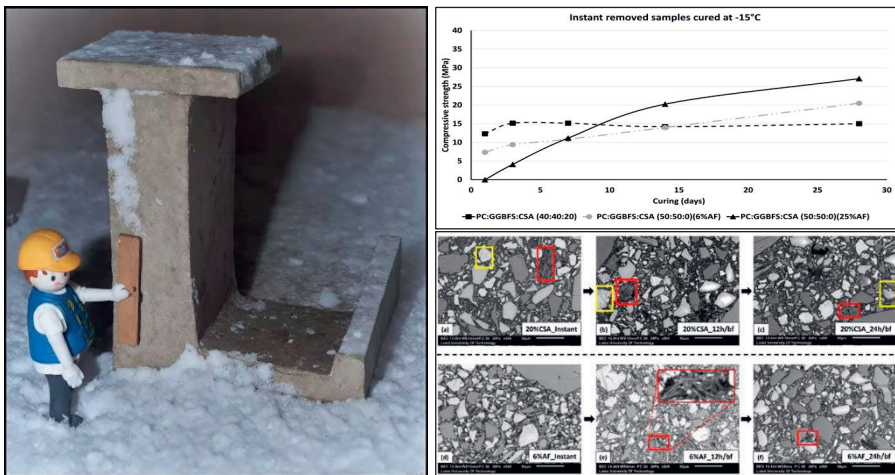


Low Portland cement content concretes at freezing and subfreezing temperatures



Ankit Kothari

Building Materials



DOCTORAL THESIS

Low Portland cement content concretes at freezing and subfreezing temperatures

Ankit Kothari

Building Materials

Department of Civil, Environmental and Natural Resources Engineering

Luleå University of Technology

SE-97187 Luleå, Sweden

June 2024

Front page: the cover image shows the overview of this PhD research results.

COPYRIGHT © ANKIT KOTHARI

Printed by Luleå University of Technology, 2024

ISSN 1402-1544

ISBN: 978-91-8048-540-1 (Print)

ISBN: 978-91-8048-541-8 (Electronic)

Luleå 2024

www.ltu.se

Academic Thesis

For the Degree of Doctor of Philosophy (Ph.D.) in Building Materials, which by due permission of the Technical Faculty Board at Luleå University of Technology will be publicly defended on:

Tuesday, June 18th, 2024, 10:00
Room F1031, Luleå University of Technology

Opponent Examiner:

Assoc. Prof. **Aleksandra Radlinska**
Pennsylvania State University, USA

Examining committee:

Professor of Practice, **Jouni Punkki**
Aalto University, Finland

Assoc. Prof. **Lukasz Sadowski**
Wrocław University of Science and Technology, Poland

Assoc. Prof. **Karel Dvořák**
Brno University of Technology, Czech Republic

Principle Supervisor:

Prof. **Andrzej Cwirzen**
Luleå University of Technology, Sweden

Assistant Supervisors:

Adj. Prof. **Hans Hedlund**
Luleå University of Technology, Sweden

Assoc. Prof. **Karin Habermehl-Cwirzen**
Luleå University of Technology, Sweden

Chairperson:

Thanyarat Buasiri, PhD
Luleå University of Technology, Sweden

From me, everyone receives the same level of importance.

To me no one is more, or less. I do see everyone with same love and care.
Sometimes I express and sometimes I don't.

On the contrary, I seek out and pay attention to a select handful. And those are very important
in my life, and I don't have words to express my gratitude.

Change is circle of life! But keep it simple and naive, with a desire to learn more!

As I always say...
"Life is a bliss, Yet a myth."

When in problem or in confusion or in frustration always share it with the person whom you
believe of having pure heart. Do not expect any solutions, but just sharing will solve the most!

Pure heart is synonym to Positive vibes and their smile is like cherry on the top.

To sum up with a beautiful phrase that states,
"Regardless of what happens - The show must go on."

..... *It's me*

Acknowledgment

This doctoral thesis has been prepared at Building Materials Group, Department of Civil, Environmental, and Natural Resource Engineering of Lulea Technical University, Sweden. This research was financed by the: Interreg Nord, Vinnova, Trafikverket - Swedish Transport Administration, SBUF - Svenska Byggbranschens Utvecklingsfond (Development Fund of the Swedish Construction Industry) and Swedish Energy Agency.

I am deeply grateful to all those who have supported and inspired me along the way of completing this PhD journey.

First and foremost, I would like to express my sincere gratitude to my main supervisor, Prof. Andrzej Cwirzen, for his invaluable guidance, unwavering support, and expert mentorship throughout this research journey. His dedication, encouragement, and insightful feedback have been instrumental in shaping the direction and quality of this thesis.

I am also indebted to my co-supervisors, Assoc. Prof. Karin Habermehl-Cwirzen and Adj. Prof. Hans Hedlund for their valuable input, constructive criticism, and scholarly insights that have enriched my research and contributed to its academic standard.

I extend my heartfelt appreciation to Carina Hannu, Göran Boström, Mats Petersson, Erik Andersson and Rikard Öhman for their administrative and technical support as and when needed.

I would like to thank Magdalena Rajczakowska for her invaluable time and support, when I needed the most during this period which made a huge impact. I sincerely appreciate Thanyarat Buasiri (Ploy)*, Vasiola Zhaka, Klaudja Telhaj, Ilda Tole, Ece Teker, Marcin Sundin, Yaser Gamil who have offered their encouragement and assistance which have made this journey memorable and rewarding.

To not forget the newly joined PhD students of Building Materials, 2024, Kyriaki Papadopoulou, Sergio Ruiz Martinez, Emmanuel Mache and Alaeddine Ben Tarzi for their short but effective interactions and being part of this remarkable journey.

I am deeply grateful to my family for their boundless support, understanding, and encouragement, especially during the challenging phases of this journey. Above all I would like to thank my wife Sakshi for her love and constant support and of course tolerating my tantrums over the past few months. Thank you for being and understanding and showing unwavering support, that has been my source of strength and motivation.

Lastly, I would like to thank Mukhtiar Ahmed and Tarun Bansal for all the support and guidance offered.

To all those mentioned above and many others who have contributed in various ways, I offer my heartfelt gratitude.

Ankit Kothari
Luleå, June 2024

Summary

Concrete is the most used building material worldwide. With the increasing growth of industries and urbanization globally, the demand for concrete is further increasing significantly. Ordinary Portland Cement (PC) is the binder used to produce typical concrete. Unfortunately, for every ton of manufactured cement about 0.61-ton CO₂ is emitted into the earth's atmosphere. As a result, several solutions have been implemented to reduce the usage of this material in the production of concrete. This includes its partial or full replacement with supplementary cementitious materials (SCMs) or alternative binders. Some of these combinations could be problematic to be used in cold climates due to a lower developed hydration heat, slower setting, or worse frost durability.

In winter the immediate exposure of fresh concrete to freezing temperatures results in pore ice formation and can delay or completely stop the hydration process. This is commonly prevented by using an additional heating system installed in concrete or the formwork. Unfortunately, it usually adds complexity, increases the price, and depending on the used power source it could increase the CO₂ footprint. Another potentially simpler and more sustainable solution is to modify the concrete itself by adjusting the mix design, by using certain chemical admixtures and special cementitious binders.

The primary objective of this research was to investigate the effects of partially replaced Portland cement with GGBFS and/or CSA cement on the properties of fresh concrete exposed to constant freezing and sub-freezing temperatures (-15°C) in a fresh state and at a young age. A special emphasis was on the application of chemical and mineral admixtures that could eliminate the need to use heat treatments. The secondary aim was to evaluate a possible application of UHPC to protect new and existing concrete structures from frost damage.

The experimental program focused on the optimization, testing, and analysis of mixes containing various combinations of chemical admixtures, CSA cement, GGBFS and Portland cement. Tests included exposure to freezing and subfreezing temperatures. The aim was to lower the freezing point of water and promote faster hydration and strength gain. The research employs techniques such as differential scanning calorimetry (DSC) to study the phase transition of pore water into ice and its effects on the binder matrix. Other tests include ultrasonic pulse velocity measurements (UPV), bond tests (pull-off), scanning electron microscopy (SEM) for microstructure analysis, frost durability evaluation with the Borås test, semi-adiabatic calorimetry to study hydration processes, and compressive strength measurements.

Various mixes containing sodium nitrate-based antifreeze admixtures (AF), or CSA cement were analyzed. Results revealed that incorporating 25 wt.% AF partially inhibited pore ice formation and prolonged hydration, while 6 wt.% AF and 20 wt.% CSA increased the risk of frost damage. Furthermore, the addition of 20 wt.% CSA led to rapid setting and increased porosity, which affected strength and microstructure. Post-curing at 20°C could enhance hydration and prevent permanent damage due to ice formation.

The study also proposed rehabilitating deteriorated normal strength concrete structures (NSCs) using an Ultra High-Performance Concrete (UHPC). High-pressure water jet scaling simulated deterioration, while freeze-thaw testing evaluated surface scaling. The UHPC overlay improved mechanical properties, durability, and bond quality. Overall, the research demonstrated how

using UHPC as a repair material can enhance sustainability by extending the lifespan of concrete structures.

Keywords: Portland cement (PC); Calcium sulfoaluminate cement (CSA); Ground granulated blast-furnace slag (GGBFS); Low curing temperature; Hydration; SEM-EDS; Antifreeze admixture (AF); UHPC; Freeze-thaw (F-T); Normal strength concrete (NSC); Interfacial transition zone (ITZ); Differential scanning calorimetry (DSC); Ultrasonic pulse velocity (UPV); Bond test (pull-off).

Table of Contents

<i>Summary</i>	<i>vii</i>
<i>List of Figures</i>	<i>xi</i>
<i>List of Tables</i>	<i>xiv</i>
1. Introduction	1
1.1 Aim, scope, and limitations	3
1.2 Research questions	4
1.3 Thesis structure	4
1.4 List of appended publications	5
1.5 Additional papers/conferences	6
2. Literature review	8
2.1 Chemical admixtures for concretes cast at zero and subzero temperatures ...	9
2.2 CSA cements for concretes cast at zero and subzero temperatures	17
2.3 UHPC overlay for restoration of deteriorated concrete structures	18
2.4 Summary	19
3. Materials and methods	20
3.1 Materials	20
3.1.1 Binders.....	20
3.1.2 Fillers and Aggregates.....	21
3.1.3 Chemical admixtures.....	22
3.1.4 Steel fibers.....	22
3.1.5 Mix designs.....	23
3.2 Methods	25
3.2.1 Mixing and curing.....	25
3.2.2 Test methods and sample preparations.....	26
3.2.3 Phase transition test setup.....	26
3.2.4 Hydration temperature development.....	27
3.2.5 Setting time.....	27
3.2.6 Workability of concrete.....	28
3.2.7 Compressive strength.....	28
3.2.8 Ultrasonic pulse velocity (UPV).....	29
3.2.9 Bond test.....	31
3.2.10 Microstructure – SEM-EDS.....	32
4. Results and discussions	34
4.1 Low Portland cement content binders at low temperatures	34
4.1.1 PC-GGBFS.....	34
4.1.2 PC-GGBFS-CSA systems.....	36
4.2 Enhancing frost durability of NSC with UHPC overlay	56
4.2.1 Fresh and hardened properties - UHPC.....	56
4.2.2 Freeze-thaw durability of UHPC.....	57
4.2.3 Compressive strength development of UHPC-NSC composite.....	58
4.2.4 Flexural strength of UHPC-NSC composite.....	59
4.2.5 UHPC-NCS interfacial transition zone.....	60
5. Conclusions	68
5.1 Concluding remarks	68
5.2 Answering research questions	70
5.3 Future research	71

6. *References*..... 72

List of Figures

Figure 1: Schematic mechanism of fresh concrete exposed to sub-zero curing temperature, [46]	8
Figure 2: Examples of primitive protection methods of concrete during cold weather, [48].	9
Figure 3: Low temperature cured/casted concrete (a) Without antifreeze admixture; (b) With antifreeze admixture; (c) Without air-entraining agent; (d) With an air-entraining agent, [63].	10
Figure 4: Particle size distribution of the used fillers and aggregates.	21
Figure 5: Visual determination of phase transition test setup.	26
Figure 6: Differential scanning calorimeter (DSC) Q100 TA.	27
Figure 7: In-house-built semi-adiabatic calorimeter box cross-section and test setup.	27
Figure 8: Vicat apparatus used to determine initial and final setting times.	28
Figure 9: The slump test setup used to determine the workability of concrete.	28
Figure 10: Scheme of UHPC-NSC cube specimen preparation (a) NSC cubes; (b) water jetting; (c) casting UHPC overlay.	29
Figure 11: Compressive strength testing machine.	29
Figure 12: UHPC-NSC column specimen preparation (a) NSC columns; (b) water jetting; (c) schematic model of the repair/rehabilitated column.	30
Figure 13: Ultrasonic Pulse Velocity (UPV) measurement nodes for UHPC-NSC column - Red (A-A'), Blue (B-B').	30
Figure 14: Bond test locations on the column (marked in red) and schematic representation of a cross-section of the drilled core.	31
Figure 15: Scanning Electron Microscope - Energy-dispersive X-ray spectrometer (SEM-EDS) used in this study.	33
Figure 16: Compressive strength gain of concrete cubes cured at 20°C, 5°C, 0°C and -5°C.	35
Figure 17: Hydration temperature development.	36
Figure 18: Visual observation of the phase transitioning time. The point marked as “slush state – red square” denotes solution transitioned and retained to slush; and “liquid state – green triangle” denotes no transition of solution into ice.	37
Figure 19: Exothermic heat flow of the pure PC, CSA, and PC:GGBFS:CSA pastes. The freezing rate was 1°C/min.	39
Figure 20: Endothermic heat flow of the pure PC, CSA, and PC:GGBFS:CSA pastes. The thawing rate was 1°C/min.	40
Figure 21: The development of the hydration temperature of pastes containing PC, CSA, and a mix of PC:GGBFS:CSA.	42

Figure 22: Initial and final setting times of pastes based on PC, CSA, and mix of PC:GGBFS:CSA.....	43
Figure 23: Concrete slump measured immediately after mixing concrete.....	44
Figure 24: Early age - 7 days compressive strength development of concretes cubes cured at ambient room temperature.....	45
Figure 25: The compressive strength development of samples tested immediately after removal from curing at -15°C.....	46
Figure 26: The compressive strength development of samples tested after 12 hours of curing at room temperature after their removal from -15°C.....	47
Figure 27: The compressive strength development of samples tested after 24 hours of curing at room temperature after their removal from -15°C.....	48
Figure 28: Average Ultrasonic Pulse velocity (UPV) measured on -15°C cured, 1-day-old composite binder-based concrete samples at distinct time intervals.....	49
Figure 29: Average Ultrasonic Pulse velocity (UPV) measured on -15°C cured, 28-day-old composite binder-based concrete samples at distinct time intervals.....	50
Figure 30: SEM images showing recovery of 3-day-old samples cured at -15°C. Note: red color boxes indicate areas with detected ettringite crystals and yellow boxes indicate unhydrated CSA cement.....	51
Figure 31: SEM images showing recovery of 28-day-old samples cured at -15°C. Note: red color boxes indicate areas with detected ettringite crystals and yellow boxes indicate unhydrated CSA cement.....	52
Figure 32: Pore segmentation of 3-day-old samples cured at -15°C. Note: White color indicates pores.....	53
Figure 33: Pore segmentation of 28-day-old samples cured at -15°C. Note: White color indicates pores.....	54
Figure 34: Effect of curing on porosity of 3-day-old concrete samples.....	54
Figure 35: Effect of curing on porosity of 28-day-old concrete samples.....	55
Figure 36. Slump flow test results.....	56
Figure 37: Compressive strength development of normal strength concrete (NSC), and UHPC without and with fibers.....	57
Figure 38: Cumulative surface scaling of UHPC exposed to 56 freeze-thaw (F-T) cycles.....	58
Figure 39: Compressive strength development of NSC and composite UHPC-NSC concrete cubes.....	59
Figure 40: Load vs displacement measured in 3-point bending for NSC and UHPC – NSC column specimens.....	59
Figure 41: Cracking of beam at failure.....	60

Figure 42: Average ultrasonic pulse velocity (UPV) measurement of UHPC – NSC composite columns.	61
Figure 43: Bond strength development using pull-off test on UHPC– NSC composite columns at different locations.	62
Figure 44: Binarized images of the core surface showing fragments of UHPC and NSC in column 1. Note: On right images, the black color indicates UHPC and white color indicates NSC.	62
Figure 45: Binarized images of the core surface showing fragments of UHPC and NSC in column 2. Note: On right images, the black color indicates UHPC and white color indicates NSC.	63
Figure 46: Interfacial bond zone of composite UHPC – NSC column 1 using SEM at 150X and 2000X magnifications.	64
Figure 47: Interfacial bond zone of composite UHPC – NSC column 2 using SEM at 150X and 2000X magnifications.	64
Figure 48: Percentage change of porosity away from NSC binder – UHPC interface of composite - UHPC – NSC columns.	65
Figure 49: Percentage change of porosity away from NSC aggregate – UHPC interface of composite -UHPC – NSC columns.	65
Figure 50: Percentage change of unhydrated cement away from NSC binder–UHPC interface of composite -UHPC – NSC columns.	66
Figure 51: Percentage change of unhydrated cement away from the interface between NSC aggregate and UHPC overlay.	66
Figure 52: Average atomic Ca/Si ratio vs. distance from the NSC binder–UHPC interface. ..	67
Figure 53: Average atomic Ca/Si ratio vs. distance from the NSC aggregate–UHPC interface.	67

List of Tables

Table 1: Summarized cold weather chemical admixture for winter concreting, [63].	11
Table 2: Efficiency of antifreeze admixtures for PC and composite concrete based on the available data, [63].	13
Table 3: Efficiency of commercial AE for PC and composite concrete, [63].	14
Table 4: Summarized PC and admixtures exposed to lower curing temperature, [63].	14
Table 5: Summarized SCM mixes, and chemical admixtures exposed to lower curing temperature, [63].	16
Table 6: Chemical composition of the used binders.	20
Table 7: Physical properties of the used binders	20
Table 8: Chemical composition of the used fillers.	21
Table 9: Solid and water contents in wt.% of used chemical admixtures.	22
Table 10: Properties of the used steel fibers	22
Table 11: Pastes mix compositions.	23
Table 12: Concrete mix compositions.	24
Table 13: Mix composition of UHPC and normal strength concrete (NSC).	25
Table 14: Pull-off test bond failure modes.	31

1. Introduction

Concrete is the most widely used construction material and stands second in usage after water. With the increasing growth of industries and urbanization globally, the demand for concrete is increasing significantly. Concrete is held together by a cementitious binder, usually Portland Cement (PC). To produce PC, a mixture of raw materials including limestone, and clay are heated together in a kiln at a temperature of 1450°C resulting in high CO₂ emission. For every ton of PC production, about 0.61-ton CO₂ is emitted. This accounts for around 8% of the world's carbon footprint, [1]. To reduce the negative impact, PC is commonly replaced partially with pozzolanic materials. These include industrial by-products such as slag, fly ash, and silica fume identified as supplementary cementitious materials (SCM). Incorporating mine tailings from mining industries and recycled concrete fines obtained from construction and demolition waste shows promising potential for enhancing concrete properties. These materials exhibit pozzolanic activity following mechanical activation and can be used as a partial substitute for cement. Additionally, recycled aggregates extracted from construction demolitions, either fines or coarse, can be used as partial or complete replacements for conventional natural aggregate, further contributing to greener concrete production and reducing production costs. These concretes have a significantly lower greenhouse gas emission and could be a constructive way of using industrial wastes rather than causing serious impacts on society and the environment, such as landfill or illegal dumping, emission of harmful gases, and water pollution.

PC-based concrete performs well when produced at external temperatures between 10°C to 20°C, [2]. As temperature is directly influencing the hydration rate and its strength-developing properties. In contrast, despite the ambient curing conditions SCM-based composite concrete shows a delay in hydration rate and strength development at an early age due to its slow reactivity but gains equivalent strength as PC at later ages. However, in cold climates when the temperature falls to 5°C and below, PC-based concrete shows a significantly retarded hydration rate and subsequently delays the setting time, strength development, and the construction period, [3–6]. And similarly, much more adverse effects are observed with SCM-based concrete. On exposure of fresh concrete to freeze temperatures, about 92% of water inside the pores freezes and expands by around 9% in volume, causing internal cracks and subsequently a high potential for frost damage, and developing false strength from the frozen pores, [7–9]. Furthermore, such exposures will not only reduce the compressive strength by 20-40% but also the frost durability is reduced by 40-60% i.e., on repeated freeze-thaw cycles, [2,10,11]. Additionally, research from ACI stated, that only minor frost damage shall be observed if concrete gains a critical compressive strength of 3.5 MPa at an early age, [6,12]. But these effect gets more aggravated on the usage of low-carbon footprint binder/concrete in similar climatic conditions.

Over the years many alternatives were researched and have been adapted to promote construction activities in winter. Such as heating the aggregates and water; using enclosures and protective insulations; pre-heating the concrete laying area; adding more cement than required; and usage of cold-weather chemical admixtures, [13]. Except for the use of chemical admixtures, the other alternatives not only increase the cost of concrete but also increase the carbon footprint from the heating processes. Chemical additives are technically simple and cost-effective to protect the fresh concrete from freezing, while also accelerating the strength development. Their fundamental role is to lower the freezing point of water, minimize the ice expansive pressure, and speed up the cement hydration, [2,14,15]. The available possible options are only certified for PC-based concrete, as there is a lack of understanding of the behavior of chemical admixtures on low-carbon footprint concretes at low temperatures. The scope of this study is to bridge this knowledge gap. As well as how to speed up the hydration

rate is of concern for the composite type of binder containing high amounts of SCMs when cured at sub-zero temperatures.

Another cost-effective alternative is utilizing a mineral accelerator (CSA-based) as an additive or partial replacement for binder instead of chemical admixtures was approached to promote the strength gain at sub-zero temperatures. The explicit quality of its faster hydration rate and ettringite formation at early stage resulting from the rapid liquid absorption capability of CSA pronounced the anti-freeze-permeable property and resulted in a potential approach for winter casting, [16–19]. Further, with an optimized partial replacement of CSA with PC along with pre-curing accelerated the strength by 300% relative to PC based concrete in cold weather conditions, [19].

Furthermore, with the urge of a circular economy, the existing concrete structures shows durability-related issues. Most durability-related problems are observed from the freeze-thaw effect i.e., cracks and surface scaling. The direct approach to preserve structures and extend their service life is to cover them with an external protective covering made of a more durable substance, rather demolish, and rebuild. The promising material for such purpose is ultra-high-performance concrete (UHPC), [20]. The essential qualities are its high compressive strength (>150 MPa), tensile strength (>8 MPa), increased flowability, and highly dense microstructure, [21–28]. However, the main disadvantage of UHPC is the usage of a large amount of binder (1100-1300 kg/m³), which greatly increases the CO₂ footprint, [29,30]. Conversely, due to the extremely low moisture content resulting in an extremely low w/b ratio, most of the binder is left unhydrated and can be replaced with relatively inexpensive locally accessible limestone powder as filler, [31–33]. Furthermore, since UHPC is applied as an overlay layer over the old concrete element, it is substantially less expensive and may be used in a wider range of applications. The interfacial transitional zone between the UHPC overlay and the substrate concrete is very critical and was another focus point of the study.

1.1 Aim, scope, and limitations

The aim of this research was to better understand how partial replacement of Portland cement with GGBFS and/or CSA cement affects the properties of concretes exposed to freezing and subfreezing temperatures in a fresh state and at a young age. The secondary aim was to evaluate a possible application of UHPC to protect new and existing concrete structures from frost damage.

The research included a literature review of methods used to produce concrete structures at zero and subzero temperatures. A special emphasis was on the application of chemical and mineral admixtures that could eliminate the need to use heat treatments. The output of this analysis enabled to narrow the scope of the research.

The experimental program focused on the optimization, testing, and analysis of mixes containing various combinations of chemical admixtures, CSA cement, GGBFS and Portland cement. Tests included exposure to freezing and subfreezing temperatures up to -15°C . The aim was to lower the freezing point of water and promote faster hydration and strength gain. Fresh and hardened properties were determined for all produced concretes. The phase transition of pore water into ice, the ice-forming temperature, and their effects on the binder matrix were studied using differential scanning calorimetry (DSC). Other tests included ultrasonic pulse velocity measurements (UPV), bond test (pull-off), scanning electron microscope (SEM) for analysis of the microstructure and phase composition, frost durability evaluation with Borås test, semi-adiabatic calorimetry to study hydration processes, compressive strength measurements.

All the investigations and experiments were conducted within the university laboratory. The concrete's sub-freezing curing temperature was simulated by using an industrial refrigerator (Schleibinger Slabtester, Germany).

The performed research had the following limitations:

- Only one type of Portland cement was used, i.e., Rapid Hardening Cement (SH cement – CEM I) from Cementa AB (Sweden).
- Only one type of GGBFS delivered by Swecem (Sweden) was used.
- All concretes were produced at ambient temperature and immediately after casting all specimens were exposed to various curing temperatures.
- The maximum aggregate size was limited to 8 mm.
- Only selected chemical admixtures were used and their choice was based on preliminary test results (not included in this thesis).
- Only sodium nitrate-based chemical antifreeze admixture was used, its selection was based on the performed literature study.

1.2 Research questions

The following research questions were formulated:

RQ (1): What is the best approach to produce concretes with low Portland cement content that is exposed shortly after casting to freezing and subfreezing temperatures? (Paper I)

RQ (2): How does a high amount of GGBFS affect hydration heat development and strength of normal concrete when cured at close and sub-zero temperatures? (SBUF report, Paper VIII)

RQ (3): How does the sodium nitrate-based antifreeze admixture influence the strength development and pore water phase transitions of binder systems based on the combination of PC and GGBFS when cured at subzero temperatures? (Paper II)

RQ (4): How effective are calcium sulfoaluminate (CSA) cements as alternatives to accelerators and antifreeze admixtures when used in combination with PC-GGBFS binders for concretes exposed to sub-zero curing temperature? What are their effects on the strength development strength and formed microstructure? (Paper III, IV)

RQ (5): Can a thin layer of UHPC applied on an existing deteriorated concrete element enhance its properties and frost durability? (Paper V, VI)

1.3 Thesis structure

The Ph.D. thesis is composed of five chapters, including:

Chapter 1: Contains a brief introduction to the research topic, followed by the research aim, its limitations, and formulate research questions.

Chapter 2: This chapter contains a literature review focusing on the composite binder-based concrete exposed to extreme cold temperatures with the usage of chemical admixtures and or mineral accelerators. Furthermore, it describes the potential application of UHPC in repair and restoration works.

Chapter 3: This chapter describes in detail the used materials, mix design, and test methodology.

Chapter 4: The main test results are analyzed and discussed in this chapter.

Chapter 5: Summarizes the findings of the research and presents conclusions drawn from the outcomes of this study.

1.4 List of appended publications

This thesis is structured as a composite compilation, incorporating below mentioned publications that are appended at the end of the thesis.

PAPER I **A Review of the Mechanical Properties and Durability of Ecological Concretes in a Cold Climate in Comparison to Standard Ordinary Portland Cement-Based Concrete.**

Ankit Kothari*, Karin Habermehl-Cwirzen, Hans Hedlund and Andrzej Cwirzen
Materials 2020, 13(16), 3467.
<https://doi.org/10.3390/ma13163467>

PAPER II **Effects of sodium nitrate and concrete mix composition on phase transition of pore water at subzero temperatures.**

Ankit Kothari*, Hans Hedlund, Mirja Illikainen and Andrzej Cwirzen
Construction and Building Materials 2022, 327(April), 126901.
<https://doi.org/10.1016/j.conbuildmat.2022.126901>

PAPER III **Partial replacement of OPC with CSA cements – effects on hydration, fresh-, hardened- properties.**

Ankit Kothari*, Ilda Tole, Hans Hedlund, Tommy Ellison, and Andrzej Cwirzen
Advances in Cement Research 2022, 35(5), 207–224.
<https://doi.org/10.1680/jadcr.22.00054>

PAPER IV **Early Age Performance of OPC-GGBFS-Concretes Containing Belite-CSA Cement Cured at Sub-Zero Temperatures.**

Ankit Kothari*, Thanyarat Buasiri, and Andrzej Cwirzen
Buildings 2023, 13(9), 2374.
<https://doi.org/10.3390/buildings13092374>

PAPER V **Eco-UHPC as Repair Material—Bond Strength, Interfacial Transition Zone, and Effects of Formwork Type.**

Ankit Kothari*, Magdalena Rajczakowska, Thanyarat Buasiri, Karin Habermehl-Cwirzen and Andrzej Cwirzen
Materials 2020, 13(24), 5778.
<https://doi.org/10.3390/ma13245778>

PAPER VI **UHPC overlay as sustainable solution to preserve old concrete structures.**

Ankit Kothari*, Magdalena Rajczakowska, and Andrzej Cwirzen
MATEC Web Conf., 364 (2022) 04014; ICCRRR 2022
<https://doi.org/10.1051/mateconf/202236404014>

Conference IRRCCC - 6th International Conference on Concrete Repair, Rehabilitation and Retrofitting, Cape Town, October 2022.

1.5 Additional papers/conferences

PAPER VII **Monitoring temperature and hydration by mortar sensors made of nanomodified Portland cement.**

Thanyarat Buasiri*, Ankit Kothari, Karin Habermehl-Cwirzen, Lukasz Krzeminski and Andrzej Cwirzen
MaterStruct 57, 1 (2024).
<https://doi.org/10.1617/s11527-023-02275-w>

PAPER VIII **Geopolymer Based on Mechanically Activated Air-cooled Blast Furnace Slag.**

Ilda Tole*, Magdalena Rajczakowska, Abeer Humad, Ankit Kothari and Andrzej Cwirzen
Materials 2020, 13(5), 1134.
<https://doi.org/10.3390/ma13051134>

PAPER IX **The Effect of Blast Furnace Slag/Fly Ash Ratio on Setting, Strength, and Shrinkage of Alkali-Activated Pastes and Concretes.**

Abeer M. Humad*, Ankit Kothari, John L. Provis, and Andrzej Cwirzen
Front. Mater., 14 February 2019
<https://doi.org/10.3389/fmats.2019.00009>

PAPER X **Restoration of Deteriorated Concrete Columns by Wrapping with an Ecological UHPC.**

Ankit Kothari*, Louise Andersson, and Andrzej Cwirzen
Proceedings 2019, 34 (1), 4.
<https://doi.org/10.3390/proceedings2019034004>

Conference The 1st International Conference on Smart Materials for Sustainable construction (SMASCO), Luleå, Sweden, December 2019

SBUF report **Not published**

2. Literature review

Ordinary Portland cement concrete's performance is significantly influenced by the properties of the cementitious binder and the exposure conditions. Temperature is a key factor influencing how concrete develops strength, as it affects the rate and degree of cement hydration. At lower temperatures as of lower magnitude, the hydration rate of the cement is significantly retarded with prolonged setting time, and the strength development is reduced by 20-40% [2,10,11]. When the temperature drops below -4°C during freezing, moisture migrates within the binder matrix and about 92% of it is converted into ice [7]. Concrete cured at 20°C hydrated to $\sim 91.9\%$ after 28 days, while those exposed to -5°C to $\sim 16.7\%$ after 1 day and $\sim 63.2\%$ after 90 days. Irrespective of the exposure to -5°C , the dissolved Ca^{2+} , K^{+} , Na^{+} , OH^{-} , and SO_4^{2-} ions can sustain a slow hydration process, [34]. Consequently, the pore ice formation could be inhibited by a lower freezing point of water but only to a certain limiting temperature, [34–37]. Longer exposure to sub-zero temperatures, causes the mixing and pore water to freeze within the binder matrix. The extensive formation of ice can result in the development of some strength which can be mistaken for the actual concrete strength originating from hydrated cement. Consequently, this can lead to faster removal of formwork as it appears to have reached enough strength. However, when exposed to high temperatures, the structure fails to take the external load and loses its integrity caused from the pore ice melting and the so-called strength finally gradually disappears, resulting in a catastrophic outcome. Figure 1 shows the schematic representation of the involved mechanism.

In the case of hardened concrete, freezing pore water increases its volume by $\sim 9\%$ which can damage the binder matrix, [7]. The ice formation depends on the pore size, [38–40]. Water present in larger pores tends to freeze earlier, while the smaller pore size increases the vapor pressure within and consequently decreases the freezing temperature, [19,41,42]. Another important parameter influencing the ice formation is the cooling rate, i.e., a slower cooling rate provides more time for the ice front to penetrate deeper into the binder matrix, [9]. A faster cooling tends to result in the freezing of only the outer concrete layers while hydration can continue in the core. If the saturation degree of the pore system exceeds 92%, cracking of the binder matrix might occur, as a result of significant stresses and strains caused by the formed pore ice [2–4,8,9,34,43–45]. The frost damage can appear as surface scaling and internal cracking of the binder matrix, [2,10,11].

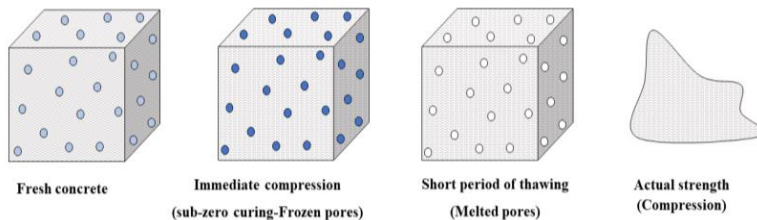


Figure 1: Schematic mechanism of fresh concrete exposed to sub-zero curing temperature, [46]

Engineering guidelines and standards require the application of extra precautionary actions if the air temperature is below 5°C or below 10°C for at least 12 hours during the day in the recorded three consecutive days [3–6]. These include heating of the mixing water or aggregates, covering concrete with isolative blankets, and windbreaks, or adding heating systems to the

formworks, [13]. An application of heating systems increases in most cases the ultimate CO₂ footprint and costs, Figure 2. Another alternative is using rapid hardening Portland cement and various types of chemical admixtures or to employ mineral accelerator that has the ability to increase the hydration heat and/or lower the freezing point of water, [2,14,15].

Replacing Portland Cement (PC) partially or fully with supplementary cementitious materials (SCMs) or alternative binders aims to reduce the carbon dioxide footprint of concrete. Unfortunately, exposure of these concretes to freezing and subfreezing temperatures can in some cases cause short- and long-term problems. Currently, PC-based concretes can be produced at temperatures as low as -10°C, [7,47]. However, some binder systems containing high amounts of SCMs showed significantly lower hydration rates and slower strength development, when subjected to subfreezing temperatures immediately after casting. Additionally, chemical admixtures optimized for PC can perform significantly differently or worse when used in composite binders. Alterations could include fresh and hardened properties, as well as durability. The knowledge in this area is still rather limited.



Figure 2: Examples of primitive protection methods of concrete during cold weather, [48]

It is commonly agreed that concrete should reach at least 3.5-5 MPa of compressive strength before it can be exposed to freezing and avoid permanent frost damage, [6,12]. A minimum compressive strength of 24 MPa is required before concrete can be exposed to multiple freeze-thaw cycles [6]. Furthermore, certain measures shall be applied before and after placing concrete during winter, [49]. For example, wooden formwork is recommended due to its lower thermal conductivity and better thermal insulation compared to metal formwork. The formwork must be cleaned of snow and ice. Frozen subgrade and steel reinforcement should be preheated, [6,12].

2.1 Chemical admixtures for concretes cast at zero and subzero temperatures

Chemical admixtures are frequently used in concrete to be cast at subzero temperatures. They can lower the freezing point of mixing water, shorten the setting time, and accelerate the strength development. Two types of antifreeze admixtures were commonly used in the early 1950s, chloride and non-chloride-based, [2,3,50,51]. Calcium chloride (CaCl₂) not only accelerates the strength development but also improves the rheology of concrete. Studies have shown that additions between 2 wt.% and 4 wt.% of CaCl₂ are optimum for concreting at temperatures as low as -7°C, [52–55]. Unfortunately, chloride-based admixtures increase steel corrosion and promote water uptake [56]. The frost durability can worsen, [52]. Additionally, the expansive oxychloride compounds can decrease the compressive strength by 30%–50%, [57].

The effects of antifreeze and air-entraining admixtures are shown in Figure 3 (a, b) and Figure 3 (c, d). The antifreeze admixtures decrease the water's freezing point. The air-entraining admixture reduced the surface scaling by introducing an evenly spaced system of air voids in the binder matrix, [58,59]. On the negative side, for every 1% increase in the air content of concrete, the 28-day compressive strength can decrease by up to 5%, [60][58][61]. These losses can be comparatively prevented when combined with antifreeze admixtures, [62].

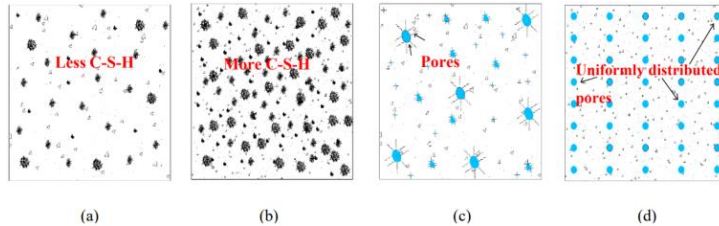


Figure 3: Low temperature cured/casted concrete (a) Without antifreeze admixture; (b) With antifreeze admixture; (c) Without air-entraining agent; (d) With an air-entraining agent, [63].

Table 1, lists the most used chemical admixtures for winter concreting. Calcium chloride, sodium chloride, calcium nitrate, and sodium nitrite are examples of inorganic salts. The novel non-chloride-based calcium nitrate admixture demonstrated similar acceleration effects, even at -10°C , without any detected steel corrosion [12]. This admixture, while soluble in water, acts solely as a set accelerator through an early Portlandite formation [64,65]. However, at lower temperature of -20°C , concrete showed deteriorated performance due to micro-cracking, but upon subsequent curing at room temperature improved strength, [3,12,66,67]. Further, in a study PC concrete with 6 wt.% of calcium nitrate and 0.5 wt.% of superplasticizer achieved compressive strengths of 33.21 MPa, 10.76 MPa, 5.35 MPa, and 4.13 MPa when cured at -5°C , -10°C , -15°C , and -20°C for 28 days, respectively. Subsequent 28 days of water curing at room temperature substantially increased these strengths to 57.51 MPa, 52.93 MPa, 51.35 MPa, and 47.02 MPa, respectively [12].

Furthermore, a curing procedure that included also pre- and post-curing, limited the admixture dosage to 1 wt.% of calcium nitrate or 1 wt.% of polyhydroxy amine antifreeze admixtures and enabled to achieve comparable results. PC concrete was cured at temperatures between 0°C and -20°C for 2 days, followed by 26 days of storage at room temperature, [68]. Mixes containing calcium nitrate reached compressive strength between 23.24 MPa and 14.8 MPa. Mixes with polyhydroxy amine admixture between 25.53 MPa and 15.98 MPa. Similarly, concrete incorporating a calcium nitrite admixture and cured at -4°C for 3 days, followed by 25 days of further curing at 10°C , showed improvements in several parameters. For example, the setting time was shortened by six hours, The compressive strength increased by 170% increase at 3 days and a 117% increase. The 28-day compressive strength was comparable to concrete without admixtures but subjected to the same curing regime [51].

Using a research setup like that of Karagöl et al. (2013) but incorporating additional room temperature curing, Demirboga et al. (2014) investigated the effectiveness of 6 wt.% of urea admixture. The maximum compressive strength was 16.38 MPa and 6.95 MPa after 28 days of curing at -5°C and -10°C , respectively. Subsequent 28 days of curing at room temperature increased the strength values to 30.28 MPa and 22.12 MPa, respectively [13]. Specimens cured at -10°C developed dense microstructures with higher amounts of formed calcium silicate

hydrate (C-S-H) and calcium hydroxide. In contrast, control specimens showed more unhydrated cement particles and delayed hydration processes. Furthermore, concrete mixes containing 6 wt.% of calcium nitrate, or 6 wt.% of urea were studied by Polat (2016). Both mixes were exposed to freeze-thaw testing immediately after casting in the temperature range of +/-10°C. Concrete with the calcium nitrate admixture achieved a 28-day compressive strength of 28.05 MPa, while the urea-based concrete was only 18.32 MPa [10]. In another study, the combined effects of urea and calcium nitrate admixtures were examined. Both admixtures were used in equal amounts (4.5 wt%) in concrete samples cured at various temperatures (-5°C, -10°C, -15°C, and -20°C). The best results were observed at -5°C and -10°C, with compressive strengths of 41.91 MPa and 24.28 MPa, respectively, after 28 days. However, curing at -15°C and -20°C resulted in lower strengths of 8.86 MPa and 3.99 MPa, respectively, [7]. The strength development can be attributed to urea's acceleration of the hydration process, calcium nitrate's promotion of rapid crystallization, and the eutectic points of both admixtures. Urea and calcium nitrate ranged between (-6.3°C to -7.4°C) and (-7.6°C to -11.5°C), which, if surpassed, could lead to reduced strength due to ice formation and microcracking, [7,12].

Combinations of 6 wt.% of sodium nitrite with 2 wt.% of calcium nitrite and 6 wt.% of sodium nitrites with 0.06 wt.% of potassium carbonate were assessed by Korhonen and Cortez (1991). After 28 days and exposure to -10°C, the test concretes reached 35 MPa [16]. The research indicated that pre-curing of specimens for six hours at room temperature enhanced their strength. However, prolonged curing at room temperature accelerated the transformation of ettringite into monosulphate and caused microcracking [57][39]. Potassium carbonate can be used as accelerators and antifreezing admixtures, producing more fiber-like products at an early age due to the faster hydration process, resulting in the development of high internal stresses and micro-cracks, thereby lowering the effectiveness of the admixture, [69].

Table 1: Summarized cold weather chemical admixture for winter concreting, [63].

Admixture	Years	References
Calcium Chloride	1951, 1952, 1958, 1970, 1976, 1990, 1995, 1998, 2007, 2008, 2013	[2,3,70,12,52–55,57,66,67]
Sodium Chloride	1976, 1990, 1998	[2,3,70]
Calcium Nitrate	1991, 1999, 2003, 2013, 2015, 2016, 2018	[7,10,12,58,61,71–73]
Calcium Nitrite	1989, 1991, 1995, 1996, 1998, 2007, 2013	[3,12,15,51,66,67,74,75]
Magnesium chloride	2008	[57]
Sodium Nitrate	1997	[76]
Sodium Nitrite	1991, 1996, 2012	[15,74]
Sodium Sulfate	1985, 1990, 1997,	[2,76,77]
Potassium carbonate	1983, 1991, 2019	[15,69,78]
Urea	2014, 2015, 2016	[7,10,13]
Calcium thiocyanate	1995, 2007	[67,79]
Polyhydroxy amine	2011	[68]
Sodium thiocyanate	1988, 1998, 1999, 2003	[3,5,71,80]
Polyglycolester based	1991, 1999	[71,72]
Hydroxyethylamine	2011, 2014	[68,81]
Polyethylhydrosiloxane	2007	[59]

Air entraining agents (AE) have a crucial role in enhancing the frost resistance of concrete. Many researchers proposed to blend the air-entraining agent with antifreeze or accelerating admixtures to limit the adverse effect. Franke et al. (2015) proposed a concrete mix with an admixture combination comprising 4 wt.% of calcium nitrate and 0.16 wt.% of air entraining agent (SIKA LPS A-94). The AE increased porosity, while calcium nitrate supported the formation of fine air voids and enhanced frost durability. This approach accelerated the strength development and low surface scaling of 82 g/m² after 56 freeze-thaw cycles exposed to 3% NaCl solution. In contrast, concrete without these admixtures showed a surface scaling of 11851 g/m², [58,61,73].

Partially replacing PC with SCMs is a common practice to reduce the CO₂ footprint of concretes. However, fresh, and hardened state properties can deteriorate more extensively in comparison with PC concretes when cured at subfreezing temperatures. Jiang et al. (2013) investigated composite concrete mixes comprising 6 wt.% fly ash, 4 wt.% of "LNC-53" non-chloride antifreeze admixture, a naphthalene-based water reducer, and 5.3 wt.% air entraining agent. The length of the applied pre-curing at room temperature, followed by 28 days of curing at -10°C, resulted in strengths ranging from 12.6 MPa to 38.6 MPa. Specimens pre-cured for 48-72 hours formed a dense binder matrix, and showed a minimal weight loss and a 15% RDME loss after 300 freeze-thaw cycles, [82]. Dong et al. (2013) increased the fly ash content to 10 and 20 wt.% of PC and observed a decreased strength regardless of the applied curing. Despite the lower 28-day compressive strength values, the 90-day strength reached 48 MPa and 40 MPa. These values were comparable with the 28-day compressive strength results obtained for the reference concretes cured at room temperature, [82–84]. An increase of the fly ash amount to 30 wt.% of PC, but without the addition of any cold weather admixtures (CWA), produced the compressive strength of 68.1 MPa strength after 90 days of standard curing. However, after 100 F-T cycles, the strength dropped by 84%, [85].

The incorporation of silica fume altered frost damage mechanisms, promoting denser microstructure formation and less water penetration during freezing, even without air entrainment, [56,86–91]. Jang et al. (2015) investigated high-performance concrete (HPC) with 5% silica fume that was cured at 5, -5, and -15°C. Strength values gradually declined with lower temperatures, reaching 25.41 MPa, 23.76 MPa, and 14.02 MPa after 28 days, [91]. Concrete with up to 7 wt.% silica fume and a w/b of 0.3 showed the surface scaling of 500 g/m² and 90% RDME after 56 freeze-thaw cycles. However, increasing the w/c ratio has widened the ITZ and increased the porosity, leading to a greater uptake of the freezing media during freeze-thaw cycles, [92–94]. On the contrary, strength reached approximately 70 MPa after 90 days, with a 108% increase in the residual compressive strength for composite concrete up to 30 wt.% of fly ash replacement, 10 wt.% silica fume, and a w/b ratio of 0.28. Further increase in the amount of fly ash decreased the strength development and worsened the frost durability despite the added silica fume, [95]. Furthermore, introducing an air-entraining agent to mixes resulted in the RDME and durability factor of over 80%, with minimal to moderate surface scaling after 300 F-T cycles. Increased fly ash content, however, led to an unstable air-void system due to the adsorption of the air-entraining agent, [90,96,97].

Ground granulated blast furnace slag (GGBFS), a byproduct from steel industries, has a negative impact on concrete properties at low temperatures. Concrete containing 50 wt.% of GGBFS showed an RDME of up to 80% after 180 F-T cycles without entrained air [98,99]. Increasing replacement levels led to extensive internal damage, with an RDME dropping below 20% after 180 cycles due to ice formation in capillary pores. This ice-stress mechanism can be

mitigated by reducing pore volume or inducing entrained air, [100–102]. Conversely, concrete with 5 wt.% of silica fume and 50 wt.% of GGBFS showed RDME of 95%. Yet, maintaining GGBFS at 50% and increasing the silica fume content to 15 wt.% reduced the F-T resistance (RDME – 65%) after 180 cycles, [100]. Sobolev and Batrakov (2007) studied the frost durability concretes containing 15 wt.% of silica fume and with either 15 wt.% ponded ash or 45 wt.% finely ground blast furnace slag. All mixes, with 1.8 wt.% of SNF type superplasticizer and 0.0625 wt.% of PEHSO air-entraining admixture, resisted F-T action over 700 cycles with minor deformation below 0.05% [59]. Increasing pond ash content to over 15 wt.% showed deterioration even before reaching 200 F-T cycles due to its slow reaction, leaving partially unhydrated ash particles [103].

The efficiency of the cold weather chemical admixtures is summarized in Table 2, Table 3, Table 4 and Table 5. Only the nitrate-based and urea mixed with calcium nitrate-based AF admixture appeared to be equally efficient for concretes based on PC and PC with SCMs.

Table 2: Efficiency of antifreeze admixtures for PC and composite concrete based on the available data, [63].

Antifreeze Admixture	PC	Composite	Comments	References
Calcium Chloride	×	–	Expansive oxychloride Susceptible to reinforcement corrosion	[2,3,52–55,70]
Sodium Chloride	×	–		
Calcium Nitrate	××××	–	Accelerates hydration reaction. Efficient up to –10 °C	[10,12,15,51,74]
Calcium Nitrite	××××	–	Needs additional standard curing	
Polyhydroxy amine	×××	–	Post-curing boosts strength and microstructure	[68]
Polyglycolester-based	×××	–	Depends on the dosage of admixture	[71,72]
Urea	×××××	–	Efficient with calcium nitrate Breaks hydrogen bond and	[7]
Calcium thiocyanate	××	–	Accelerator	[67,79]
Sodium thiocyanate	×	× (OPC + FA) ×× (OPC + Slag)	Risk of alkali–aggregate reaction	[3,5,71,80]
Sodium Nitrate	××××	××××	Prolonged pre-curing will develop cracks	[75]
Potassium carbonate	×××	–	Detrimental effect at standard temperature	[69]
Sodium Sulfate	××	–	Need pre-curing	[78]
Hydroxyethylamine	××	–	Does not withstand corrosive environment	[68,81]
MC Rapid 25/15	–	××××	Dissolute silica compound and maintain liquid phases	[44,104]

Note: (×) not acceptable performance; (××) barely acceptable; (×××) reasonable; (××××) acceptable; (×××××) very good performance; (–) no data available.

Table 3: Efficiency of commercial AE for PC and composite concrete, [63].

Air-Entraining (AE) Admixture	PC	Composite	Comments	References
Diamidoamine salt	xxx	-	Closed spaced air-void. Promote strength development at later age	[105]
Saponin based	-	xxxx (OPC + FA)	Stable in acidic and alkaline environment	[106–109]
Resin based	-	× (OPC + SF)	High porosity	[110,111]
Polyethylhydrosiloxane (PEHSO)	-	xxxx (OPC + SF + Slag) xxxx (OPC + FA + SF)	High reactive with hydroxyl group	[59,112]

Note: (×) not acceptable performance; (××) barely acceptable; (×××) reasonable; (××××) acceptable; (×××××) very good performance; (-) no data available.

Table 4: Summarized PC and admixtures exposed to lower curing temperature, [63].

Convention PC concrete				
Admixtures	Curing Temp (°C)	F-T cycles	Notes	Reference
Calcium chloride + sodium chloride	-10	-	Dosage 2% - 4% efficient, no adverse effects	[2,3,52–55,70]
3wt% calcium thiocyanate	-5	-	74% strength increase compared to normal cured concrete	[67,79]
1wt% polyhydroxy amine antifreeze	0 -5 -10 -15 -20	-	2 days cured at respective temperature, followed by normal water curing for 26 days	[68,81]
10wt% sodium thiocyanate	-7	-	Over 10% risk of alkali aggregate reaction	[3,5,71,80]
6wt% sodium nitrite + 2 wt% calcium nitrite.	-10	-	Strength gain 35 MPa	[15,74]
6wt% sodium nitrite + 0.06 wt% potassium carbonate		-		
3 wt% potassium carbonate antifreeze	10 to -5	-	30% strength increase -Exposed to winter, varying temperature	[69]

8.1% calcium nitrite	-4 and 10	-	117% strength increase – Initial 3days cured at -4°C and followed by 10°C until test	[51]
Calcium nitrite + polyglycolester	-5	-	5 liters per 100 kg of cement is the optimum dosage	[71,72]
6 wt% urea	-5 -10	-		[13]
6 wt% calcium nitrate + 0.5 wt% plasticizer	-5 -10 -15 -20	-	Workable, additional normal curing increased strength	[12] [10]
4.5 wt% urea + 4.5 wt% calcium nitrate	-5 -10	-	Over -10°C, strength decreased	[7]
4 wt% calcium nitrate + 0.16 wt% air entraining agent (SIKA LPS A-94)	20	56	Less surface scaling relative to conventional concrete without admixtures	[58,61,73]

Table 5: Summarized SCM mixes, and chemical admixtures exposed to lower curing temperature, [63].

Mix	Admixtures	Curing Temp (°C)	F-T cycles	Notes	Reference
12.5% Fly ash + 5.4% silica fume	0.4 wt% sodium nitrite antifreeze (AF)	-5 and +20	-	7 days cured at -5°C, followed by +20°C for 21 days	[75]
20% fly ash	-	-5	-	Lower modulus of elasticity compared to 20°C cured samples	[91]
23% fly ash	Sodium thiocyanate (AF)	-4	-	Concrete measured 27°C while casting	[3]
50% slag	-		180	Excessive internal damage	[100]
50% slag +5% silica fume	-		180	RDME 95%	
20% to 30% silica fume	lignosulfonic acid water reducing agent + sulfonated naphthalene formaldehyde + AE		300	Deterioration of concrete due to high air void spacing factor	[110]
0% to 65% slag + 25% silica fume	-		100	Extremely dense binder matrix	[99]
7% silica fume	-		56	High performance concrete, less surface scaling 500 g/m ²	[92]
15% silica fume	-		28	Surface scaling 80 g/m ²	[87]
10% silica fume	-		300	7% strength decrease	[113]
15% silica fume or fly ash	1.5% Sikament (SP) + 0.15% Sika AER (AE)		28	Dense microstructure, less surface scaling	[87,88,114]
15% silica fume + 40% fly ash	1.25% PCE (SP)	20	210	Extensive internal damage	[115]
5% silica fume	5% AE	20	300	Dense and durable	[85,97]
5% silica fume + 15% to 35% fly ash	5% AE	20	300	Fly ash is affecting durability	
Silica fume (0% - 20%) + fly ash (0% -40%)	-	20	120	Internal damage, need of AE agent	[116]
15% cement kiln dust (CKD)	-	20	300	Internal frost damage for excess CKD	[117]
10% slag + 10% metakaolin	-	20	300	Optimization of pore structure	[118]
15% silica fume + 45% slag	1.8% sulfonated naphthalene formaldehyde (SP) + 0.0625% polyethylhydrosiloxane (AE)	20	56	Admixtures improved frost durability	[59]
20% fly ash	0.5% naphthalene-based (SP) +4.2% SJ-3 (AE)	20	400	Less internal damage	[107,108]

2.2 CSA cements for concretes cast at zero and subzero temperatures

CSA cements are known for their rapid setting, low shrinkage, excellent anti-freeze properties, and superior sealing characteristics, [16–19]. Some of their hydration products can adsorb liquid phase, thereby preventing the formation of larger ice crystals, [19]. CSA cement production requires approximately 60% less limestone compared to Portland Cement (PC), which results in lower clinkering between 1250°C and 1350°C, with the potential to be further reduced to 1100°C, [119,120]. CSA cement has a lower density in comparison with PC clinker therefore it requires less energy for grinding, and emits less CO₂ during production, [18,121–123]. The composition of CSA cement typically includes 30-70 wt.% of ye'elimite (C₄A₃S̄), 10-25 wt.% of calcium sulfate (anhydrite) (C̄S), up to 25 wt.% of belite (C₂S) and some brownmillerite (C₄AF), [19,124,125]. Upon reaction with water, the main hydration phases formed are calcium monosulfate aluminate (AFm) (C₄ASH₁₂) and gibbsite (AH₃) from ye'elimite. The presence of anhydrite led to the production of ettringite (AFt) (C₆A₃H₃₂) and gibbsite, [126,127]. High early strength and rapid drying, accelerated setting, are linked with non-expansive large ettringite crystals, [16]. On the contrary, expansive, self-stressing, and shrinkage-resistant properties are observed in the presence of lime. In that case, ettringite (AFt) (C₆A₃H₃₂) is formed upon hydration of ye'elimite. Additionally, optimized anhydrite dosage often leads to a higher later-age strength due to a slower dissolution, [128,129].

A partial replacement of PC by CSA cement has shown promising results, leading to accelerated setting and faster strength development, [130,131]. The formed larger amount of ettringite fills the pore system, absorbing excess water that can limit the formation of large ice crystals, and enhancing the density of the binder matrix, [19,132]. Additionally, in PC-CSA systems, the presence of gibbsite promotes the synthesis of strätlingite and portlandite through interaction with alite (C₃S), [133,134]. Belite-rich CSA as the sole binder along with gibbsite (AH₃) primarily promotes the formation of strätlingite, resulting in slower strength development, [135]. Concretes based on PC-CSA binders cured -5°C showed 300% higher early compressive strength due to the ettringite formation, [19]. On the contrary, studies by Huang et al. (2019) showed a 65% and 83% reduction in strength for concretes cured at -5°C and -10°C, [136]. The maximum replacement of PC with CSA appeared to be <20 wt.%, [19]. The presence of CSA in PC systems does not alter the hydration process of C₃S but modulates aluminate dissolution, [137,138]. Blended PC-CSA has a 2.5 times faster hydration rate in comparison with pure PC systems. Higher concentrations of sulfates and free lime led to increased heat release, [19,125,132,137]. The primary factors were faster wetting, dissolution, and partial hydration. Gypsum (C̄SH₂) from PC accelerates the dissolution of anhydrite (C̄S) and enhances the hydration kinetics of ye'elimite, ultimately resulting in the formation of ettringite crystals as the principal reaction products, [123]. After complete consumption of calcium sulfates and calcium hydroxide, the main reactions involve the formation of calcium monosulfate aluminate (AFm) and gibbsite (AH₃) as the principal hydration phases during the interaction of ye'elimite with water, [139].

Furthermore, maintaining the CSA cement and having GGBFS replace some parts of the PC could further lower the CO₂ footprint. However, incorporating CSA into the PC+GGBFS system has the potential to enhance the early-age mechanical properties, [131]. The primary hydration phases, including ettringite, monosulfate, gibbsite, and strätlingite, were comparable to those found in pure CSA-based concrete, [120,131,140]. These systems exhibited a reduced risk of alkali-silica reaction (ASR) and enhanced resistance to sulfate attack, [131,141]. However, studies have noted that the dilution effect and limited reactivity of GGBFS in binary

GGBFS-CSA mixtures led to a decline in mechanical properties and durability, [120,142,143]. Additionally, the behavior of these blended composite mixtures under freezing and subfreezing curing conditions remains uncertain, as of a very limited number of studies.

2.3 UHPC overlay for restoration of deteriorated concrete structures

Ultra-high-performance concrete (UHPC) has high compressive strength (>150 MPa), tensile strength >8 MPa, enhanced flowability, and a very dense microstructure leading to superior frost durability, [21–28]. UHPC has been successfully applied in strengthening and repairing deteriorated reinforced concrete structures [144,145]. Ensuring a sufficient bonding between UHPC overlays and deteriorated concrete substrates is a crucial factor. Parameters such as substrate roughness, moisture content, and water-cement ratio play key roles in determining the properties of the interfacial bond zone [146–150]. Studies showed that a high porosity in the interface zone could weaken bonding between the layers due to the limited water available for proper hydration. Low porosity may reduce mechanical interlock between the substrate and the overlay, [150]. Jackhammering, sandblasting, and water jetting are commonly used to roughen the substrate surface, [151]. However, microcracking caused by jackhammering can lead to weaker bonds [151]. In contrast, studies have shown that preparing the substrate surface through sandblasting or water jetting promotes better bonding due to well-exposed aggregates [22,152]. Zhang et al. (2020) evaluated the interfacial bond properties between UHPC and normal concrete with varying moisture levels and substrate roughness using slant shear, split tensile, and direct tensile tests. The results indicated a significantly higher bond with rough and adequately wetted substrate concrete compared to smooth substrates [26]. Curing conditions also directly influence bond properties. Application of high temperatures resulted in higher early shrinkage and decreased interfacial bond strength compared to ambient-cured specimens [155,156]. The interface shear strength was investigated using a Z-shaped single-sided push-out test on untreated and grooved (water-jetted) substrates. The results showed better strength for rough and grooved substrates compared to untreated substrates [153,154]. Others applied epoxy as an adhesive agent on a rough substrate surface. The results showed mixed effects due to the uneven distribution of the epoxy agent, [155]. Some have recommended an overlay thickness of only 25-50 mm, to minimize materials consumption and lower the weight while maintaining high tensile strength [156–158]. Such thin overlays are susceptible to early-age shrinkage cracks caused by restraint effects [159].

UHPC often requires a significant amount of cement compared to conventional concrete, resulting in 2-3 times higher CO₂ emissions [29,31–33]. Partially replacing PC with slag, fly ash, silica fume, limestone powder, and quartz filler not only reduces production costs but also decreases shrinkage while enhancing mechanical properties and durability, [160–165]. The inclusion of limestone powder as a filler in UHPC has different effects on fresh and hardened concrete properties. Its fineness accelerates cement hydration, [166–168]. Some studies indicate that calcium carbonate in limestone powder reacts with C₃A to form low and high forms of calcium carboaluminate (CCA) during cement hydration, thus enhancing strength, [163,169–171]. Additionally, it expels water and fills voids, thereby improving fresh concrete properties and facilitating secondary pozzolanic reactions between portlandite and silica fume [171]. Using quartz filler reduces paste thickness, resulting in lower porosity and better homogeneity, making UHPC more brittle [172,173].

2.4 Summary

Casting concrete in cold weather is challenging and costly, as it can lead to delayed setting times, slow strength development, and increased risk of freezing. Two approaches are typically used to address these issues: heating systems, protective covers, or alternative binders and chemical admixtures. Existing research indicates that PC-based concretes can perform well at temperatures as low as -10°C without the need for additional measures. Hydration heat combined with chemical admixtures is sufficient to achieve adequate strength and freeze-thaw durability in these conditions.

Only limited research has been done on composite binders incorporating, alternative cements, supplementary cementitious materials (SCMs), chemical admixtures, and their performance in subzero temperatures.

The application of UHPC to protect old and new PC concrete structures from frost damage has been also investigate only to a limited extend. Especially, when using low PC content UHPC.

3. Materials and methods

3.1 Materials

3.1.1 Binders

The following types of binders were used: Rapid hardening Portland cement (CEM I 52.5R) and Anl aggningcement (CEM I 42.5N) from Cementa AB – Heidelberg Materials Sweden, ground granulated blast furnace slag (GGBFS) from SWECHEM – Merit – Sweden and commercially available belite based CSA cement identified as Calimex BeliCem (CSA) from Caltra Nederland B.V. The chemical compositions of all binders are shown in Table 6 and physical properties on Table 7.

The CSA cement contained ~25% of belite (C₂S), > 60% of Ye'elimitite (C₄A₃Ŝ), and 10% of calcium sulfate (CŜ).

Table 6: Chemical composition of the used binders.

Oxides (%)	CEM I 42.5 N	CEM I 52.5R	GGBFS	CSA
CaO	63.30	62.5	30.3	40-44
SiO ₂	21.20	18.8	34	6-10
Al ₂ O ₃	3.40	5.4	11.6	≥32
Fe ₂ O ₃	4.12	3.2	0.3	≤2.2
MgO	2.20	1.3	12.1	≤1.5
Na ₂ O	0.18	0.14	0.53	-
K ₂ O	0.56	1.3	0.81	-
SO ₃	2.70	3.7	1.5	9-10
Cl	0.02	0.03	0.02	-
LOI	2.50	2.6	-0.9	≤3

Table 7: Physical properties of the used binders

Binder	Type	Producer	Fineness cm ² /g	Density g/cm ³
PC	CEM I 52.5R	Cementa	5400	3.2
Slag	GGBFS	SWECHEM	4350	2.9
CSA	Belite-CSA	Caltra Nederland B.	5000	2.9

3.1.2 Fillers and Aggregates

The used fine fillers included a fine quartz filler type "Norquartz 45" from Sibelco Nordic (Lillesand, Norway), condensed micro-silica 920D from Elkem (Oslo, Norway), limestone powder type "Nordkalk Limus 40" from Nordkalk AB, and fine sands with maximum particle sizes of 350 μm (B35) and 150 μm (B15) supplied by Baskarpsand AB (Habo, Sweden). Table 8 shows their chemical compositions. Concretes contained natural granite aggregates having particle size 0-4 mm and 4-8 mm, from Jehander – Heidelberg Materials, Sweden. Figure 4 shows the particle size distribution of the used fillers and aggregates.

Table 8: Chemical composition of the used fillers.

Oxides (%)	Limestone Powder	Silica Fume	Quartz	Fine sand (B15, B35)
CaO	50.2	1	99.6	-
SiO ₂	4.6	≥85	-	90.5
Al ₂ O ₃	1	1	0.25	4.9
Fe ₂ O ₃	1	1	0.02	0.5
MgO	2	1	-	-
Na ₂ O	0.1	0.5	-	1.2
K ₂ O	0.3	1.2	-	2
SO ₃	0.02	2	-	-
Cl	<0.01	0.3	-	-
LOI	-	4	0.15	-

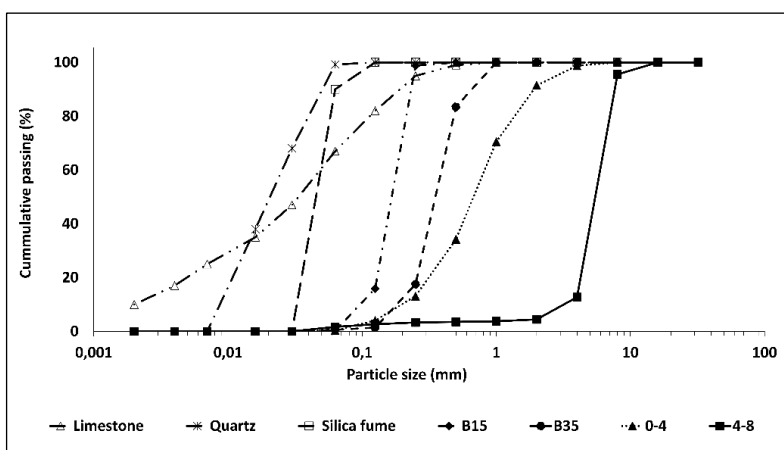


Figure 4: Particle size distribution of the used fillers and aggregates.

3.1.3 Chemical admixtures

To enhance the workability and accelerate the hydration process of pastes and concretes several chemical admixtures were used in this study. These included a polycarboxylate ether-based superplasticizer "MasterGlenium ACE 30" (SP), a sodium nitrate-based antifreeze admixture "MasterSet AC 220" (AF), an accelerator "Master X-Seed 130" (ACC), and an air-entraining admixture "MasterAir 105" (AE), all of which were provided from Masters Builders (Rosersberg, Germany). The water content within these chemical admixtures was subtracted from the water added during mixing. The solids and water contents are shown in Table 9.

Table 9: Solid and water contents in wt.% of used chemical admixtures.

Chemical admixtures	Solid content (wt.%)	Water content (wt.%)
MasterGlenium ACE 30 (SP)	30	70
MasterSet AC 220 (AF)	40	60
Master X-Seed 130 (ACC)	22.5	77.5
MasterAir 105 (AE)	12.5	87.5

3.1.4 Steel fibers

Steel fibers of lengths 6 mm and 13 mm from Krampe Harex-Germany (Hamm, Germany) were used in the production of UHPC. The properties of these fibers are shown in Table 10.

Table 10: Properties of the used steel fibers

Properties	DM 6/0.175	DG 13/0.3 – E430
Material	Steel – brass coated	Stainless steel
Type of fiber	Wire fiber – microfiber	Wire fiber – straight steel
Length (L)	6 mm	13 mm
Diameter (d)	0.175 mm	0.3 mm
Ratio (L/d)	34.3	43
Tensile strength (MPa)	2800	1100
Modulus of elasticity (GPa)	210	200
Quantity of fibers/kg	882,000	144,174

3.1.5 Mix designs

The total binder content for all pastes and concretes was set to 400 kg/m³. The binary or the tertiary mixes of PC, GGBFS, and CSA contained 50 wt.% of PC and 50 wt.% of GGBFS, while the replacement of PC and/or GGBFS with CSA cement was limited to 20 wt.%. The water-to-binder ratio was 0.31 and 0.42 for paste and concrete respectively. In addition, the chemical admixture dosage i.e., superplasticizer (SP), accelerator (ACC), and air entraining agent were kept constant at 0.75 wt.%, 10 wt.%, and 0.1 wt.% of the binder weight, respectively. The antifreeze admixture was added in different dosages i.e., 0 wt.%, 6 wt.%, 10 wt.%, 15 wt.%, 20 wt.%, 25 wt.%, and 30 wt.%. Table 11 and Table 12 show the detailed mix composition of pastes and concretes.

Table 11: Pastes mix compositions.

Mix	CEM I 52.5R	GGBFS	CSA	w/b	Chemical admixture			
	(kg/m ³)	(kg/m ³)	(kg/m ³)		(wt.%)			
PC (100%)	400	0	0	0.31	SP – 0.75			
CSA (100%)	0	0	400	0.31	SP – 0.75			
PC:GGBFS:CSA (80:0:20)	320	0	80	0.31	SP – 0.75			
PC:GGBFS:CSA (0:80:20)	0	320	80	0.31	SP – 0.75			
PC:GGBFS:CSA (40:40:20)	160	160	80	0.31	SP – 0.75			
PC:GGBFS:CSA (50:50:0)(0%AF)	200	200	0	0.31	SP – 0.75			
PC:GGBFS:CSA (50:50:0)(6%AF)	200	200	0	0.31	SP	AF	ACC	AE
					0.75	6	10	0.1
PC:GGBFS:CSA (50:50:0)(10%AF)	200	200	0	0.31	0.75	10	10	0.1
PC:GGBFS:CSA (50:50:0)(15%AF)	200	200	0	0.31	0.75	15	10	0.1
PC:GGBFS:CSA (50:50:0)(20%AF)	200	200	0	0.31	0.75	20	10	0.1
PC:GGBFS:CSA (50:50:0)(25%AF)	200	200	0	0.31	0.75	25	10	0.1
PC:GGBFS:CSA (50:50:0)(30%AF)	200	200	0	0.31	0.75	30	10	0.1

Table 12: Concrete mix compositions.

Mix	CEM I 52.5R kg/m ³	GGBFS kg/m ³	CSA kg/m ³	w/b	Chemical admixture wt. %				Filler kg/m ³		Aggregate kg/m ³	
									Quartz	B15	0-4	4-8
CSA (100%)	0	0	400	0.42	SP – 0.75				90	90	1075	537
PC (100%)	400	0	0	0.42	SP – 0.75				90	90	1075	537
PC:GGBFS:CSA (80:0:20)	320	0	80	0.42	SP – 0.75				90	90	1075	537
PC:GGBFS:CSA (0:80:20)	0	320	80	0.42	SP – 0.75				90	90	1075	537
PC:GGBFS:CSA (40:40:20)	160	160	80	0.42	SP – 0.75				90	90	1075	537
PC:GGBFS:CSA (50:50:0) (0%AF)	200	200	0	0.42	SP – 0.75				90	90	1075	537
					<u>SP</u>	<u>AF</u>	<u>ACC</u>	<u>AE</u>				
PC:GGBFS:CSA (50:50:0) (6%AF)	200	200	0	0.42	0.75	6	10	0.1	90	90	1075	537
PC:GGBFS:CSA (50:50:0) (10%AF)	200	200	0	0.42	0.75	10	10	0.1	90	90	1075	537
PC:GGBFS:CSA (50:50:0) (15%AF)	200	200	0	0.42	0.75	15	10	0.1	90	90	1075	537
PC:GGBFS:CSA (50:50:0) (20%AF)	200	200	0	0.42	0.75	20	10	0.1	90	90	1075	537
PC:GGBFS:CSA (50:50:0) (25%AF)	200	200	0	0.42	0.75	25	10	0.1	90	90	1075	537
PC:GGBFS:CSA (50:50:0) (30%AF)	200	200	0	0.42	0.75	30	10	0.1	90	90	1075	537

Anläggningscement (CEM I 42.5N) was used to produce UHPC. The normal strength concrete (NSC) was supplied by a locally ready-mix concrete distributor (Snells Betong och Ballast, Luleå, Sweden). Detailed mix compositions of both concretes are shown in Table 13. The UHPC mix contained steel fibers having lengths of 6 mm and 13 mm with dosages of 10 wt.% and 15 wt.% respectively, and 5 wt.% of the superplasticizer (SP). The water-to-binder ratio was 0.33.

Table 13: Mix composition of UHPC and normal strength concrete (NSC).

Materials	UHPC (kg/m ³)	NSC (kg/m ³)
Cement type	CEM I 42.5N	CEM II/A-V 52.5N
Cement	651	340
Silica Fume 920D	130.2	-
Limestone	651	-
Dolomite filler – KM200	-	160
Quartz	65.1	-
Sand – B15 (150 µm)	227.9	-
Sand – B35 (350 µm)	227.9	-
Fine aggregate (0-4mm)	-	1021
Coarse aggregate	(4-8mm)	-
	(8-16mm)	802
MasterGlenium ACE 30 – (SP)	32.6	3.4
Water	192 (w/b 0.33)	187 (w/b 0.55)
Steel fibers 6 mm	65.1	-
Steel fibers 13 mm	97.7	-

3.2 Methods

3.2.1 Mixing and curing

The mixing sequence for composite binder-based concretes included 2 min of dry mixing, followed by the addition of water with all chemical admixtures, and mixing for another 2 min. Similarly, the UHPC was dry mixed for 2 min, followed by the addition of water with superplasticizer and mixed for another 5–6 min. The steel fibers were added at the end and mixed for another 2 min. In total, the mixing time for UHPC was approximately 9–10 min. A pan mixer having 75 liters capacity type Zyklos – ZZ 75 HE from Pemat- Germany was used.

Freshly cast concrete cubes were covered with plastic foil and cured at an ambient room temperature, of approximately 20°C ± 2°C for the preliminary studies. In contrast, for the main studies, the cubes were placed in a refrigerator with a set temperature of -15°C. The UHPC

layer cast over the deteriorated NSC element was covered with a plastic foil for 24 hours, followed by a surface curing using water sprinklers for the following 7 days.

3.2.2 Test methods and sample preparations.

All produced concretes were tested for initial and final setting time, hydration temperature development, slump, and compressive strength. The phase transition of pore water into ice and its transitioning temperature, as well as their impacts on the binder matrix, was studied using differential scanning calorimetry (DSC). Ultrasonic pulse velocity (UPV) was used to detect either the formation of internal cracks or ice within the binder matrix. A bond strength between UHPC and substrate concrete was determined using a pull-off method. Microstructure was studied using a scanning electron microscope (SEM) coupled with an energy-dispersive spectrometer (EDS).

3.2.3 Phase transition test setup

Visual examination and differential scanning calorimetry (DSC) were used to determine the phase transition for the seven admixture combinations and twelve paste mixes shown in Table 11. For the visual assessment of the phase transition in admixture solutions, the prepared samples were sealed in a plastic container, that was exposed to -15°C , Figure 5. The visual assessments were performed every 30 min with a compulsion of determining the transition either between from water to slush or from slush to ice.

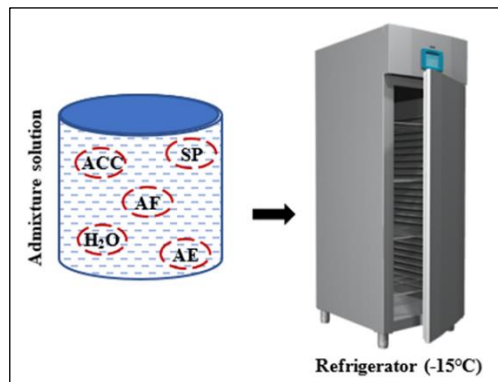


Figure 5: Graphical representation of phase transition test setup – visual determination.

The phase transition of pore water to ice was studying differential scanning calorimetry type Q100 TA, Figure 6. The test included placing 15 mg of paste into a sealed aluminum crucible that was installed into the DSC chamber next to the empty reference crucible, Figure 6. The instrument's freezing and thawing rate was set to $1^{\circ}\text{C}/\text{min}$ with an operating temperature cycle from $+10^{\circ}\text{C}$ to -30°C . This temperature cycle was selected to simulate the real-case scenario for casting in winter. As a result, the phase transition was observed based on either the endothermic or the exothermic heat flow. Followed by determining the times of freezing, melting, and glass transition.

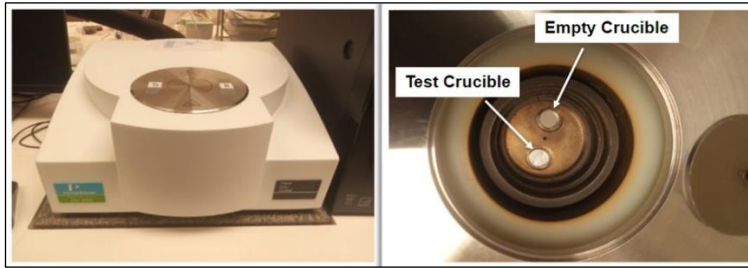


Figure 6: Differential scanning calorimeter (DSC) Q100 TA.

3.2.4 Hydration temperature development

An in-house semi-adiabatic calorimeter was used to analyze the temperature development due to hydration. The calorimeter, shown in Figure 7, was made of Styrofoam with a wall thickness of 60 mm. The PicoLog6 TC-08 instrument with a K-type thermocouple was adopted to record the temperature for 7 days for the pastes that were selected based on the phase transition test results. To monitor the temperature, the thermocouple was inserted into a freshly made paste sample that measured 60 mm x 60 mm x 60 mm.

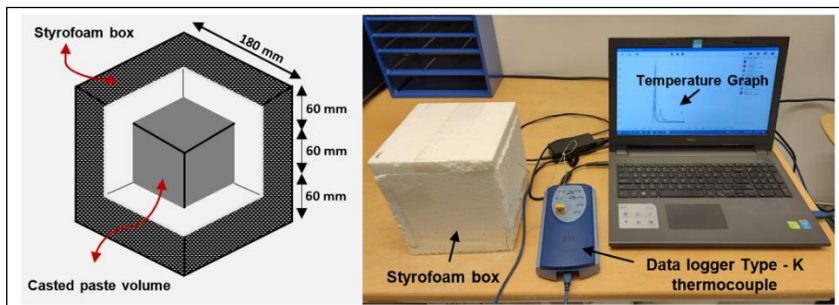


Figure 7: In-house-built semi-adiabatic calorimeter box cross-section and test setup.

3.2.5 Setting time

Initial and final setting times were determined on paste samples manually following the ASTM C191-19, [174]. Figure 8, shows the used Vicat needle apparatus provided from Form+Test Prüfsystemeas, Riedlingen – Germany.

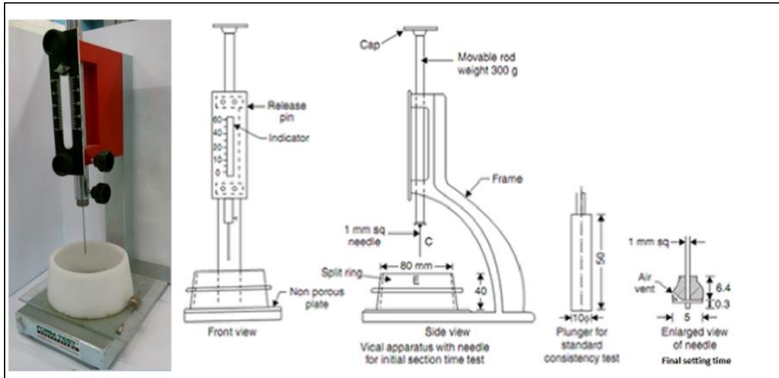


Figure 8: Vicat apparatus used to determine initial and final setting times.

3.2.6 Workability of concrete

Concrete's workability was determined by performing a slump test following the SS-EN 12350-8:2019 standard [175], Figure 9.



Figure 9: The slump test setup used to determine the workability of concrete.

3.2.7 Compressive strength

The compressive strength of concrete cubes having dimensions of $100 \times 100 \times 100 \text{ mm}^3$, were determined after 1, 3, 7, 14, and 28 days of casting. The loading rate was constant and set at 10 kN/s . For every curing period of -15°C , the samples were taken out of the refrigerator at three different time intervals and tested i.e., directly for testing at 0 hours (instant), 12 hour-before testing (12h/bf) and 24 hour-before testing (24h/bf). During the waiting period, the concrete samples were kept at room temperature until the test.

Composite concretes made of UHPC and NSC were cast as cubes having dimensions of $150 \times 150 \times 150 \text{ mm}^3$. The compressive strength was determined after 7 and 28 days of casting the UHPC layer over the substrate element. The loading rate was set to 13.5 kN/s . The reference NSC cubes of $150 \times 150 \times 150 \text{ mm}^3$ were tested on the same day as the composite UHPC-NSC concrete samples. Note: The substrate concrete and the NSC-only sample were of the same age at the time of testing. Figure 10 shows the preparation scheme for composite concretes. After

producing the NSC cube that was used later as a substrate for casting UHPC, the specimens were stored in laboratory conditions for three months. One month before casting the UHPC overlay, the external surfaces were water-jetted. The UHPC overlay thickness was 1.5 cm covering all the surfaces of the cube, except the top and bottom surfaces.

The compressive strength for all concrete specimens was determined using Toni Technik compression testing machine following the SS-EN 12390-3:2019 standard, Figure 11, [176].

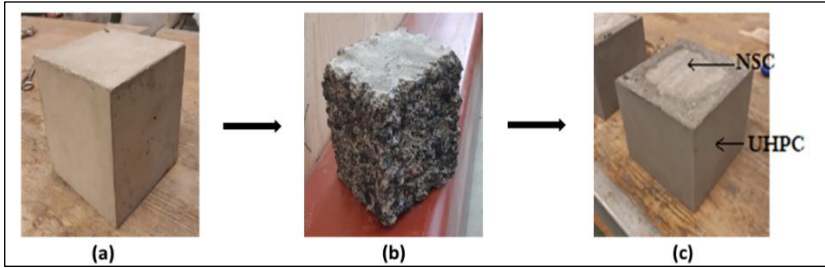


Figure 10: Scheme of UHPC-NSC cube specimen preparation (a) NSC cubes; (b) water jetting; (c) casting UHPC overlay.



Figure 11: Compressive strength testing machine.

3.2.8 Ultrasonic pulse velocity (UPV)

The ultrasonic pulse velocity (UPV) test was performed to detect either internal cracking, debonding between layers of new and old concrete, and/or ice formation within the binder matrix of the concrete. Pundit Lab ultrasonic instrument (Proceq, Zurich, Switzerland) with exponential transducers at 54 kHz was used. To analyze the transit time, the direct transmission method was used following the SS-EN 12504-4:2004 standard [177].

In the case of concrete cubes cured at -15°C , the test was performed on 1-day and 28-day-old samples and having a measuring path length of 100 mm. The transit time was measured at different time intervals i.e., immediately after removal from the refrigerator (instant), 6 hours-

after (6 h/af), 12 hours-after (12 h/af), 18 hours-after (18 h/af) and 24 hours-after (24 h/af). The samples were stored at room temperature during the waiting period.

The test was also performed on a large-scale UHPC-NSC column having dimensions of 360x360x2500 mm³ after 288 days of casting the UHPC layer. The measuring path length was limited to 360 mm. The measuring sequence was different compared to the concrete cubes. The column was prepared in the same way as for the UHPC-NSC cubes Figure 12. However, the UHPC overlay thickness was set to 3 cm. Measurements were performed on Red A-A1 and Blue B-B1 nodes of the grid formed on the surface of the column, Figure 13. The transit time was recorded for every 100 mm from the center (0 mm) up to 1000 mm in either direction (i.e., top and bottom). Furthermore, the readings were separated into top, middle, and bottom sections as per column level. In both cases, three consecutive readings were done without lifting the transducers.

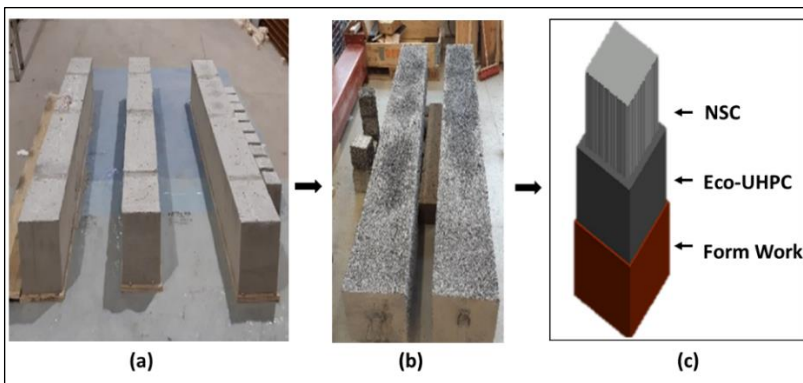


Figure 12: UHPC-NSC column specimen preparation (a) NSC columns; (b) water jetting; (c) schematic model of the repair/rehabilitated column.

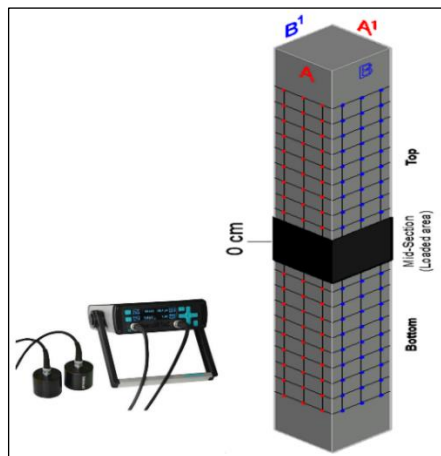


Figure 13: Ultrasonic Pulse Velocity (UPV) measurement nodes for UHPC-NSC column - Red (A-A'), Blue (B-B').

3.2.9 Bond test

The bond test between NSC and UHPC was evaluated in columns having dimensions of 360x360x2500 mm³, 28 days after casting the UHPC overlay. The main aim was to measure the interfacial bond strength between the substrate NSC concrete and the UHPC overlay. This is a common method enabling the avoidance of friction between interfacial surfaces and other types of stresses [26,178]. ASTM C1583 standard was followed, [179]. The test was carried out using commercially available "Proceq dy-216" equipment with a 50 mm aluminum disc and at a loading rate of 35 kPa/s. Using a 50 mm diameter drill core, in depth of 60 mm deep core was drilled, inclusive of 30 mm depth of substrate layer. In total three sides of the column (A, B, and C) were assessed, with 6 tests per side, i.e., three at the top and three at the bottom Figure 14. The bond strength was calculated using Eq 1.

$$f_p = \frac{4F}{\pi d^2} \text{ MPa} \quad \text{Eq(1)}$$

where: f_p = bond (pull-off) strength (MPa); F = failure load (N); d = the core diameter (mm).

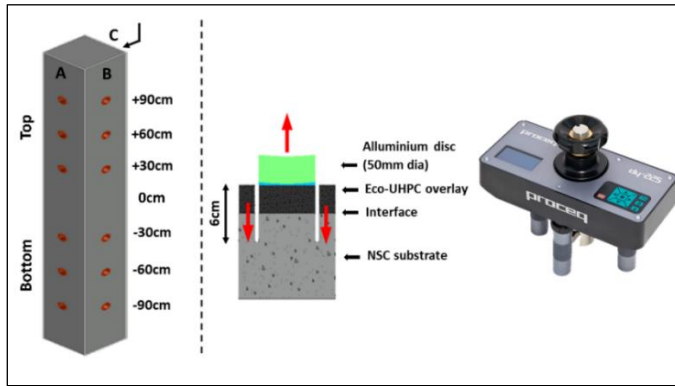


Figure 14: Bond test locations on the column (marked in red) and schematic representation of a cross-section of the drilled core.

Based on the visual observation of the bond failure, its failure mode was categorized as shown in Table 14. Additionally, the failure mode was verified using SEM images analyzed with Image processing techniques on fractured core samples. The FIJI ImageJ software (Version 1.53C) was used for the analysis and the calculation was performed on the binarized image of the core surface, showing UHPC as black pixels and NSC as white pixels [180].

Table 14: Pull-off test bond failure modes.

ID	Bond Failure Mode	Fraction of residue (%) on detached
SBF	Substrate failure	85-100% NSC
OF	Overlay failure	100% UHPC
IF	Interface failure	0% NSC (no fracture surface)
PISF	Partial interface-substrate failure	1-85% NSC

3.2.10 *Microstructure – SEM-EDS*

The microstructure and phase composition were analyzed using a Scanning Electron Microscope (SEM)—JSM-IT100 (JEOL Ltd, Tokyo, Japan) coupled with an energy-dispersive X-ray spectrometer (EDS) from Bruker (Bruker Corporation, Billerica, MA, USA), Figure 15. Small concrete samples having a volume of 15 to 18 mm³ were taken from the core or the interface. These samples were immersed in isopropanol for 24 hours to stop the hydration and then dried for another 24 hours in a vacuum chamber. Dried samples were impregnated with a low-viscosity epoxy resin under vacuum. After hardening, all samples were polished using diamond spray with particle sizes ranging from 9, 3, and 1 μm. Lamp oil was used as a lubricant and coolant, [181].

The SEM analysis was performed with the following parameters: backscattered electron (BSE) detector for images, 15 kV electron beam accelerating voltage, 50 mA electron beam current, chamber vacuum of 30 Pa, and 50,000 counts per analysis for the SEM-EDS data points. The EDS analysis was performed on areas occupied predominantly by the calcium silicate hydrate (C-S-H). These areas were selected based on the grey-level histograms of the BSE images, [181,182]. Unhydrated cement and porosity were segregated from images based on the greyscale histograms and quantitatively analyzed using the ImageJ software, [180].

Concrete samples cured at -15°C were analyzed 3 and 28 days after casting. Before preparing the macro samples for SEM analysis, concrete cubes were removed from the refrigerator and held at room temperature additionally for at 0 hours (instant), 12 hour-before (12 h/bf), and 24 hour-before (24 h/bf) respectively and followed by core extraction and isopropanol immersion and epoxy impregnation. The SEM-BSE Images were taken at a magnification of 500x [183,184], and 1000x magnification. The EDX analysis was done using images taken at 1000x magnification.

The SEM analysis of UHPC-NSC concrete was performed on 28-day-old samples at magnifications of 150x, 2000x, and 5000x. The aim was to determine variations of phase composition with an increasing distance from the interface, [183,185]. Images with 5000x magnification were used for the EDS analysis. Analysis was done in the interface between exposed old aggregate and UHPC, and between the old binder and UHPC.

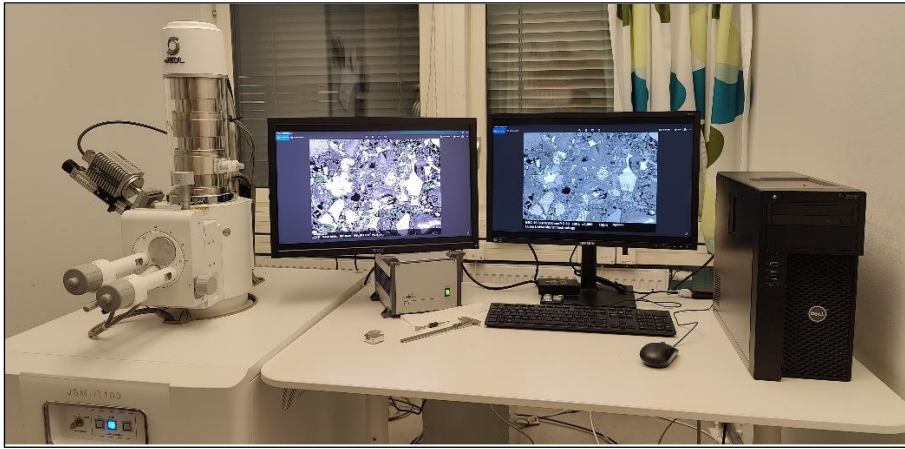


Figure 15: Scanning Electron Microscope - Energy-dispersive X-ray spectrometer (SEM-EDS) used in this study.

4. Results and discussions

The results and discussions are divided into two parts. The first section 4.1 addresses the studies that focused on the effects of subfreezing curing temperatures on the performance of low PC content systems. The second section 4.2 addresses results obtained from additional studies that verified the performance of composite elements composed of NSC and UHPC.

4.1 Low Portland cement content binders at low temperatures

The first, and the main part of this PhD research was to study the performance of fresh and young concretes having a low PC content and significant amounts of GGBFS and CSA cement at subfreezing temperatures. The work has been divided into two stages.

The first stage included an initial study that aimed to assess the effects of various curing temperatures on the performance of PC-GGBFS concretes. Compressive strength and temperature developments were recorded.

The second stage of this study consisted of extensive tests performed on systems containing various combinations of PC, GGBFS, CSA cement and chemical admixtures. The aim was to determine the effects of curing temperature on several key parameters, i.e., ice formation, hydration temperature, strength development, microstructure, etc.

4.1.1 PC-GGBFS

The study started with the determination of the effects of curing temperature on the development of the compressive strength and hydration temperature of concretes based on Portland cement replaced by 50% of GGBFS. Concrete samples were cured at 20°C, 5°C, 0°C, and -5°C. Except for 0°C and -5°C, the concrete samples were placed in the curing water baths having temperatures of 20°C and 5°C immediately after casting. In contrast, samples cured at -5°C and 0°C were stored at ambient room temperature for the first 24 hours before being placed in a refrigerator at the temperatures of 0°C and -5°C. This curing sequence replicated conditions that could occur during winter casting. The development of the hydration temperature was assessed using a semi-adiabatic calorimeter. Two types of concrete were tested: 100 wt.% Anläggningcement (ANL) and 50 wt.% Anläggningcement with 50 wt.% of GGBFS (ANL: GGBFS). Only superplasticizer was used as a chemical admixture.

Figure 16 and Figure 17 shows the strength development of concrete at different curing temperature and hydration temperature development respectively. The compressive strength of concretes containing 50 wt.% of GGBFS was generally lower, independently of the curing temperature, which complies with previous test results and common knowledge. The most interesting observation from this part of the research work is the high strength values of the ANL (100) concrete that was cured at a constant temperature of 5°C. Up to 5 days, the strength was lower in comparison with mixes cured at other temperatures. However, later the strength increased and was the highest after 7 and 28 days even in comparison with the concrete that was continuously cured at 20°C. On contrary, development of the compressive strength was different for concrete containing 50 wt.% of GGBFS. Here the highest overall values were reached for mix that was continuously cured at 20°C. The 28-day compressive strength for

mixes cured at that temperature was very similar even despite replacing 50 wt.% of PC with GGBFS and reaching around 50 MPa.

The effect of lower curing temperatures, i.e., 5°C, 0°C, and -5°C, even with initial 24 h curing at 20°C for samples later cured at -5°C and 0°C, was significantly stronger. All concrete samples made of 100 wt.% of PC reached the ultimate 28-day compressive strength values close to the reference cured at 20°C. On the contrary, concrete samples containing 50 wt.% of GGBFS reached only around 30 MPa. The observed strength is related to a lower hydration rate which is also seen on the hydration temperature plot, Figure 17, [186–189]. The maximum recorded temperature decreased from nearly 50°C to just about 30°C for mixes with GGBFS. These results indicate that the application of a larger amount of GGBFS in concrete exposed to subfreezing temperature can be problematic even despite the initial curing for the first 24 hours at 20°C. Others observed similar trends. For example, mixes containing 50 wt.% of GGBFS cured at 10°C, showed a 64% decline in strength compared to 100% PC concrete [186,190]. Producing concrete with no chemical antifreeze admixtures for cold regions are of high susceptible of pore ice formation at constant freezing temperatures could therefore be a challenging issue. Thus, by employing different kinds of chemical admixtures, the composition of the concrete mix (irrespective of the binder type) could be altered to produce higher hydration temperatures and decrease the freezing point of water, [2,14,15].

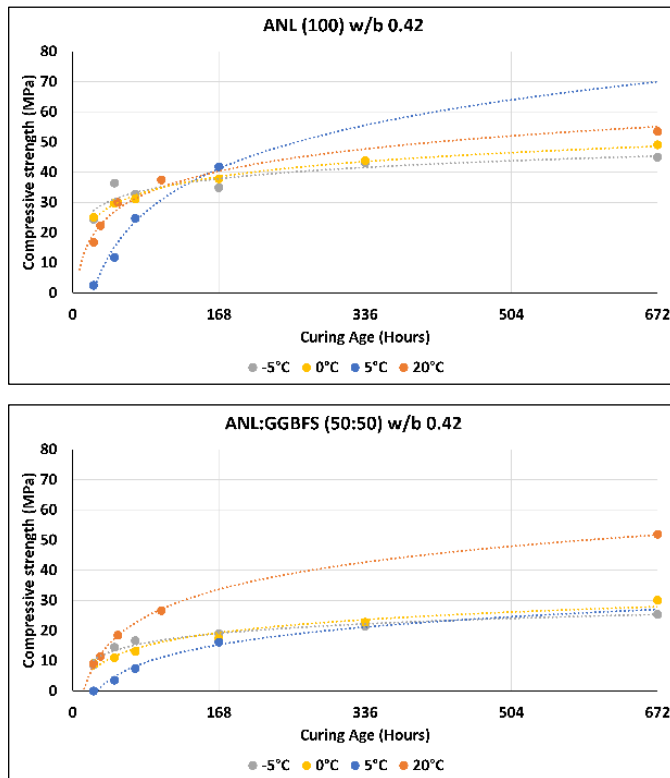


Figure 16: Compressive strength gain of concrete cubes cured at 20°C, 5°C, 0°C and -5°C.

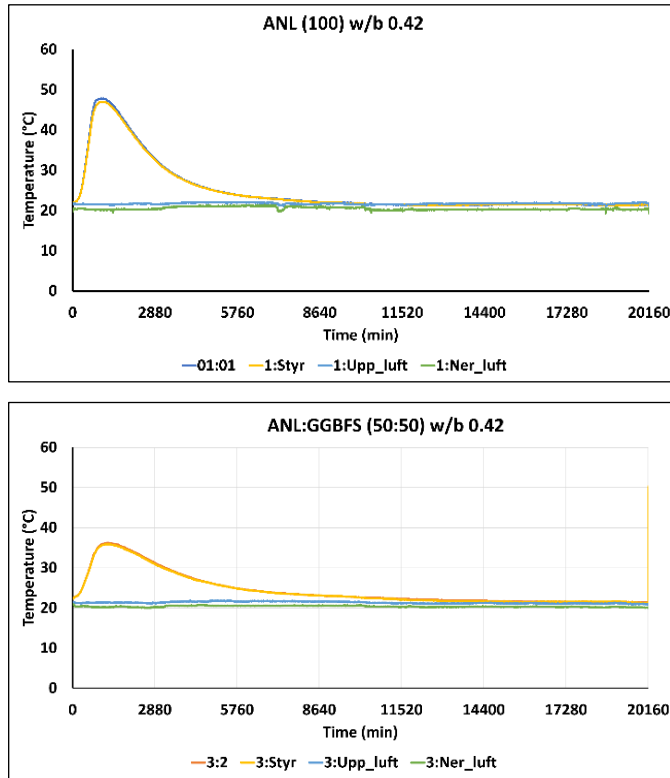


Figure 17: Hydration temperature development.

4.1.2 PC-GGBFS-CSA systems

Based on initial test results presented in section 4.1.1, it appears that producing concrete based on PC with a high amount of GGBFS used as SCM requires the application of additional means to support the hydration process. This could include either heating or chemical admixtures. The following part of this research focuses on diminishing the negative effects of low-temperature curing on concretes containing PC, GGBFS, and CSA.

4.1.2.1 Phase transitioning (Liquid ↔ Slush ↔ Ice)

The first stage included a study on the effects of sodium nitrate on the phase-transitioning temperatures of various binders with reduced PC content. Tests were divided into systems comprising only water with sodium nitrate and binder pastes with sodium nitrate.

- Effects of sodium nitrate on the phase transition of water

In general, bulk solutions are susceptible to freezing earlier than the same solutions present in the concrete binder matrix due to the vapor pressure [19,36,37]. The main function of the antifreeze admixture is to lower the freezing point of water and to enable continued hydration.

This research aimed to enable hydration at -15°C . The visual phase transitioning times to slush/ice, recorded at this temperature are shown in Figure 18.

The results showed that a higher concentration of antifreeze admixture extended the duration of phase change from liquid to slush and ice. This delay correlates directly with the diminishing quantity of freezable water. Furthermore, each molecule of the antifreeze admixture operates as a molecular shield, impeding the rupture of intermolecular bonds among water molecules and constrain the crystallization of ice. The results showed that the sodium nitrate antifreeze dosage of up to 15 wt.%, did not prevent the formation of ice when exposed to a constant temperature of -15°C . The solution transitioned to a slush state 3 hours after placement. After another 2 hours, the slush transitioned to a thick ice lens. On the contrary, an antifreeze dosage of 25 wt.% initiated transitioning to slush after 48 hours and maintained that state even after 168 hours with only a few ice lenses forming, see the red square in Figure 18. Thus, this amount of sodium nitrate prolonged the hydration without the need for additional heating. Solutions containing 30 wt.% of the antifreeze admixture retained their liquid state even after 168 hours of exposure to -15°C , see the green triangle in Figure 18. This could be inferred to the segregation of ions with high concentration of solid sodium nitrate content present in antifreeze admixture limited the transitions [56].

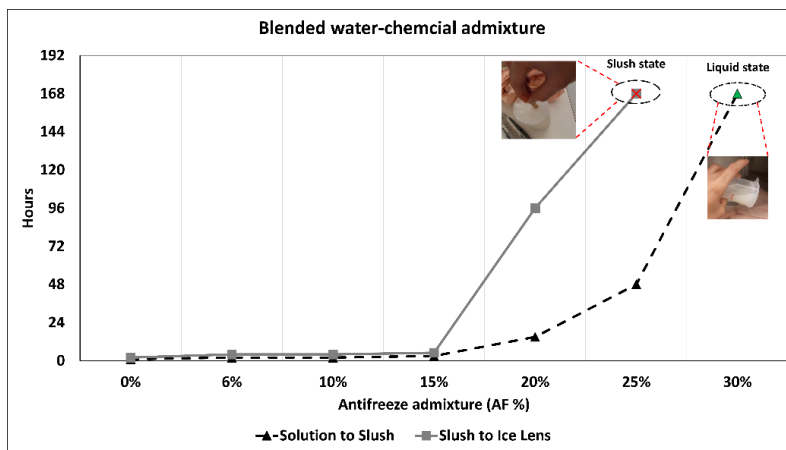


Figure 18: Visual observation of the phase transitioning time. The point marked as “slush state – red square” denotes solution transitioned and retained to slush; and “liquid state – green triangle” denotes no transition of solution into ice.

- Effects of sodium nitrate on phase transition of binder pastes

Several paste samples listed in Table 11 were tested using DSC to determine the phase transitioning temperature of the paste pore solution to ice. The DSC curves consist of an exothermic peak on freezing and an endothermic peak on thawing, [38]. Using the eutectic point of the used chemical admixtures and/ or mineral based accelerators the freezing point of an aqueous solution can be determined, [12][46]. However, due to the fusion of the interacting components, estimating the eutectic temperature for pastes is complicated. During freezing and thawing processes, pastes containing different amounts of antifreeze admixtures or the CSA-based mineral accelerator showed a significant energy release, resulting in a single dominant

peak on the DSC that correlated to the cluster of the same pore size Figure 19 and Figure 20. Similar results were also observed by others, [9]. Furthermore, the mass of the sample and the rate of heat transfer (enthalpy change) have an impact on the measured heat flow peaks (mW), [37]. However, it was also reported that the sample mass has only a minor influence on the phase transitions [191]. The test used paste samples weighing on average 15 mg.

The first exo-peak was observed at around -12°C for PC:GGBFS:CSA (50:50:0) with no added AF admixture. This low freezing temperature could be attributed to the presence of dissolved ions originating from PC and GGBFS which altered the kinetics of the pore solution [34–36]. Pastes containing over 15 wt.% of AF showed further delayed ice formation and the formation of two DSC peaks. The first peak corresponded to the initiation of the pore ice crystallization, while the second peak to the freezing of the confined isolated pores due to the supercooling temperature [37,192]. Zhang et al. (2020) observed ongoing hydration and formation of a dense binder matrix during the cooling stage but still before reaching the freezing temperature [19]. Mix PC:GGBFS:CSA (50:50:0) with 20 wt.% and 25 wt.% of AF significantly depressed the freezing point to around -29°C . The mix PC:GGBFS:CSA (50:50:0) containing 30 wt.% of AF admixture showed first pore ice crystallization at around -22°C . This result could be explained by the theory of thermodynamics and redistribution of pore solutions due to the high concentration of ions [37,193]. High concentrations tend to segregate the ions from inducing an aqueous path between the pores (smaller and larger) causing an ice front to penetrate and freeze with high internal hydraulic pressure [37,194].

In the present study the depressed freezing temperature in all cases are associated with the dissolved ionic concentration in the pore solution. The latter “concentration effect” results in the decreased pore radius and enhanced network structure, according to the Raoult’s law and Clausius-Clapeyron relation, [19]. Generally, the pore solution present in larger pores freezes faster, whereas, in smaller pores, the vapor pressure is increased which depresses the freezing point, [41,42]. Both reference paste mixes PC (100%) and CSA (100%), showed freezing at around -14°C . Mixes containing 80 wt.% PC and 20 wt.% CSA cement showed a slightly lower freezing temperature at around -15°C . The addition of CSA cement caused the formation of additional ettringite which could absorb some pore solution. This could lead to an increased concentration of ions thus limiting the ice formation, [19,124]. Other studies showed that replacing <10 wt.% of PC with CSA cement has adversely affected the hydration of systems exposed to freezing temperatures. This led to the formation of coarser microstructure and worse frost durability, [19].

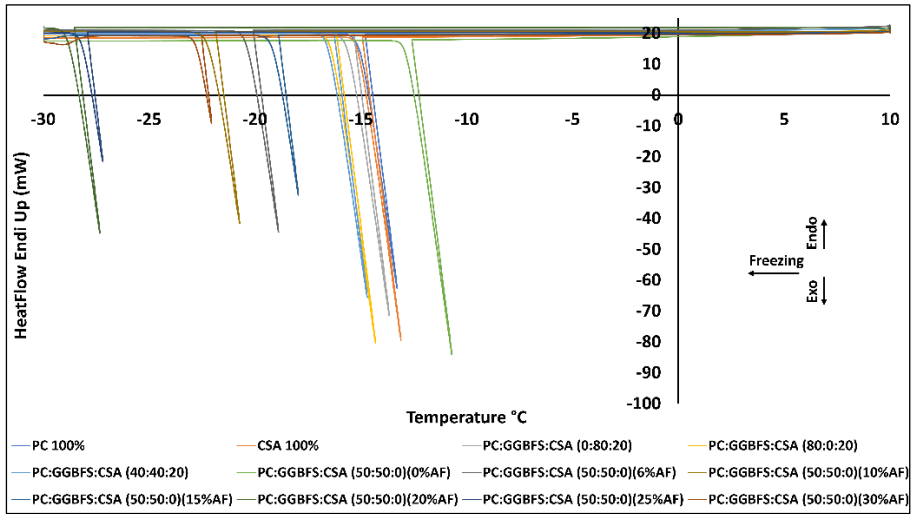


Figure 19: Exothermic heat flow of the pure PC, CSA, and PC:GGBFS:CSA pastes. The freezing rate was $1^{\circ}\text{C}/\text{min}$.

During the thawing process, from -30°C to $+10^{\circ}\text{C}$, the formation of an endothermic peak was observed at different temperatures corresponding to the energy absorption of the formed pore ice Figure 20. Paste PC:GGBFS:CSA (50:50:0) with no chemical admixture (0 wt.% AF) showed a well-defined peak at 0°C , [37,195]. Pastes containing AF admixture showed the formation of two peaks. The position of these peaks corresponded to the geometry of the pore system, and dissolved ion concentration [9,40]. Pastes containing >20 wt.% of AF, showed initial melting peaks at around -20°C , and at -10°C when less than 15 wt.% of the AF was used. The energy absorbed during thawing was lower and showed less variation with the amount of AF. This trend could be related to the earlier initiation of the melting process. The pastes containing 20 wt.% and 25 wt.% of AF absorbed the lowest amount of energy to initiate the breaking of bonds between ice molecules and cause the phase transition. Interestingly, pastes containing <20 wt.% and >25 wt.% of the AF, absorbed more heat energy to initiate the melting process. All pastes containing CSA showed a dominant endothermic peak just after 0°C and a shoulder before it. According to previous research, the early peak generated during melting refers to the melting of ice formed in finer pores, and the later peak, to melting in larger pores, [9,196,197]. The melting of ice is a continuous process, which is limited at very low temperatures, [38,198]. The presence of AF limited the difference in the amount of heat expelled during freezing and heat absorbed during thawing [37,38].

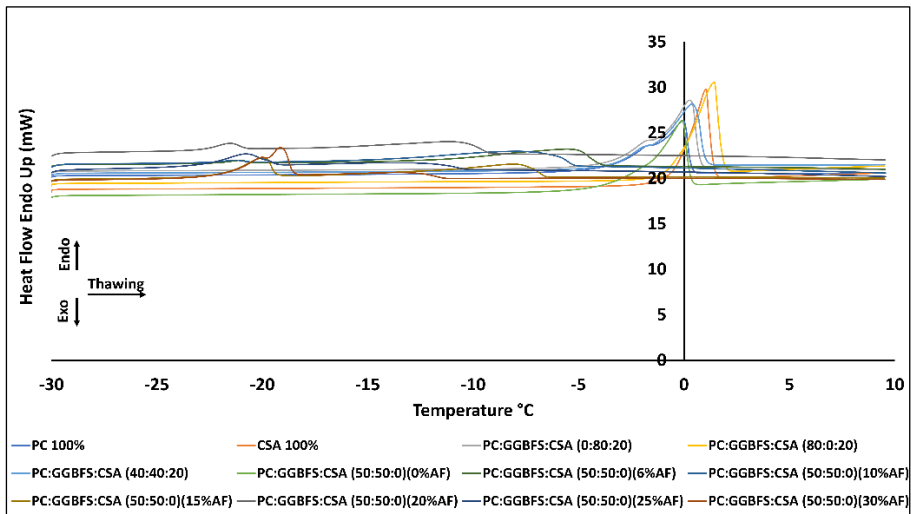


Figure 20: Endothermic heat flow of the pure PC, CSA, and PC:GGBFS:CSA pastes. The thawing rate was 1°C/min.

4.1.2.2 Development of temperature due to hydration

The hydration temperature development was measured using a simple semi-adiabatic setup on the following pastes: reference pastes, pastes containing CSA, and pastes containing 6 wt.% and 25 wt.% of AF admixtures, Table 11. The tested mixes were chosen based on the DSC test results and the obtained results are shown in Figure 21.

The length of the induction period was ~250 min for the reference PC and 140 min for the CSA cement. The initial temperature peak observed for the CSA cement can be related to the rapid breakdown of gypsum and Ye'elinite, resulting in the formation of ettringite and amorphous AH₃. After 30 min of the induction period, a second exothermic peak evolved, which is associated with the synthesis of ettringite and the fast hydration of ye'elinite [199,200]. The main hydration peaks for PC and CSA cement were detected after 360 min and 240 min respectively. The current setup enabled the first reading of the temperature only 5 min after mixing, thus preventing the detection of early-age hydration peaks. It was also impossible to detect the third peak at later ages, which has been related by others to the crystallization of ettringite [200].

Earlier research studies showed the formation of three distinctive hydration peaks of conventional CSA cement i.e., multistage acceleration-deceleration-acceleration. These stages were related to the ye'elinite hydration and the repeated development of ettringite. The concentration of sulfate diminished over time, [199,201]. On the contrary, the studied CSA cement showed a longer induction period, which was presumably related to the 25 wt.% content of belite. It delayed the early age reaction which was followed by a temperature increase due to the formation of more ettringite and strätlingite, [202].

In general, the composite binder systems containing PC and ≥ 10 wt.% of the CSA cement showed more intensive initial reactions and shorter induction periods [125,137]. This was

caused by faster precipitation of ettringite and accelerated dissolution of alkali-sulfate phases due to the high concentration of K, Na, and sulfates. Based on earlier results it can be assumed that the calcium and sulfate concentrations were steady for the first several hours and then began to decline sharply as the gypsum disappeared. An equilibrium between the formation of the C-S-H and AFt phases is achieved, [125,137].

Replacement of PC by 20 wt.% CSA shortened the induction period and resulted in lower hydration temperature compared to pure PC, Figure 21. Similar results were obtained by others, [19]. The pastes PC:GGBFS:CSA (80:0:20), PC:GGBFS:CSA (40:40:20), and PC:GGBFS:CSA (50:50:0)(25%AF) had a short induction period of 9 minutes, 8 minutes, and 25 minutes, respectively. This is related to the faster dissolution, the partial hydration of gypsum and ye'elimite, and the formation of ettringite and amorphous AH₃ [137,199,200]. Furthermore, sulphates and calcium hydroxide derived from PC, another factor to contribute PC-CSA hydration rate, [126,137,138]. Additionally, a shallow peak corresponding to the formation of AFm was also discovered in the PC-CSA pastes at a later age. This could be related to the binding of gypsum sulfates to C₃A, [203]. Other researchers assumed that it could also be related to the decelerated hydration rate of C₃S. With the increased CSA content a simultaneous precipitation of calcium aluminate and ettringite causes faster consumption of water, which in turn could delay the nucleation of C-S-H, [19,204]. Furthermore, the developed lower hydration temperature compared to the pure PC system could be also related to the sulfates present in the CSA cement. The used CSA cement contained 10 wt.% of anhydrite and >60 wt.% of ye'elimite. Which is significantly lower in comparison with CSA cements studied by others. For example, CSA cement tested by Le Saoût et al., (2013) contained 47.7 wt.% of anhydrite and only 22.5 wt.% of ye'elimite [137]. Thus, they needed a larger proportion of CSA to enhance the hydration process in comparison with the reference PC. Sulfates impact the hydration of CSA by regulating the reaction of ye'elimite with water and the subsequent development of AFt and AFm phases, [205,206].

The PC:GGBFS:CSA (0:80:20) binder developed a very low maximum hydration temperature of just 40°C, Figure 21. The ye'elimite was replaced by GGBFS which limited the continuous hydration of CSA cement and the predomination of ettringite, [120]. Similar research showed that decreased formation of AFt, AFm, and AH₃ phases in systems with higher content of GGBFS (>30 wt%) can be linked to the dilution effect and low reactivity, [120,142,143]. The PC:GGBFS:CSA – 50:50:0 binders containing 0 wt.% and 6 wt.% AF admixtures showed a delayed hydration peak compared to other tested binders. The delay corresponded to the absence of CSA and the slow reactivity of slag. On the contrary, the same mix but with 25 wt.% of AF admixture showed the main hydration peak, earlier at 60-65 min. This could be related to the higher amount of sodium nitrate which presumably accelerated the C₃S reaction, [207].

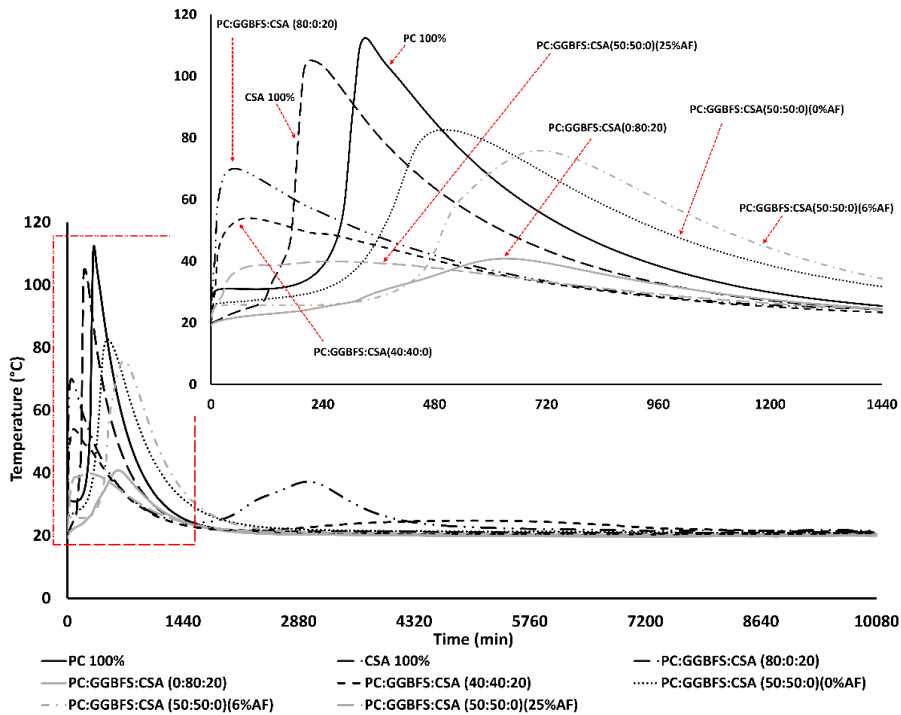


Figure 21: The development of the hydration temperature of pastes containing PC, CSA, and a mix of PC:GGBFS:CSA.

4.1.2.3 Setting time

The setting time test results for pastes are shown, Figure 22. CSA cements typically have shorter setting times than PCs and can be used as accelerators in PC-based concretes, [16]. The reference mixes containing 100 wt.% of PC and 100 wt.% of CSA cement showed the initial setting times of 80 min and 31 min respectively. The final setting times were 530 min and 605 min, respectively. The mixes PC:GGBFS:CSA – 80:0:20 and PC:GGBFS:CSA – 40:40:20 had the initial setting time of 9 min and 7 min, respectively. The shorter times can be attributed to the fast hydration rate of CSA's - ye'elinite and gypsum, ettringite formation, and the early age moisture loss leading to the rapid loss of plasticity, [125]. Additionally, based on earlier results, gypsum and calcium hydroxide from PC could have further supported the hydration of CSA, [126,138].

On the contrary, the partial replacement of GGBFS by 20 wt.% of CSA showed the initial setting after 70 minutes. These results are comparable with mixes containing 100% PC. Despite the slow reaction of the GGBFS, the addition of the CSA cement stimulated the hydration reaction at a very early age. Others observed the formation of ettringite (AFt), monosulphate (AFm), $Al(OH)_3$, and strätlingite, [120]. At the same time, the final setting time has been delayed to 1227 min. This could be attributed to the excess of the GGBFS which induced the dilution effect, and limited the amount of formed AFt and AFm phases, [120,143]. The PC:GGBFS (50:50) with neither containing chemical admixtures nor the CSA cement showed

the initial setting times delayed to 323 minutes. This could be explained by the presence of the GGBFS and slower hydration of the PC. In contrast, the addition of synthetic C-S-H shortened the initial and final setting times, [208,209].

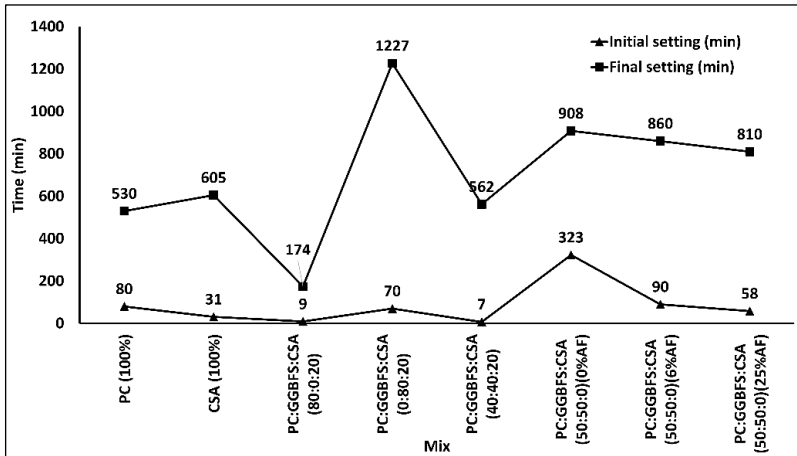


Figure 22: Initial and final setting times of pastes based on PC, CSA, and mix of PC:GGBFS:CSA.

4.1.2.4 Workability.

The workability of the fresh concrete was determined by measuring the slump immediately after mixing, Figure 23. The reference PC showed the lowest slump of all the studied concrete mixes i.e., 3 cm. The maximum slump of 20 cm was observed for mix PC:GGBFS:CSA – 50:50:0 incorporating 25 wt.% of AF. On the contrary, a similar mix containing 50 wt.% of PC and 50 wt.% of GGBFS, with 0% AF and 6% AF had a slump lower than the same mix but incorporating 25 wt.% of AF. Further, the test concretes PC:GGBFS:CSA – 80:0:20 and PC:GGBFS:CSA – 0:80:20 had a lower slump of 4 cm and 5 cm, respectively. This could be attributed to the CSA stimulating the formation of ettringite crystals at a very early age. Less available free water and more strätlingite formation in systems with higher GGBFS content could contribute to the lower workability, [120,137,141]. Despite similar CSA dosage, the mix PC:GGBFS:CSA (40:40:20) showed a higher slump of 13 cm. The final measured slump was a result of several, often contradicting factors. For example, calcium sulfate and calcium hydroxide from PC could accelerate the hydration of CSA at a very early age. However, the GGBFS could control the availability of calcium sulfate and its acceleratory effect, [202]. Additionally, the lower reactivity of GGBFS and its coarser particle size could enhance the workability, [210].

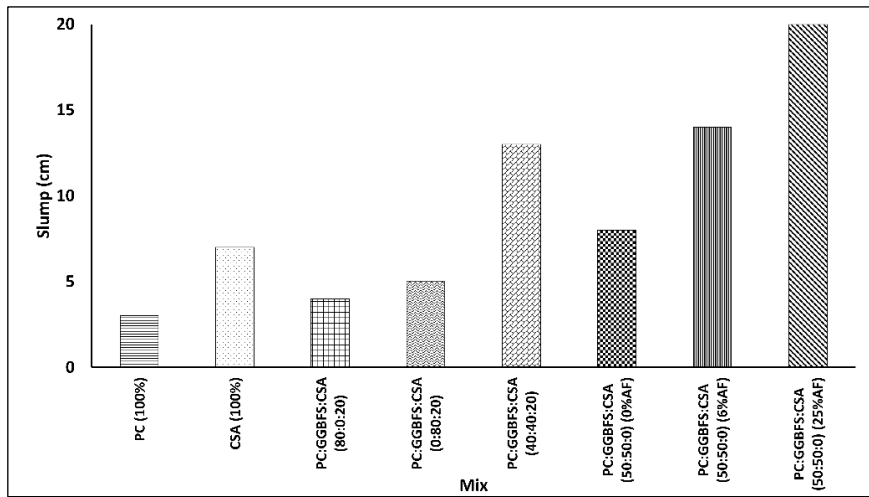


Figure 23: Concrete slump measured immediately after mixing concrete.

4.1.2.5 Early age compressive strength of concretes cured at ambient temperature.

The highest 1-day compressive strength of 42 MPa was developed by reference PC (100%), CSA (100%), and PC:GGBFS:CSA (80:0:20), Figure 24. While mixes containing major proportion GGBFS i.e., PC:GGBFS:CSA (0:80:20) showed the lowest strength of all mixes, ranging between 6 MPa to 7 MPa, irrespective of the curing age. These results are similar to previous earlier published data showing the degradation of physiochemical properties of CSA types of cement due to the presence of GGBFS, [120,211–213]. The decreased strength could be related to the dilution effect and low reactivity of GGBFS. Additionally, the mix containing >30 wt.% of GGBFS other observed a limited formation of ettringite, strätlingite phase, and increased porosity and total voids, [143,188,214]. Conversely, GGBFS replacement level ≤ 30 wt.% with CSA concrete can achieve strength values that are comparable with mixes containing only CSA cement, [120]. Ettringite, monosulfate, strätlingite, and AH_3 were recognized as the main hydration phases that formation leads to denser concrete microstructure, [120].

It can be assumed that the PC:GGBFS:CSA (80:0:20) mixes are characterized by the formation of AFt phases along with more C-S-H / C_2ASH_8 and Portlandite, even though the used CSA cement contained 25 wt.% of belite (C_2S), ye'elinite ($C_4A_3\hat{S}$) content >60 wt.% and calcium sulfate ($C\hat{S}$) 10 wt.%, [134,205]. Several studies found that belite present in CSA resulted in the formation of only strätlingite after 7 days of curing, [202,215]. The PC:GGBFS:CSA - (80:0:20) mix had reduced strength at all ages except for day 1 when compared to the CSA (100%) concrete, Figure 24. At 3 days, the strength difference was 12.84%, and at 7 days, 10%. This could be related to the co-existence of two types of cement and the resulting quick ettringite crystal formation, the high early age strength could be related to the rapid dissolution and accelerated hydration rate [125]. Nevertheless, the formation of microcracks due to the overlapping ettringite on the C-S-H particles over time has a negative influence on the microstructure, [125,134].

Similar strength values were observed for mixes of the PC:GGBFS:CSA (50:50:0) containing 25 wt.% AF and the PC:GGBFS:CSA (40:40:20). In both mixes the dosage of chemical admixtures and CSA cement were the key elements for synergistic hydration reaction and increased strength gain. After 1 day of curing the strength reached almost 18 MPa and 37 MPa after 7 days, Figure 24. The mix PC:GGBFS:CSA (50:50:0) but without AF or with just only 6 wt.% AF showed very low strength values. However, GGBFS used as a partial replacement of PC reacts with $\text{Ca}(\text{OH})_2$ to produce more C-S-H. The used synthetic C-S-H seeds accelerated additional hydration and early strength development. Furthermore, ye'elimite, alite, belite, and anhydrite were added to the system by CSA cement and additionally impacted the result. For example, overlapping crystals of ettringite, strätlingite, monosulphate, and AH_3 could increase the early age strength. Others observed improved durability, [213]. The GGBFS alone could increase the matrix cohesion and densify the microstructure, [131].

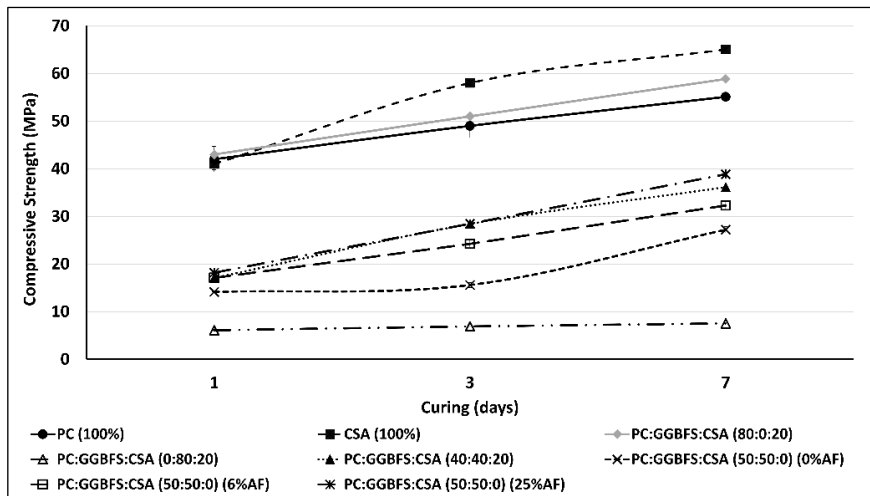


Figure 24: Early age - 7 days compressive strength development of concretes cubes cured at ambient room temperature.

4.1.2.6 Compressive strength development of concretes cured at -15°C .

The development of the compressive strength for concrete mixes PC:GGBFS:CSA – 40:40:20, PC:GGBFS:CSA – 50:50:0 (6% AF), and PC:GGBFS:CSA – 50:50:0 (25% AF) cured at a constant temperature of -15°C , is shown in Figure 25, Figure 26, Figure 27. Samples were removed from the refrigerator and tested either immediately (instant), 12 hours before testing (12h/bf), or 24 hours before testing (24h/bf). During the waiting period, the concrete samples were stored at room temperature.

Generally, concrete mixes containing 25 wt.% of AF admixture developed higher compressive strength values in comparison with samples containing 6 wt.% of AF and 20 wt.% of the CSA cement. Furthermore, concrete samples containing 25 wt.% of the AF admixtures tended to show a reduced difference between the compressive strength measured immediately after removal from the freezer vs when measured on samples additionally stored at room temperature for 12 hours, Figure 25 and Figure 26 respectively.

The concrete samples containing 6 wt.% of the AF admixture and 20 wt.% of the CSA cement and tested immediately after removal from the freezer reached the one-day strength of 7.4 MPa and 12.3 MPa. The concrete containing 25 wt.% of the AF admixture showed no strength development, Figure 25. The observed strength could be related to the initial hydration of the CSA cement, and the formation of ettringite, [19], but mostly to the ice formation and thus could be classified as a false strength. An earlier study showed that, at a constant freezing temperature, the concentration and strength of ice lenses increase linearly [216]. Consequently, an internal pressure on the binder matrix is created which results in microcracking of the formed binder matrix and thus a lower ultimate strength, [34,44,45].

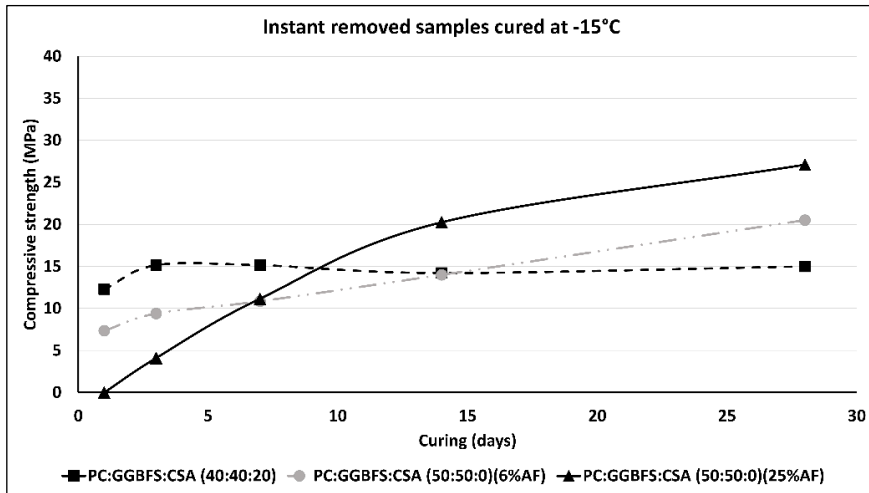


Figure 25: The compressive strength development of samples tested immediately after removal from curing at -15°C.

Samples cured for 12 hours after their removal from the freezer showed a linear increase of compressive strength at all ages only when 25 wt.% of AF admixture was used, Figure 26. The concrete mix containing 20 wt.% of the CSA cement showed a constant strength value. The mix containing 6 wt.% of the AF admixture showed variable values over the measured period of 28 days with an average of no significant increase. The reasons, as described also earlier can be related to the formation of ice, damage to the binder matrix, and limited hydration.

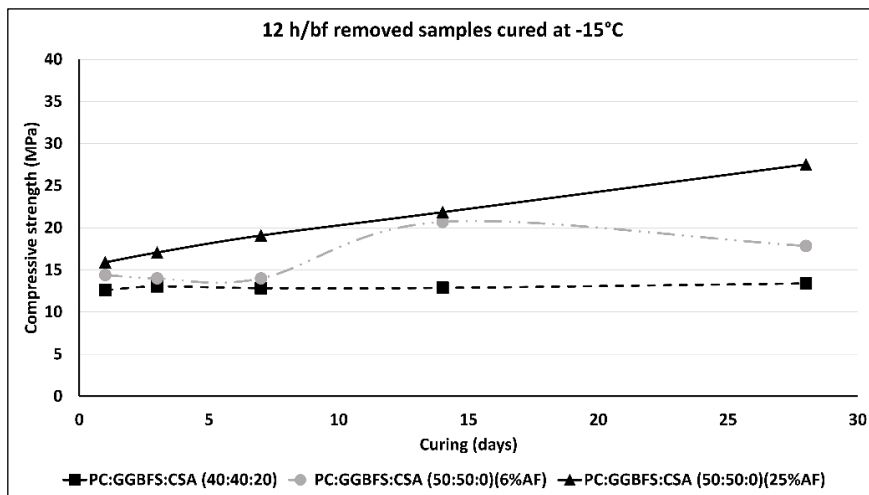


Figure 26: The compressive strength development of samples tested after 12 hours of curing at room temperature after their removal from -15°C.

The compressive strength of samples that were cured for 24 hours in room conditions after their removal from the freezer is shown in Figure 27. Concrete containing 25 wt.% of the AF admixture and additionally cured at room temperature for 24 hours reached 35 MPa after 28 days. This result further confirms that the high dosage of the AF admixture prevented the excessive formation of ice that would lead to the permanent damage of the binder matrix. At the same time, concrete containing 20 wt.% of the CSA cement showed regression of the compressive strength with age. The strength value decreased from the initial 20 MPa measured after 1 day to around 17 MPa measured after 28 days. The additional curing at room temperature did not enhance this value. The reason for this regression in the compressive strength is unclear and needs more future research.

Generally, samples exposed to room temperature for 24 hours showed a lower strength gain. This could be also related to the microcracking of the binder matrix due to the ice formation, [7,35]. In addition, the high CSA cement content resulted in a presumable intensive formation of ettringite crystals which could, induce additional microcracks, [125]. Concrete samples containing 6 wt.% of the AF admixture and 20 wt.% of the CSA cement reached the maximum strength of 24 MPa and 17 MPa respectively. Others reported limited compressive strength values of concretes containing 40 wt.% of CSA and cured at -5°C, [124]. Heat curing of concrete for at least 6 hours at room temperature appeared to mitigate the detrimental effects of later exposure to subfreezing temperatures, [19,125].

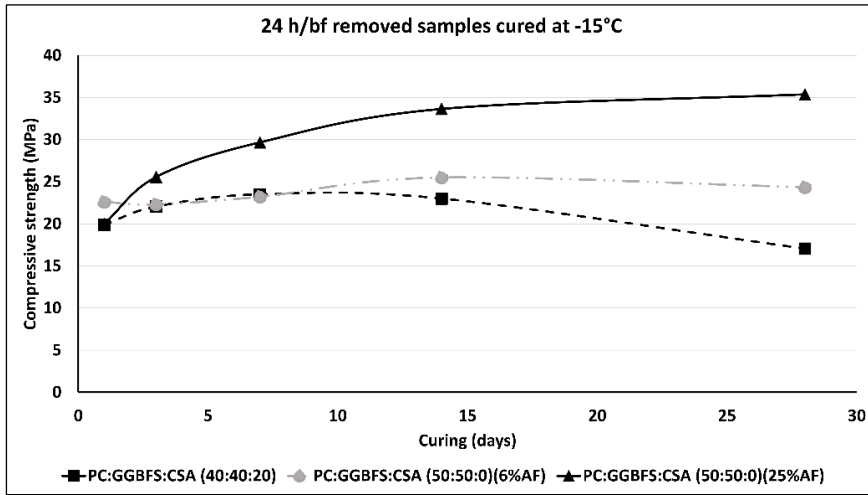


Figure 27: The compressive strength development of samples tested after 24 hours of curing at room temperature after their removal from -15°C.

4.1.2.7 Validation of the ice formation with UPV measurements.

Ultrasonic pulse velocity tests were performed to identify and validate the formation of pore ice within the binder matrix of a composite binder-based concrete cured at -15°C. The test was executed on 1 and 28-day-old concrete samples after being removed from the freezer and held at room temperature for varied periods, Figure 28 and Figure 29 respectively. Samples containing 20 wt.% of the CSA cement showed the highest pulse velocity of 4768 m/s and 4510 m/s when measured on 1- and 28-day-old respectively after being measured immediately on removal from the freezer. Concretes containing 6 wt.% of the AF admixture showed a similar trend of higher pulse velocity of 4608 m/s and 4926 m/s on 1- and 28-day-old samples, respectively. However, the following 6 hours of ambient exposure, the UPV of 1 day-old decreased to 3775 m/s and 3818 m/s, respectively, Figure 28. The trend of high initial pulse movement and followed by its sudden drop after 6 hours of ambient exposure could be inferred to the pore ice formation within the binder matrix which causes a faster movement of the ultrasonic waves and conversely the thawing of ice cause the formation of empty voids and low pulse, [37,192]. Another reason could be also microcracking of the binder matrix due to the initial ice formation, [15,217]. Others found that fresh concrete exposed to freezing had an abnormally high UPV, but did not correspond to the developed compressive strength, [218]. Others demonstrated that water at ambient temperature measured pulse movement of 1482 m/s, whereas dense ice with no air inside had an average pulse velocity of 3894 m/s at a low temperature of -20°C, [37,192,218].

On the contrary, mixes containing 25 wt.% of the AF admixture showed significantly lower UPV when measured on samples being immediately removed from the freezer, i.e., 3367 m/s on 1-day-old and 4464 m/s on 28-day old, Figure 28 and Figure 29, respectively. Exposure of these mixes to ambient conditions, resulted in an increased UPV, unlike it was observed in mixes containing 20 wt.% of the CSA cement and 6 wt.% of the AF admixture. These results

can be directly linked to the limited or the lack of ice formation due to the significantly lowered freezing point of the pore solution, [43,208].

Despite the notable decline in the UPV values observed during the initial 6 hours of ambient exposure for concrete mixes containing 20 wt% CSA and 6% AF, the pulse gain was observed in the following hours. The concrete samples containing 20 wt.% of the CSA cement showed the lowest increase of the UPV. This limited pulse gain may be attributed to irreversible damage caused by prolonged exposure to freeze conditions. Additionally, after a 24-hour thawing period, both 1- and 28-day old samples incorporating 20 wt% CSA exhibited a maximum pulse velocity of 4000 m/s, whereas those containing 6% AF recorded velocities of 4695 m/s and 4428 m/s, on 1- and 28-day respectively, Figure 28 and Figure 29. Generally, The water released from the ice could potentially resume the hydration of Portland cement and fill the pores with hydration products, [219]. These findings were consistent with the measured compressive strength and indicate that the incorporation of 6% AF and 20 wt.% CSA failed to effectively inhibit pore ice growth within the binder matrix.

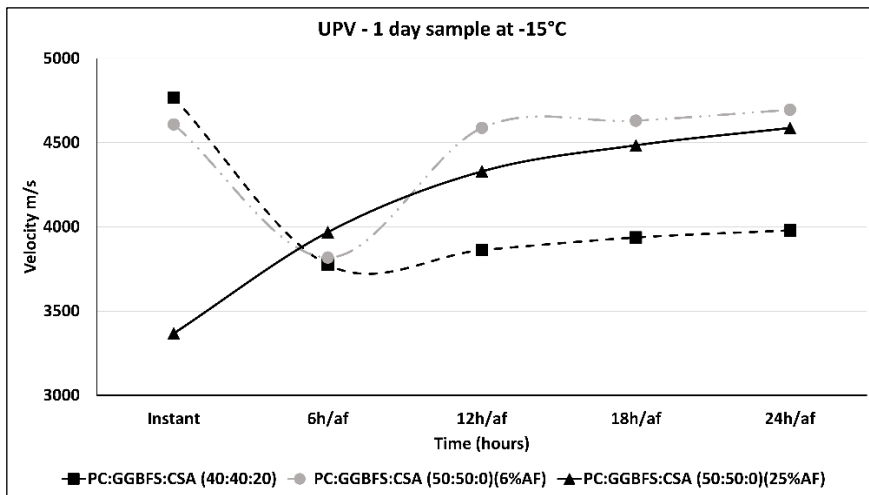


Figure 28: Average Ultrasonic Pulse velocity (UPV) measured on -15°C cured, 1-day-old composite binder-based concrete samples at distinct time intervals.

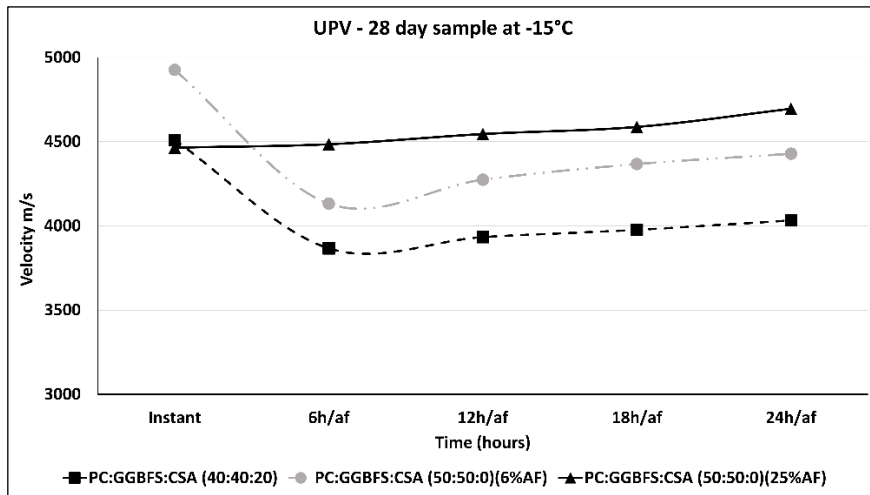


Figure 29: Average Ultrasonic Pulse velocity (UPV) measured on -15°C cured, 28-day-old composite binder-based concrete samples at distinct time intervals.

4.1.2.8 Microstructure of concretes cured at -15°C .

SEM analysis was carried out on 3 and 28-day-old concrete samples cured at -15°C , including the following mixes PC:GGBFS:CSA – 40:40:20, PC:GGBFS:CSA – 50:50:0 (6%AF), and PC:GGBFS:CSA – 50:50:0 (25%AF). At 3 days, samples containing 20 wt.% of the CSA cement and 6 wt.% of the AF admixture showed a relatively large number of unhydrated cement particles compared to the samples containing 25 wt.% of the AF admixture, Figure 30. The application of additional ambient curing resulted in a lower porosity and fewer unhydrated cement particles for samples containing 6% AF and 25% AF, Figure 30 (d, e, f), (g, h, i) and Figure 31 (d, e, f), (g, h, i).

Ettringite formation was consistently observed at all ages in concretes containing 20 wt.% of the CSA cement, Figure 30 (a, b, c) and Figure 31 (a, b, c). At the same time, the 3-day concretes containing 6 wt.% of the AF admixture contained ettringite only after an additional 12 to 24 hours of ambient exposure. This delay in ettringite formation can be attributed to the ice formation, [3,219,220]. When the temperature rises, hydration reactions resume due to the availability of water from the melted ice. The presence of ice in some of the pores limited the hydration processes in comparison with concrete containing 25 wt.% of the AF admixture, [220]. This indicates that the hydration reaction has persisted despite subzero temperatures. Furthermore, based on research performed by others, it could be assumed that alkalis from PC and from the AF admixture could activate GGBFS and promote ettringite formation at early ages, [221–224].

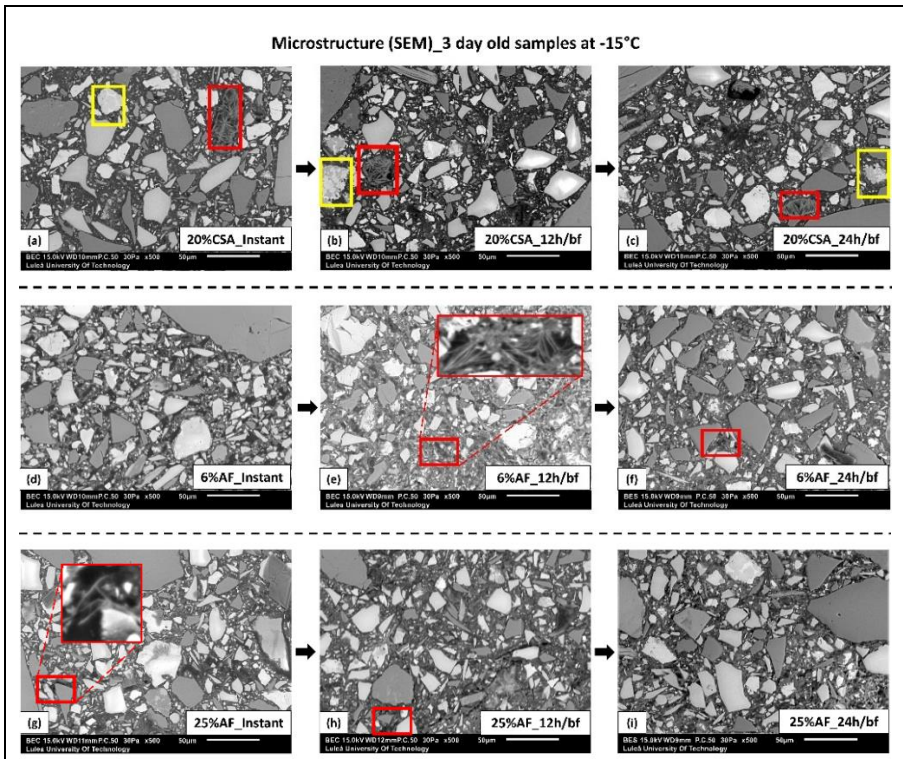


Figure 30: SEM images showing recovery of 3-day-old samples cured at -15°C. Note: red color boxes indicate areas with detected ettringite crystals and yellow boxes indicate unhydrated CSA cement.

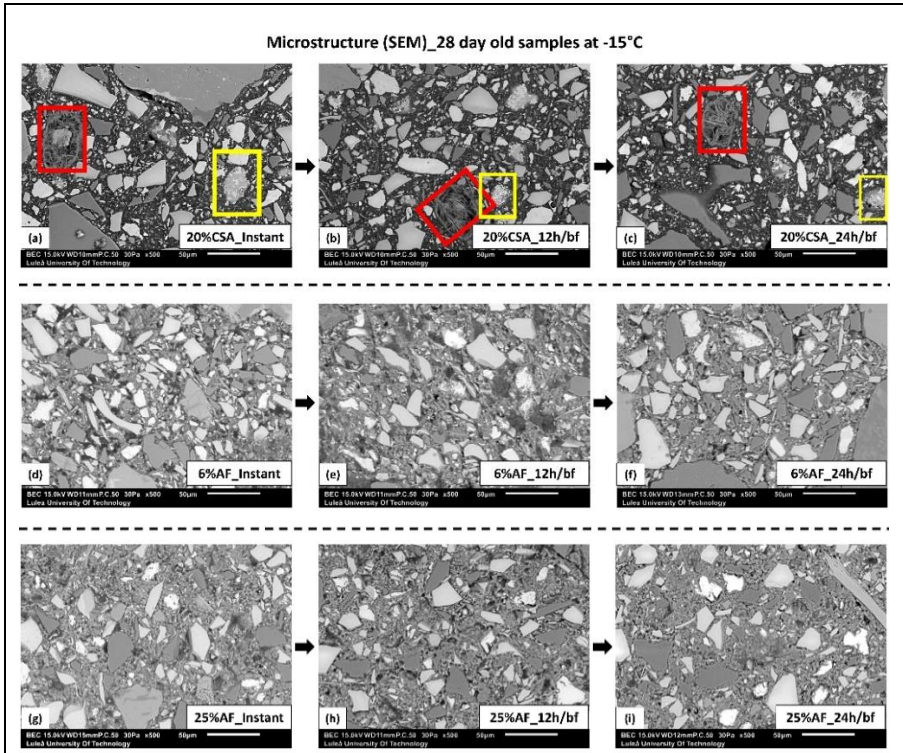


Figure 31: SEM images showing recovery of 28-day-old samples cured at -15°C. Note: red color boxes indicate areas with detected ettringite crystals and yellow boxes indicate unhydrated CSA cement.

Concretes containing 20 wt.% of the CSA cement and 6 wt.% of the AF admixture showed a higher average porosity in comparison with mixes containing 25 wt.% of the AF admixture, Figure 32, Figure 33, Figure 34 and Figure 35. The measured porosity ranged between 9-11% and 6-9%, for 3- and 28-day old concrete containing 20 wt.% of the CSA cement, respectively. Conversely, 3-day-old samples, which were studied directly after curing in the freezer and containing 6 wt.% of the AF admixture showed a relatively high porosity of 15%, which subsequently decreased upon exposure to ambient conditions, Figure 34. Furthermore, regardless of curing age, concrete containing 25 wt.% of the AF porosity ranged between 3-4%. On contrary, for AF induced 28-day old concrete samples, despite of additional 12 to 24 hours of ambient exposure, it showed relatively increased porosity compared to the 3-day old samples, Figure 34 and Figure 35. It could be related to the prolonged exposure to freezing temperatures, which enhanced the ice growth and internal microcracking, [216,225]. SEM analysis and earlier test results indicate pore ice formation in concrete samples containing 20 wt.% of the CSA cement and 6 wt.% of the AF admixture, while pore ice formation was partially inhibited in samples incorporating 25 wt.% of the AF admixture.

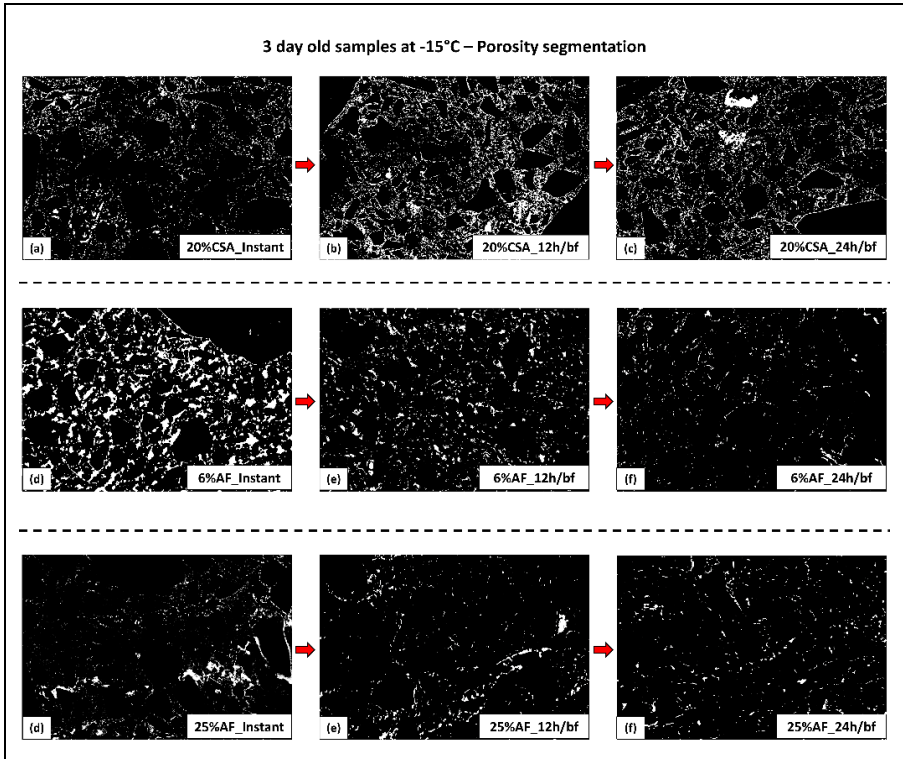


Figure 32: Pore segmentation of 3-day-old samples cured at -15°C. Note: White color indicates pores.

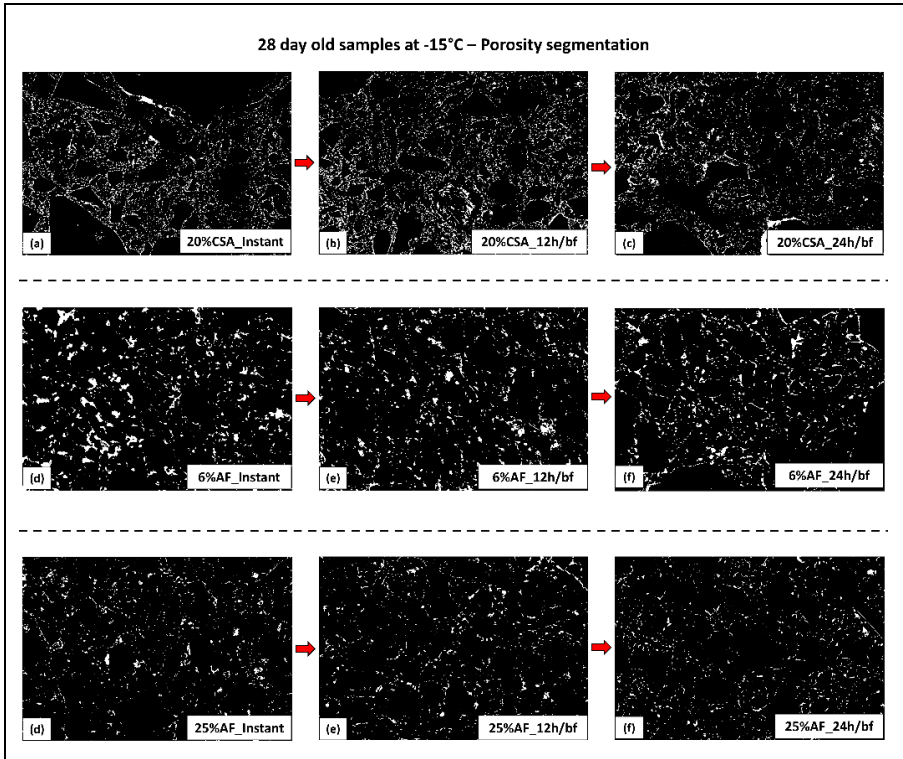


Figure 33: Pore segmentation of 28-day-old samples cured at -15°C. Note: White color indicates pores.

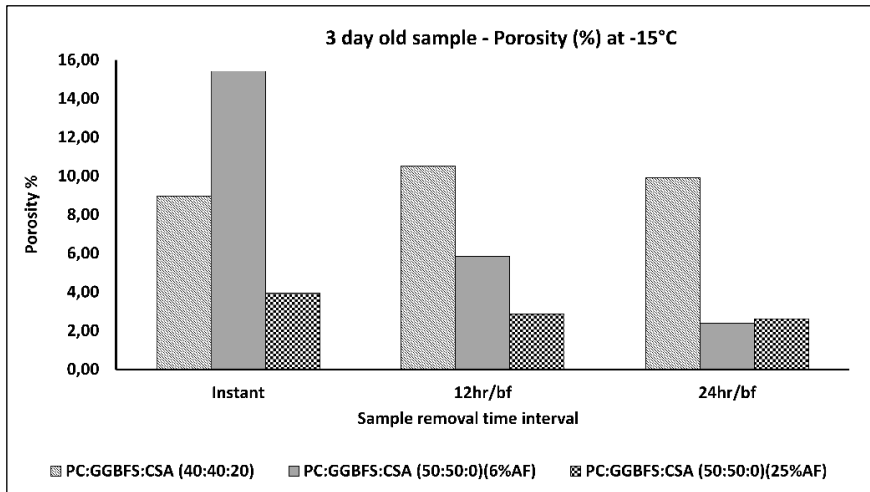


Figure 34: Effect of curing on porosity of 3-day-old concrete samples.

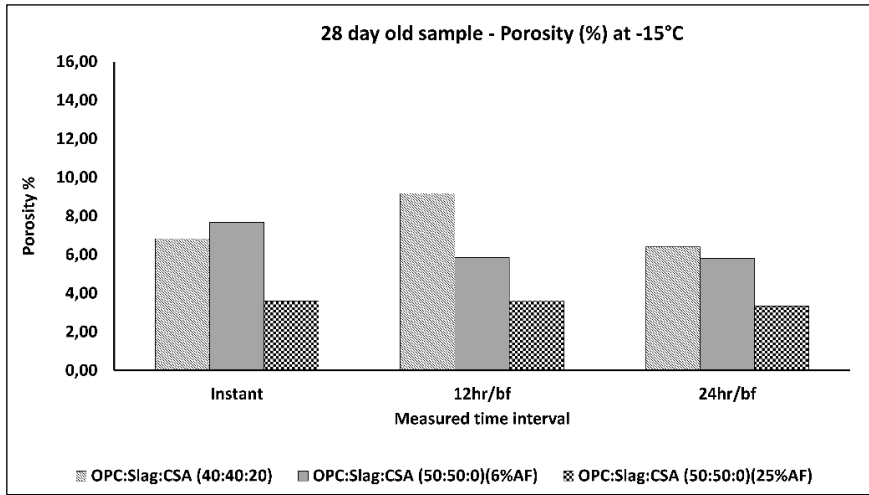


Figure 35: Effect of curing on porosity of 28-day-old concrete samples.

4.2 Enhancing frost durability of NSC with UHPC overlay

The second part of this PhD study focused on the possible application of UHPC to create a thin overlay that could be applied to existing and new concrete structures to enhance their frost durability. The study was divided into two parts: development and testing of UHPC with lower PC content and testing of hybrid elements made of NSC with thin UHPC overlay.

4.2.1 Fresh and hardened properties - UHPC

The slump flow test results are shown in Figure 36. The UHPC mix without fibers had a slump flow of 800 mm and 900 mm when fibers were present. The water demand and particle size are the major influencing factors contributing to the slump flow. Despite lower w/b (0.33), an optimized mix design that used the packing density theory enabled to decrease of the free spaces between particles to produce very a flowable material, [226–228]. The addition of limestone filler added Ca^{2+} and CO_3^{2-} ions which in contact with water react with OH^- groups leading to inter-particle electrostatic repulsion and better flow, [164,171,229–231]. Furthermore, the addition of steel fibers presumably improved the rheology by breaking up condensed silica fume agglomerates during the mixing process. The use of small-size steel fibers, 6 mm and 13 mm, prevented the interlocking effect commonly observed for regular steel fibers [232,233].

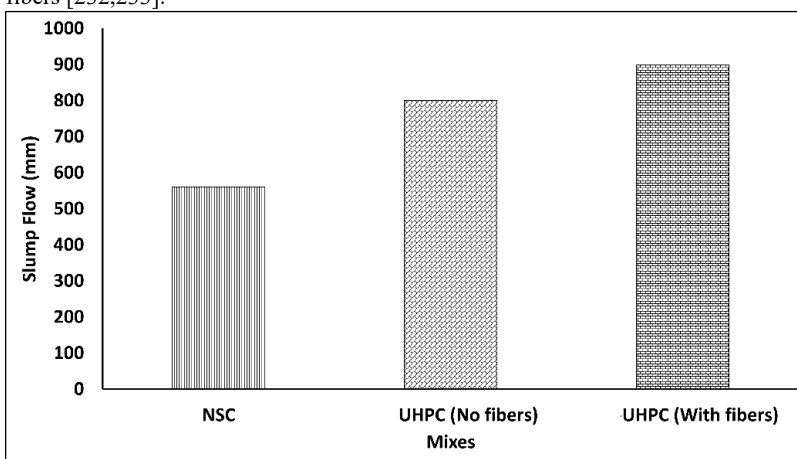


Figure 36. Slump flow test results.

The compressive strength development of the designed UHPC mix with and without steel fibers and the normal strength concrete (NSC) are shown in Figure 37. The highest 28-day compressive strength of 154 MPa was measured for UHPC with fibers. The very low water-to-binder ratio and the high amount of silica fume had the dominating effect on the compressive strength [171,226,234–236]. The limestone powder and silica fume accelerated the cement hydration process due to pozzolanic reactions and nucleation effect, [164,237,238]. Portlandite reacted with condensed silica fume to produce more C-S-H gel, followed by filling the voids and forming a dense microstructure. The steel fibers reinforced the binder matrix and delayed the micro-cracks formation leading to a higher strength. Overall, on average, over 25% of strength gain was observed for UHPC mix with fibers regardless of its age, compared to non-fiber UHPC.

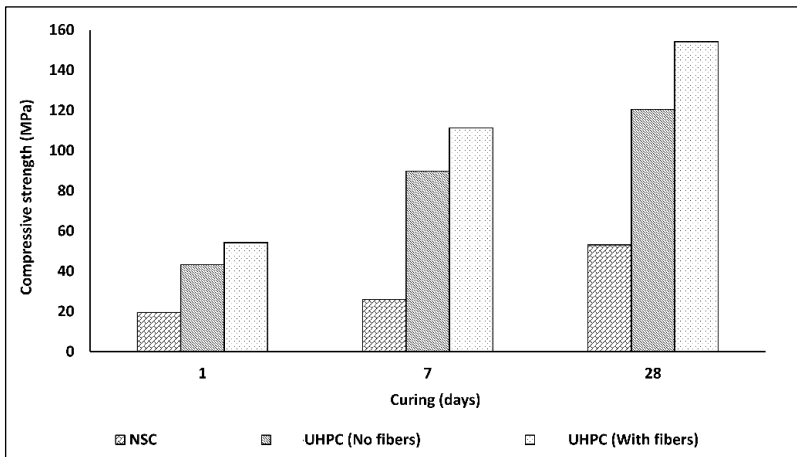


Figure 37: Compressive strength development of normal strength concrete (NSC), and UHPC without and with fibers.

4.2.2 Freeze-thaw durability of UHPC.

The cumulative surface scaling of the studied UHPC specimens exposed to 56 freeze-thaw cycles (F-T) in the presence of 3% NaCl de-icing salt solution is shown in Figure 38. About 0.01 kg/m² of surface scaling was observed for UHPC which was significantly lower compared to the standardized limit of 0.1 kg/m² following SS-EN 13 72 44:2005 standard, [239]. The low scaling could be mainly due to the very dense microstructure and low weakly interconnected capillary porosity, [240]. The majority of pores present in UHPC are gel pores, [241–243]. The use of silica fume triggered a pozzolanic reaction leading to the consumption of Portlandite and the formation of additional C-S-H. Consequently, the porosity was refined which limited the penetration of deicing salts, [244,245]. Furthermore, the added steel fibers delayed the formation of micro-cracks, which additionally delayed the ingress of salts, [240,243]. Previous studies indicated that the concretes containing an optimum dosage of steel fibers could sustain 800-1000 F-T cycles with a very low mass loss and more than 90% of relative dynamic modulus of elasticity, [243,246]. The very good frost durability of the tested UHPC concrete indicated its applicability in the studied concept to protect NSC by applying a thin external layer.

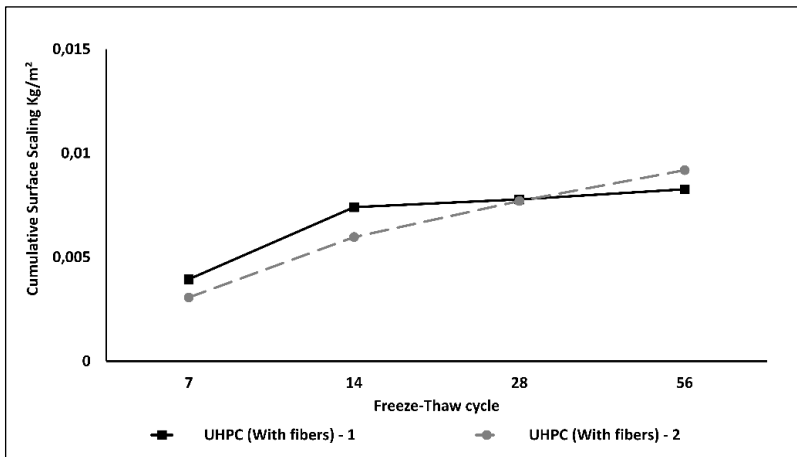


Figure 38: Cumulative surface scaling of UHPC exposed to 56 freeze-thaw (F-T) cycles.

4.2.3 Compressive strength development of UHPC-NSC composite

The compressive strength development of NSC and composite UHPC-NSC at 7 and 28 days is shown in Figure 39. The maximum compressive strength values reached 67.93 MPa and 76.33 MPa, respectively. However, the strength increase is partially related to a larger cross-section of composite cubes. Furthermore, because of the strain-hardening characteristic of UHPC, composite UHPC-NSC specimens could transfer higher loads by limiting the microcrack development. [27,246]. Due to very good bond strength, no delamination or debonding of the overlay was observed, despite the loading direction being parallel to the bond surface, Figure 39. This could be due to the substrate concrete's surface roughness, flowability of UHPC, and the used fine particles. The rough substrate surface with macro roughness and voids are filled with freshly produced concrete by capillary absorption, which complements high friction/anchoring, i.e., aggregate interlocking mechanism, and increased chemical bonding between layers [153,247–251]. The unreacted silica fume present at the interface has presumably gradually combined with Ca(OH)_2 from the NSC substrate to generate additional C-S-H which enhanced the bond, [26,252–255]. The used limestone filler could also react to produce carboaluminates, which could lead to the formation of additional C-S-H, [56].

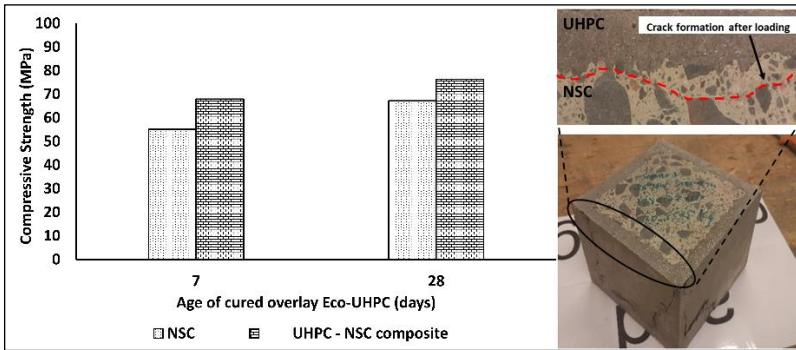


Figure 39: Compressive strength development of NSC and composite UHPC-NSC concrete cubes.

4.2.4 Flexural strength of UHPC-NSC composite

The flexural strength of the UHPC-NSC composite beam using a three-point bending test reached a strength of 7.96 MPa, 28 days after applying the UHPC overlay. This strength is 66% higher in comparison with beams made of NSC, Figure 40. Both beams showed a similar trend of crack formation with an ultimate flexural load of 165 kN and 57.6 kN, respectively, Figure 41.

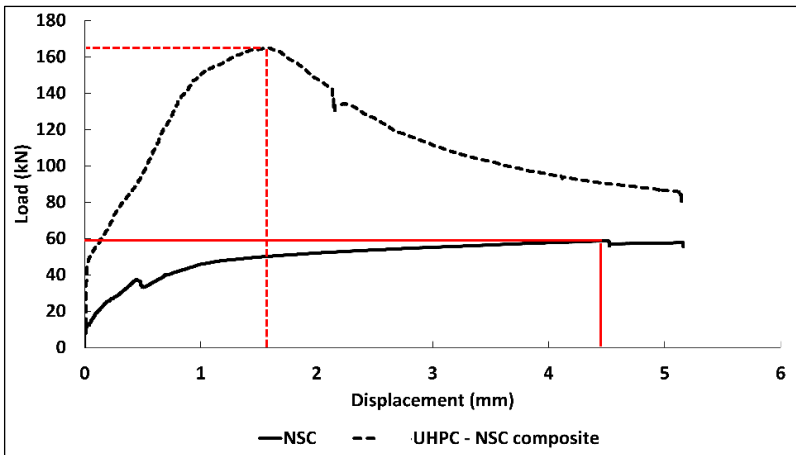


Figure 40: Load vs displacement measured in 3-point bending for NSC and UHPC – NSC column specimens.

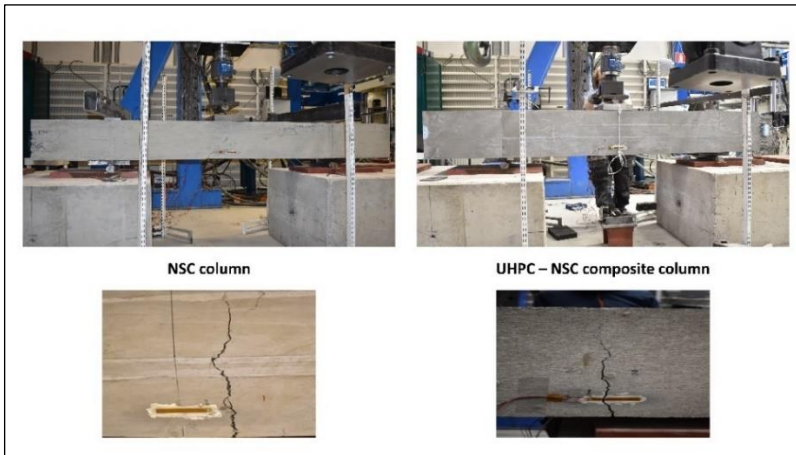


Figure 41: Cracking of beam at failure.

4.2.5 UHPC-NCS interfacial transition zone

The interfacial transition zone between UHPC and NSC has been studied by UPV measurements, the determination of the bond strength by pull-out testing, while the microstructure and phase composition were characterized using SEM combined with EDX.

4.2.5.1 UPV measurements

The UPV measurements were done every 10 cm on test columns that were 2 meters high, and the results are shown in Figure 42. Generally, the pulse velocity tended to increase with height. Despite the identical external dimensions of the two studied UHPC-NSC composite columns, there was a 3.7% difference in the recorded UPV values. The UPV for UHPC alone was 4900 m/s and for the NSC 4540 m/s, which difference could be presumably indicated as good bonding between the layers. Additionally, water from the UHPC overlay could migrate toward the interface zone and trigger the hydration of anhydrous Portland cement present in the NSC binder matrix. Some of the longer measured transition times could be attributed to a lower degree of hydration of the UHPC [26,158].

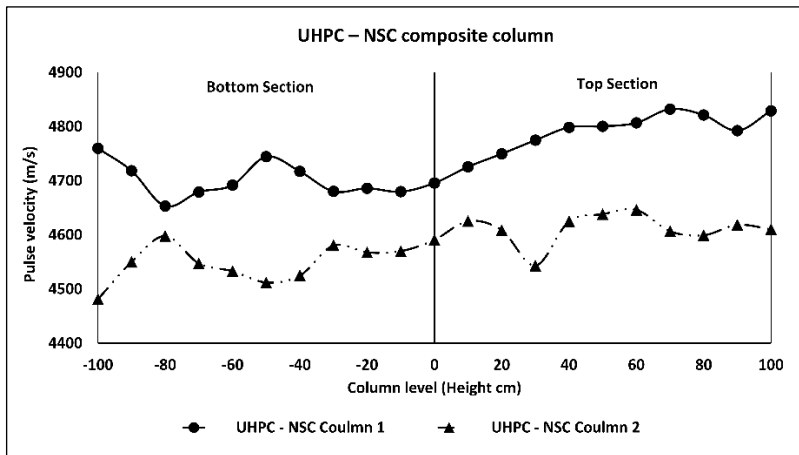


Figure 42: Average ultrasonic pulse velocity (UPV) measurement of UHPC – NSC composite columns.

4.2.5.2 Bond strength – Pull-off test.

The measured bond strength between the UHPC overlay and NSC substrate is shown in Figure 43. The strength varied between 2.0 MPa to 2.7 MPa, which can be categorized as “excellent” (≥ 2.1 MPa) according to ACI 546, Table 14 [256]. Failure was mostly seen in the NSC designated as "SBF (substrate failure)". No full interface failure was observed, in Figure 44 and Figure 45. This indicates that the bond strength exceeded the ultimate developed tensile stress [257]. A partial interface substrate failure (PISF) was observed in some locations. This could be related to a locally occurring smooth exposed aggregate surface or the presence of loose derbies, Figure 44 and Figure 45, [258].

Several studies indicated that the rougher the substrate texture and the better the overlay material, the stronger the bond will be [26,27,152,259]. Bonding is mostly affected by the substrate roughness, moisture, and properties of the overlay concrete. According to Benoit Bissonnette et al., the dry substrate concrete will absorb the water from the fresh overlay concrete leading to a lower hydration degree and weaker developed bond, [248,260]. The optimum moistening of the substrate will have a small/ negligible positive impact on the bond strength [261]. On the contrary, saturating with water the substrate surface will close the capillary pores and dilute the repair concrete resulting in an excessive w/c ratio at the interface leading to a weaker bond, [257,262].

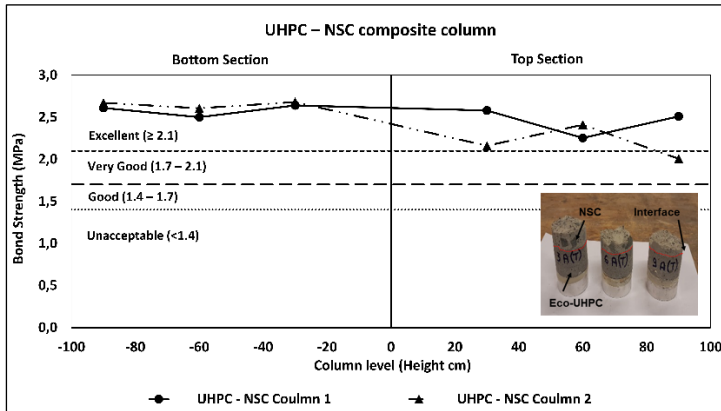


Figure 43: Bond strength development using pull-off test on UHPC– NSC composite columns at different locations.

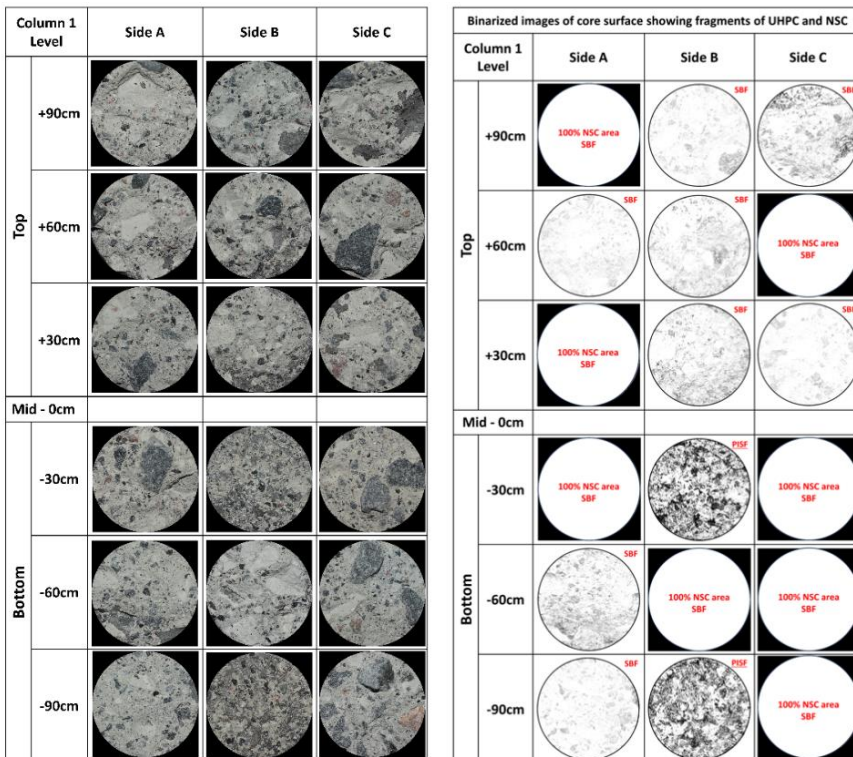


Figure 44: Binarized images of the core surface showing fragments of UHPC and NSC in column 1. Note: On right images, the black color indicates UHPC, and white color indicates NSC.

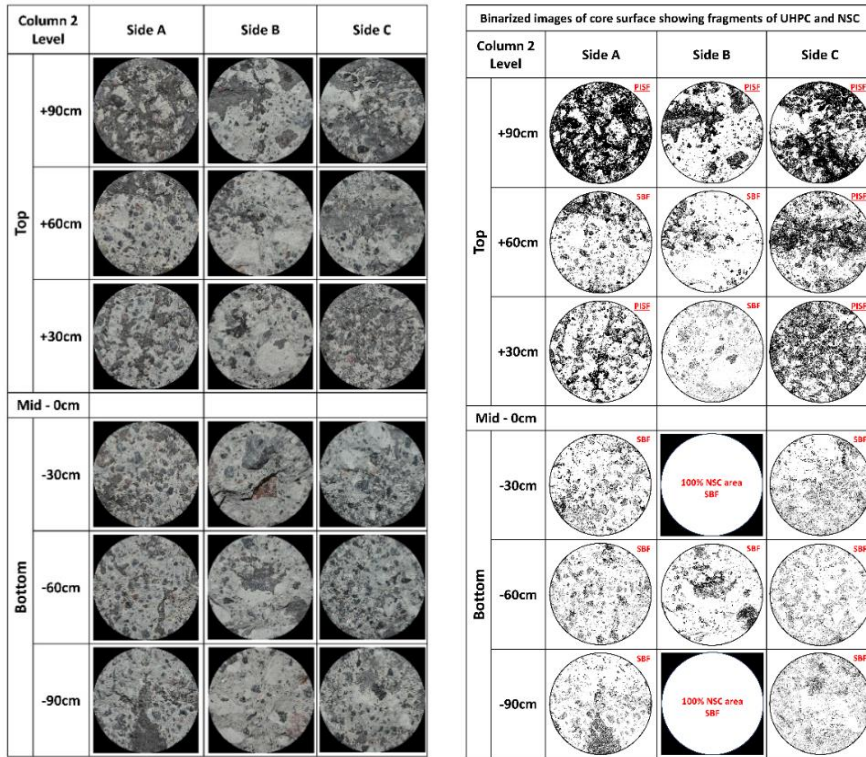


Figure 45: Binarized images of the core surface showing fragments of UHPC and NSC in column 2. Note: On right images, the black color indicates UHPC and white color indicates NSC.

4.2.5.3 Microstructure and phase composition.

The microstructure and phase composition were studied using SEM combined with an EDX analyzer. Generally, the results indicated that the UHPC–NSC interface was homogenous with a limited number of visible pores, Figure 46 and Figure 47. A well-developed ITZ (interfacial transition zone) was not observed. Some entrapped air voids were seen next to the interface as well in the bulk binder zone of both studied columns.

Variations of porosity and content of anhydrous cement were determined using ImageJ analysis software based on SEM images. The results are shown in Figure 48 - Figure 51. The porosity at the interface zone was approximately 6% and tended to decrease to around 2% with increasing distance. This could be explained, by the locally increased w/c ratio due to the wall effect, [92,263]. The fine particles located close to the exposed NSC aggregates form empty spaces that are filled with the mixing water. Consequently, a lower number of unhydrated cement particles are present in that zone. This trend was also observed in this research, Figure 50 and Figure 51.

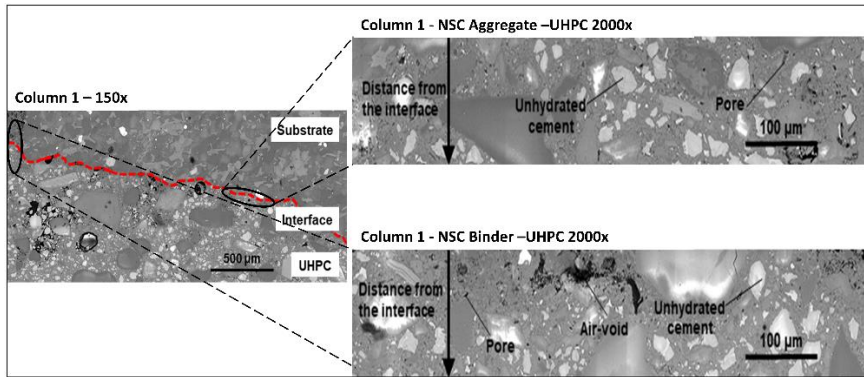


Figure 46: Interfacial bond zone of composite UHPC – NSC column 1 using SEM at 150X and 2000X magnifications.

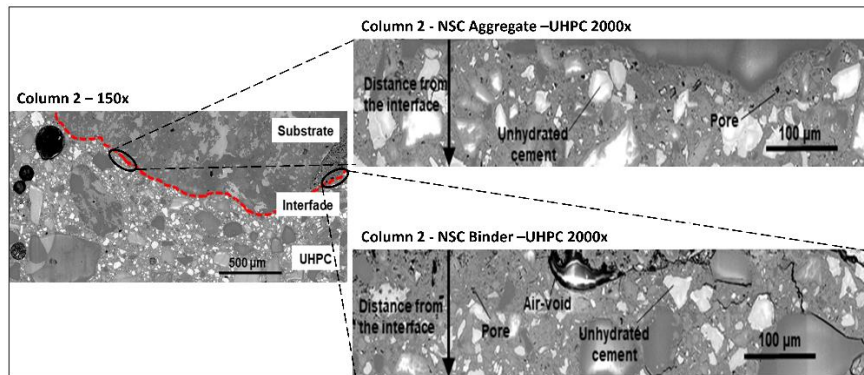


Figure 47: Interfacial bond zone of composite UHPC – NSC column 2 using SEM at 150X and 2000X magnifications.

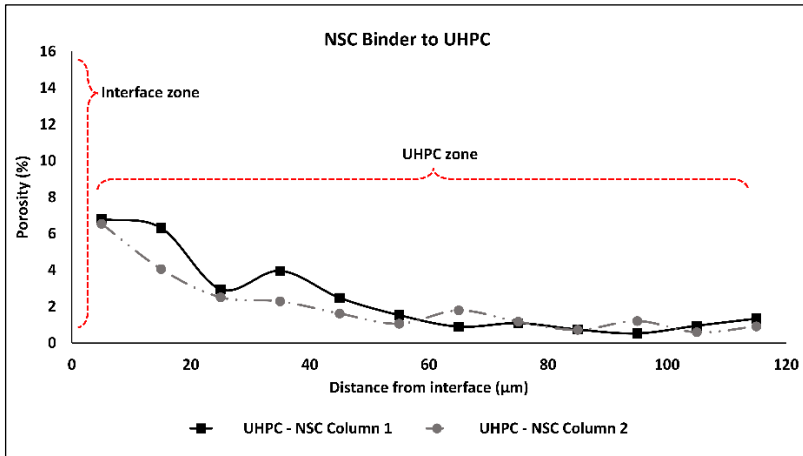


Figure 48: Percentage change of porosity away from NSC binder – UHPC interface of composite - UHPC – NSC columns.

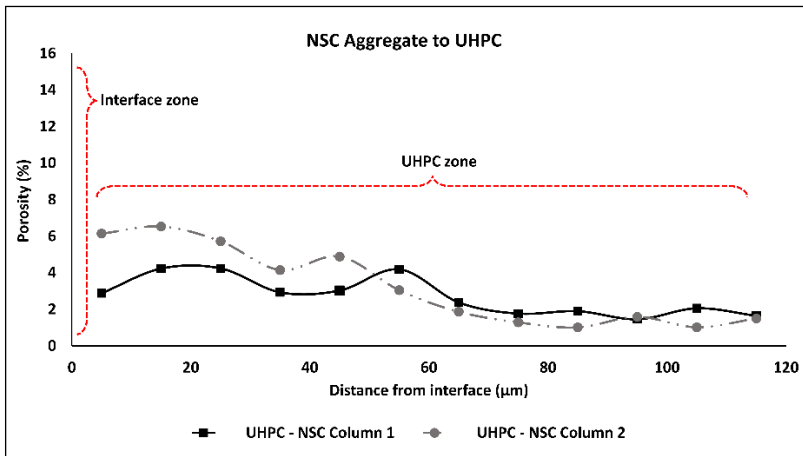


Figure 49: Percentage change of porosity away from NSC aggregate – UHPC interface of composite - UHPC – NSC columns.

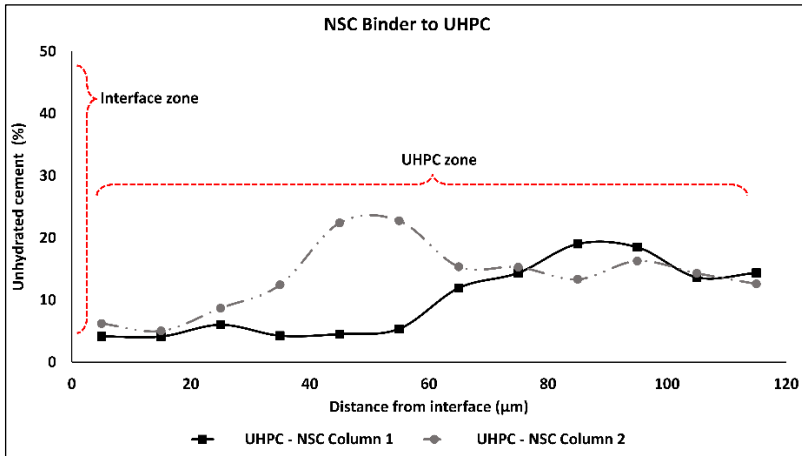


Figure 50: Percentage change of unhydrated cement away from NSC binder–UHPC interface of composite -UHPC – NSC columns.

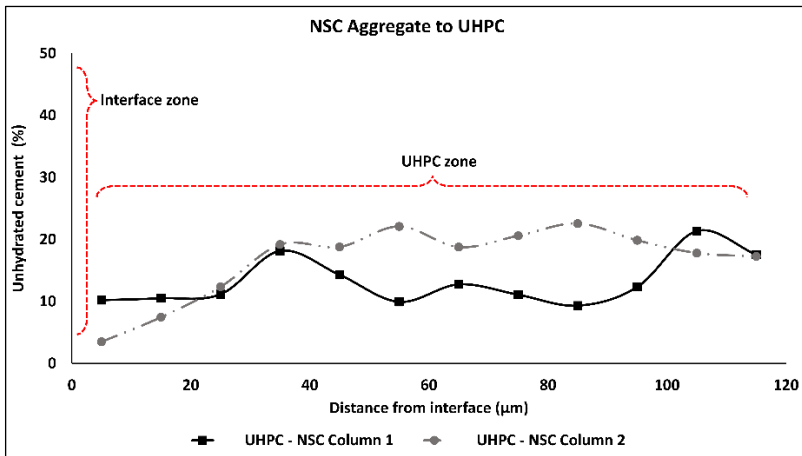


Figure 51: Percentage change of unhydrated cement away from NSC aggregate–UHPC interface of composite - UHPC–NSC columns.

The phase composition analysis focused on studying C-S-H, whose location was identified using the grey-level method and SEM-BSE images. The results of the SEM-EDS spot analysis are shown in Figure 52 and Figure 53. Both beams showed a similar trend indicating a slightly higher Ca/Si average atomic ratio at the NSC binder and UHPC interface compared to the NSC aggregate and UHPC interface. The ratio was between 1.2 to 1.6. Only a limited variation of this atomic ratio was seen when moving away from the interface which further indicates the formation of a narrow ITZ, having an average width of less than 20 μm, which translates into a generally very good bond strength measured in pull-off testing.

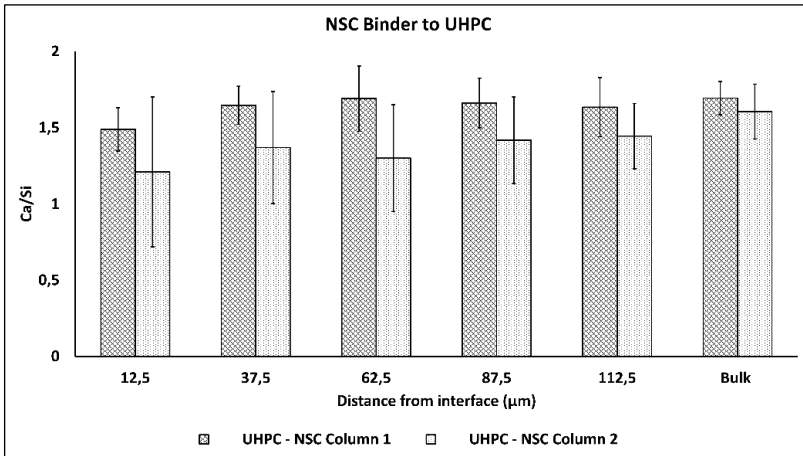


Figure 52: Average atomic Ca/Si ratio vs. distance from the NSC binder–UHPC interface.

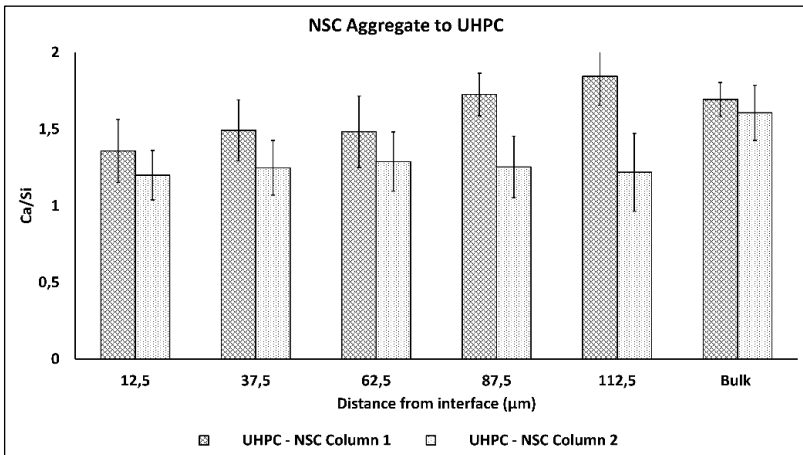


Figure 53: Average atomic Ca/Si ratio vs. distance from the NSC aggregate–UHPC interface.

5. Conclusions

5.1 Concluding remarks

This research aimed to better understand how partial replacement of Portland cement with GGBFS and/or CSA cement affects the properties of concretes exposed to freezing and subfreezing temperatures in a fresh state and at a young age.

The secondary aim was to evaluate a possible application of UHPC to protect new and existing concrete structures from frost damage and possibly to enhance its mechanical properties.

The findings can be summarized as:

Composite binder-based concrete systems for cold weather concreting

- The partial replacement of PC or GGBFS or their combinations by 20 wt.% of CSA showed a shorter initial setting time. This could be attributed to the fast hydration of CSA and the extensive formation of ettringite.
- PC and GGBFS of equal proportions with 20 wt.% CSA, 6 wt.% AF, or 25 wt.% AF showed identical strength gain when cured at room temperature. Thus, the combination can balance each other's strengths and compensate for any flaws.
- Despite high concentration of CSA (20 wt.%) and the depressed freezing point of water, it relatively gained lower strength when cured at sub-zero temperature. Ettringite formed at very early age and incorporated low reaction degree of GGBFS disrupted the physicochemical properties of CSA and thus relatively more voids.
- Sodium nitrate-based antifreeze admixture (AF) of 25 wt.% dosage considerably reduced the freezable pore water in concrete and promoted the hydration process throughout the studied 28 days.
- 6 wt.% AF and 20 wt.% CSA admixture incorporated concrete samples developed pore ice within the binder matrix when cured at -15°C and confirms the developed strength as false strength.
- At -15°C curing, UPV increased steadily for concrete with 25 wt.% AF. Conversely, samples with 6 wt.% AF and 20 wt.% CSA saw a rapid drop in UPV after 6 hours at room temperature, indicating pore ice formation, melting upon return to room temperature, causing longer transit times.
- Irrespective of the AF dosage, the frozen pores got revived and densified the binder matrix after extended post-curing at room temperature. On contrary no considerable densification effect was observed for concrete with 20 wt.% CSA.
- Prolonged curing at -15°C aggravated the porosity of PC-GGBFS based concrete incorporated with 20 wt.% CSA and thus relatively lower strength gain. Possible due to the nucleation of thick pore ice causing irreversible damage.

- PC-based concrete with up to 50 wt.% GGBFS and a larger optimized dosage of sodium nitrate-based antifreeze can be utilized in winter with temperatures as low as -15°C without additional heat curing.

Application of UHPC for enhanced frost durability

- Overlay of dense UHPC applied on deteriorated NSC, enhanced the 28-day compressive strength by 14% compared to NSC specimen.
- The reduced w/b ratio, optimum dosage of steel fibers, and fine powders (silica fume, quartz, limestone) significantly improved the F-T resistance of UHPC, by lowering the pore size and forming a dense binder matrix.
- The added steel fibers in UHPC prevented micro-cracks formation under loading and enhanced F-T resistance.
- The rough and uneven surface of the substrate significantly improved the bond strength. No delamination between the layers was observed even despite loading parallel to the interface.
- The ultrasonic longitudinal pulse velocities measured on the UHPC – NSC composite indicated a good bonding between the layers.
- Pull-off bond strength varied between 2 MPa to 2.7 MPa and most of the interface failure occurred on the weaker NSC substrate.
- The ITZ between NSC and UHPC was less than 20 μm . The estimated Ca/Si had little variability with the distance from the interface.
- The application of thin UHPC layer on water jetted concrete surface can potentially enhance mechanical properties and frost durability of composite elements.

5.2 Answering the research questions

RQ (1): What is the best approach to produce concretes with low Portland cement content that are exposed shortly after casting to freezing and subfreezing temperatures? (*Paper I*)

The optimum approach to produce concrete with low Portland cement content appeared to be using chemical admixtures and mineral accelerators. These materials can enhance the early-age strength development, reduce the freezing point of water, and reduce the susceptibility to the frost damage.

Additionally, optimizing the concrete mix design, especially in terms of the type and amount of used SCMs, should be considered.

RQ (2): How does a high amount of GGBFS affect hydration heat development and strength of normal concrete when cured at close and sub-zero temperatures? (*SBUF report, Paper VIII*)

Concretes containing GGBFS generally showed a slower hydration and slowed down the strength development thus leading to the enhanced freezing risk of young concretes. Consequently, the usage of antifreeze admixtures is more important in comparison with concretes based on PC, especially when heat treatment or additional thermal insulations are not considered.

RQ (3): How does the sodium nitrate-based antifreeze admixture influence the strength development and pore water phase transitions of binder systems based on the combination of PC and GGBFS when cured at subzero temperatures? (*Paper II*)

Sodium nitrate-based antifreeze admixture reduces the freezing point of water in the concrete mixtures, alters the phase transition of pore water. This inhibits the formation of large ice crystals, which can reduce the risk of damage due to the frost action. It enables the continuation of the cement hydration process even at subzero temperatures, albeit at a slower rate. As a result, its optimized dosage delayed the pore ice growth and enabled to maintain the strength development.

RQ (4): How effective are calcium sulfoaluminate (CSA) cements as alternatives to accelerators and antifreeze admixtures when used in combination with PC-GGBFS binders for concretes exposed to sub-zero curing temperature? What are their effects on the strength development strength and formed microstructure? (*Paper III, IV*)

CSA cement shortened the setting time by facilitating the rapid formation of ettringite in PC-GGBFS binder systems. However, it failed to effectively inhibit pore ice formation in sub-zero curing temperatures. The risk of frost damage was increased even when the "post-freezing" heat treatment was applied. These concretes exhibited reduced strength, and a more porous binder matrix was formed.

RQ (5): Can a thin layer of UHPC applied on an existing deteriorated concrete element enhance its properties and frost durability? (*Paper V, VI*)

A thin layer of Ultra High-Performance Concrete, applied to a existing deteriorated concrete element, can result in enhanced strength and better frost durability. The dense microstructure of UHPC binder matrix provides a protective layer and limits the moisture ingress, which leads to the enhanced frost durability.

5.3 Future research

Generally, the sodium nitrate-based antifreeze chemical admixtures can lower the freezing point of water but at the same time, they can increase the risk of alkali-silica reaction. This effect is not well studied for concretes based on a mix of PC with GGBFS and CSA. Therefore, tests in that area should be planned. Future research could also aim to collect additional data regarding the hydration process using isothermal calorimetry instead of the semi-adiabatic calorimetry used in the research. Other tests should also include XRD and TG. Effects of other types of industrial wastes and mine tailings, is yet another area that shows a insufficient level of knowledge.

6. References

1. Provis, J.L.; van Deventer, J.S.J. Alkali Activated Materials: State-of-the-Art Report, RILEM TC 224-AAM. *Springer* **2014**.
2. Korhonen, C.J. *Antifreeze Admixtures for Cold Regions Concreting: A Literature Review*; U. S. Army Corps of Engineers, Cold Regions Research and Engineering Laboratory, HANOVER, NH, 1990;
3. Nmai, C.K. Cold weather concreting admixtures. *Cem. Concr. Compos.* **1998**, *20*, 121–128, doi:10.1016/s0958-9465(97)00063-2.
4. Barna, L.A.; Korhonen, C.J. *Extending the Season for Concrete Construction and Repair Phase III — Guidance for Optimizing Admixture Dosage Rates Cold Regions Research and Engineering Laboratory*; U. S. Army Engineering Research and Development Center, Cold Regions Research and Engineering Laboratory: Hanover, NH, 2014;
5. Farrington, S.A.; Christensen, B.J. The Use of Chemical Admixtures to Facilitate Placement of Concrete at Freezing Temperatures. *ACI Spec. Publ.* **2003**, *217*, 71–86.
6. ACI 306R Guide to Cold Weather Concreting. *Am. Concr. Inst.* **2010**.
7. Karagöl, F.; Demirboga, R.; Khushefati, W.H. Behavior of fresh and hardened concretes with antifreeze admixtures in deep-freeze low temperatures and exterior winter conditions. *Constr. Build. Mater.* **2015**, *76*, 388–395, doi:10.1016/j.conbuildmat.2014.12.011.
8. Powers, T.C. A Working Hypothesis for Further Studies of Frost Resistance of Concrete. *ACI J. Proc.* **1945**, *41*, 245–272, doi:10.14359/8684.
9. Koniarczyk, M.; Konca, P. Kinetics of water freezing in mesopores determined by differential scanning calorimetry. *Int. J. Therm. Sci.* **2017**, *122*, 124–132, doi:10.1016/j.ijthermalsci.2017.08.015.
10. Polat, R. The effect of antifreeze additives on fresh concrete subjected to freezing and thawing cycles. *Cold Reg. Sci. Technol.* **2016**, *127*, 10–17, doi:10.1016/j.coldregions.2016.04.008.
11. Liu, J.; Li, Y.; Yang, Y.; Cui, Y. Effect of low temperature on hydration performance of the complex binder of silica fume-portland cement. *J. Wuhan Univ. Technol. Mater. Sci. Ed.* **2014**, *29*, 75–81, doi:10.1007/s11595-014-0870-2.
12. Karagöl, F.; Demirboğa, R.; Kaygusuz, M.A.; Yadollahi, M.M.; Polat, R. The influence of calcium nitrate as antifreeze admixture on the compressive strength of concrete exposed to low temperatures. *Cold Reg. Sci. Technol.* **2013**, *89*, 30–35, doi:10.1016/j.coldregions.2013.02.001.
13. Demirboğa, R.; Karagöl, F.; Polat, R.; Kaygusuz, M.A. The effects of urea on strength gaining of fresh concrete under the cold weather conditions. *Constr. Build. Mater.* **2014**, *64*, 114–120, doi:10.1016/j.conbuildmat.2014.04.008.

14. Suprenant, B.A. Designing cold weather concrete mixes. *Aberdeen's Concr. Constr.* **1990**, *35*, 882–884.
15. Korhonen, C.J.; Cortez, E.R. Antifreeze admixtures for cold weather concreting. *Concr. Int.* **1991**, *13*, 38–41.
16. Li, G.; Zhang, J.; Song, Z.; Shi, C.; Zhang, A. Improvement of workability and early strength of calcium sulfoaluminate cement at various temperature by chemical admixtures. *Constr. Build. Mater.* **2018**, doi:10.1016/j.conbuildmat.2017.11.076.
17. Wang, P.; Li, N.; Xu, L. Hydration evolution and compressive strength of calcium sulfoaluminate cement constantly cured over the temperature range of 0 to 80 °C. *Cem. Concr. Res.* **2017**, doi:10.1016/j.cemconres.2017.05.025.
18. Glasser, F.P.; Zhang, L. High-performance cement matrices based on calcium sulfoaluminate-belite compositions. *Cem. Concr. Res.* **2001**, *31*, 1881–1886, doi:10.1016/S0008-8846(01)00649-4.
19. Zhang, G.; Yang, Y.; Yang, H.; Li, H. Calcium sulfoaluminate cement used as mineral accelerator to improve the property of Portland cement at sub-zero temperature. *Cem. Concr. Compos.* **2020**, *106*, doi:10.1016/j.cemconcomp.2019.103452.
20. Huang, W.; Kazemi-Kamyab, H.; Sun, W.; Scrivener, K. Effect of cement substitution by limestone on the hydration and microstructural development of ultra-high performance concrete (UHPC). *Cem. Concr. Compos.* **2017**, *77*, 86–101, doi:10.1016/j.cemconcomp.2016.12.009.
21. Charron, J.P.; Denarić, E.; Brühwiler, E. Permeability of ultra high performance fiber reinforced concretes (UHPFRC) under high stresses. *Mater. Struct. Constr.* **2007**, *40*, 269–277, doi:10.1617/s11527-006-9105-0.
22. Tayeh, B.A.; Abu Bakar, B.H.; Megat Johari, M.A.; Voo, Y.L. Mechanical and permeability properties of the interface between normal concrete substrate and ultra high performance fiber concrete overlay. *Constr. Build. Mater.* **2012**, *36*, 538–548, doi:10.1016/j.conbuildmat.2012.06.013.
23. Prem, P.R.; Ramachandra Murthy, A.; Ramesh, G.; Bharatkumar, B.H.; Iyer, N.R. Flexural behaviour of damaged rc beams strengthened with ultra high performance concrete. In *Advances in Structural Engineering: Materials, Volume Three*; 2015; pp. 2057–2069 ISBN 9788132221876.
24. Safdar, M.; Matsumoto, T.; Kakuma, K. Flexural behavior of reinforced concrete beams repaired with ultra-high performance fiber reinforced concrete (UHPFRC). *Compos. Struct.* **2016**, *157*, 448–460, doi:10.1016/j.compstruct.2016.09.010.
25. Brühwiler, E.; Denarić, E. Rehabilitation and strengthening of concrete structures using ultra-high performance fibre reinforced concrete. In *Proceedings of the Structural Engineering International: Journal of the International Association for Bridge and Structural Engineering (IABSE)*; 2013.
26. Zhang, Y.; Zhu, P.; Liao, Z.; Wang, L. Interfacial bond properties between normal strength concrete substrate and ultra-high performance concrete as a repair material. *Constr. Build. Mater.* **2020**, *235*, doi:10.1016/j.conbuildmat.2019.117431.

27. Zhang, Y.; Li, X.; Zhu, Y.; Shao, X. Experimental study on flexural behavior of damaged reinforced concrete (RC) beam strengthened by toughness-improved ultra-high performance concrete (UHPC) layer. *Compos. Part B Eng.* **2020**, *186*, doi:10.1016/j.compositesb.2020.107834.
28. Brühwiler, E.; Denarié, E. Rehabilitation of concrete structures using Ultra-High Performance Fibre Reinforced Concrete. In Proceedings of the The Second International Symposium on Ultra High Performance Concrete; 2008; pp. 1–9.
29. Courtial, M.; De Noirfontaine, M.N.; Dunstetter, F.; Signes-Frehel, M.; Mounanga, P.; Cherkaoui, K.; Khelidj, A. Effect of polycarboxylate and crushed quartz in UHPC: Microstructural investigation. *Constr. Build. Mater.* **2013**, *44*, 699–705, doi:10.1016/j.conbuildmat.2013.03.077.
30. IS: 10262 - 2019 Indian Standard Concrete Mix Proportioning - Guidelines. *Bur. Indian Stand. Delhi* **2019**.
31. Soliman, A.M.; Nehdi, M.L. Effect of drying conditions on autogenous shrinkage in ultra-high performance concrete at early-age. *Mater. Struct. Constr.* **2011**, *44*, 879–899, doi:10.1617/s11527-010-9670-0.
32. Oey, T.; Kumar, A.; Bullard, J.W.; Neithalath, N.; Sant, G. The filler effect: The influence of filler content and surface area on cementitious reaction rates. *J. Am. Ceram. Soc.* **2013**, *96*, 1978–1990, doi:10.1111/jace.12264.
33. Yu, R.; Spiesz, P.; Brouwers, H.J.H. Mix design and properties assessment of Ultra-High Performance Fibre Reinforced Concrete (UHPFRC). *Cem. Concr. Res.* **2014**, *56*, 29–39, doi:10.1016/j.cemconres.2013.11.002.
34. Liu, Z.; Jiao, W.; Sha, A.; Gao, J.; Han, Z.; Xu, W. Portland Cement Hydration Behavior at Low Temperatures: Views from Calculation and Experimental Study. *Adv. Mater. Sci. Eng.* **2017**, *2017*, 1–9, doi:10.1155/2017/3927106.
35. Klemm, A.J.; Klemm, P. Ice formation in pores in polymer modified concrete - II. The influence of the admixtures on the water to ice transition in cementitious composites subjected to freezing/thawing cycles. *Build. Environ.* **1997**, *32*, 199–202, doi:10.1016/S0360-1323(96)00054-6.
36. Brun, M.; Lallemand, A.; Quinson, J.F.; Eyraud, C. A new method for the simultaneous determination of the size and shape of pores: the thermoporometry. *Thermochim. Acta* **1977**, *21*, 59–88, doi:10.1016/0040-6031(77)85122-8.
37. Kaufmann, J.P. Experimental identification of ice formation in small concrete pores. *Cem. Concr. Res.* **2004**, *34*, 1421–1427, doi:10.1016/j.cemconres.2004.01.022.
38. Wu, M.; Johannesson, B.; Geiker, M. Determination of ice content in hardened concrete by low-temperature calorimetry: Influence of baseline calculation and heat of fusion of confined water. *J. Therm. Anal. Calorim.* **2014**, *115*, 1335–1351, doi:10.1007/s10973-013-3520-6.
39. Diamond, S. Aspects of concrete porosity revisited. *Cem. Concr. Res.* **1999**, *29*, 1181–1188, doi:10.1016/S0008-8846(99)00122-2.
40. Farnam, Y.; Villani, C.; Washington, T.; Spence, M.; Jain, J.; Jason Weiss, W. Performance of carbonated calcium silicate based cement pastes and mortars exposed

- to NaCl and MgCl₂ deicing salt. *Constr. Build. Mater.* **2016**, *111*, 63–71, doi:10.1016/j.conbuildmat.2016.02.098.
41. Dong, S.; Feng, D.; Jiang, S.; Zhu, W. Effect of freezing temperature on the microstructure of negative temperature concrete. In Proceedings of the Advanced Materials Research; 2013; pp. 343–348.
 42. Pigeon, M. *Durability of Concrete in Cold Climates*; 2014;
 43. Barna, L.A.; Seman, P.M.; Korhonen, C.J. Energy-Efficient Approach to Cold-Weather Concreting. *J. Mater. Civ. Eng.* **2011**, *23*, 1544–1551, doi:10.1061/(ASCE)MT.1943-5533.0000262.
 44. Ogurtsova, Y.N.; Zhernovsky, I. V; Botsman, L.N. Efficiency of Composite Binders with Antifreezing Agents. In Proceedings of the IOP Conference Series: Materials Science and Engineering; Institute of Physics Publishing, 2017; Vol. 262.
 45. Polat, R.; Demirboğa, R.; Karakoç, M.B.; Türkmen, I. The influence of lightweight aggregate on the physico-mechanical properties of concrete exposed to freeze-thaw cycles. *Cold Reg. Sci. Technol.* **2010**, *60*, 51–56, doi:10.1016/j.coldregions.2009.08.010.
 46. Kothari, A.; Hedlund, H.; Illikainen, M.; Cwirzen, A. Effects of sodium nitrate and OPC-GGBS concrete mix composition on phase transition of pore water at subzero temperatures. *Constr. Build. Mater.* **2022**, doi:10.1016/j.conbuildmat.2022.126901.
 47. Dai, J.; Wang, Q.; Lou, X.; Bao, X.; Zhang, B.; Wang, J.; Zhang, X. Solution calorimetry to assess effects of water-cement ratio and low temperature on hydration heat of cement. *Constr. Build. Mater.* **2021**, *269*, doi:10.1016/j.conbuildmat.2020.121222.
 48. Kosmatka, S.H.; Wilson, M.L. Chapter 17 - Cold Weather Concreting. In *Design and Controls of Concrete Mixtures*; Portland Cement Association, 2011; pp. 327–343 ISBN 0-89312-272-6.
 49. American Concrete Institute (ACI) ACI 306R-10. *Am. Concr. Inst.* **2016**.
 50. Jokela, J.; Kivekas, L.; Kukko, H.; Ratvio, J.; Rissanen, E. *Arctic Concrete Technology - Research Report 343*; Technical Research Center of Finland (VTT), Concrete and Silicate Laboratory: Finland, 1982;
 51. Scanlon, J.M.; Ryan, R.J. Placing cold weather concrete. *Constr. Specif.* **1989**, *42*, 58–65.
 52. Klieger, P. Effect of Mixing and Curing Temperature on Concrete Strength. *J. Proc.* **1958**, *54*, 1063–1081.
 53. Stormer, C.D. *Cold Concrete - Technical Report 220*; Hanover, NH, 1970;
 54. Price, W.H. Factors Influencing Concrete Strength. *ACI J. Proc.* **1951**, *47*, 41–432, doi:10.14359/12003.
 55. Shideler, J.J. Calcium Chloride in Concrete. *ACI J. Proc.* **1952**, *48*, 537–559, doi:10.14359/11939.

56. Kessler, S.; Thiel, C.; Grosse, C.U.; Gehlen, C. Effect of freeze–thaw damage on chloride ingress into concrete. *Mater. Struct. Constr.* **2017**, *50*, 1–13, doi:10.1617/s11527-016-0984-4.
57. Sutter, L.; Peterson, K.; Julio-Betancourt, G.; Hooton, D.; Van Dam, T. Van; Smith, K. *The deleterious chemical effects of concentrated deicing solutions on Portland cement concrete*; Houghton, MI, 2008;
58. Franke, W.; Thiel, C.; Duran, F.; Gehlen, C. Effect of Calcium Nitrate on the freeze-thaw-resistance of concrete. *Betonw. und Fert. Plant Precast Technol.* **2015**, *81*, 34–42.
59. Sobolev, K.G.; Batrakov, V.G. Effect of a polyethylhydrosiloxane admixture on the durability of concrete with supplementary cementitious materials. *J. Mater. Civ. Eng.* **2007**, *19*, 809–819, doi:10.1061/(ASCE)0899-1561(2007)19:10(809).
60. Hazaree, C.; Ceylan, H.; Wang, K. Influences of mixture composition on properties and freeze-thaw resistance of RCC. *Constr. Build. Mater.* **2011**, *25*, 313–319, doi:10.1016/j.conbuildmat.2010.06.023.
61. Karagöl, F.; Yegin, Y.; Polat, R.; Benli, A.; Demirboğa, R. The influence of lightweight aggregate, freezing–thawing procedure and air entraining agent on freezing–thawing damage. *Struct. Concr.* **2018**, *19*, 1328–1340, doi:10.1002/suco.201700133.
62. Barna, L.A.; Seman, P.M.; Korhonen, C.J. *Cold Weather Admixture Systems Demonstration at Fort Wainwright, Alaska*; Hanover, NH, 2010;
63. Kothari, A.; Habermehl-Cwirzen, K.; Hedlund, H.; Cwirzen, A. A review of the mechanical properties and durability of ecological concretes in a cold climate in comparison to standard ordinary portland cement-based concrete. *Materials (Basel)*. **2020**, *13*, 32, doi:10.3390/MA13163467.
64. Justnes, H.; Nygaard, E.C. Technical calcium nitrate as set accelerator for cement at low temperatures. *Cem. Concr. Res.* **1995**, *25*, 1766–1774, doi:10.1016/0008-8846(95)00172-7.
65. Kumar, A.; Bishnoi, S.; Scrivener, K.L. Modelling early age hydration kinetics of alite. *Cem. Concr. Res.* **2012**, *42*, 903–918, doi:10.1016/j.cemconres.2012.03.003.
66. Ratinov, V.B.; Rosenberg, T.I. Antifreezing Admixtures. In *Concrete Admixtures Handbook - Properties, Science and Technology*; Noyes Publications: New Jersey, 1995; pp. 740–799.
67. Myrdal, R. *Accelerating Admixtures for Concrete. State of the Art*; COIN Concrete Innovation Centre: Norway, 2007; ISBN 9788253609898.
68. Arslan, M.; Çullu, M.; Durmuş, G. The effect of antifreeze admixtures on compressive strength of concretes subjected to frost action. *Gazi Univ. J. Sci.* **2011**, *24*, 299–307.
69. Reddy, P.N.; Naqash, J.A. Effect of Antifreeze Admixtures on Cold Weather Concrete. *Int. J. Eng.* **2019**, *32*, 366–372, doi:10.5829/ije.2019.32.03c.03.
70. Mironov, S.A.; Lagoyda, A. V; Ukhov, Y.N. *Curing Concrete with Chemical Additives in Freezing Weather*; Hanover, NH, 1976;

71. Hooton, R.; Johnston, C.; Rixom, R.; Mailvaganam, N. *Chemical Admixtures for Concrete third edition*; E & FN Spon: London, 1999; ISBN 041922520X.
72. Sakai, K.; Watanabe, H.; Nomachi, H.; Hamabe, K. Antifreeze admixture developed in Japan. *Concr. Int.* **1991**, *13*, 26–30.
73. Justnes, H. Explanation of Long-Term Compressive Strength of Concrete Caused By the Set Accelerator Calcium Nitrate. In Proceedings of the 11th International Congress on the Chemistry of Cement.; Durba, South Africa, 2003; Vol. 11, p. 475.
74. Mason, M.R.; Schroeder, H.P. Freeze-thaw durability of concrete cured below 0°C using antifreeze admixtures. In Proceedings of the Proceedings of the Eighth International Conference on Cold Regions Engineering; American Society of Civil Engineers: Alaska, U. S., 1996; pp. 185–195.
75. Mou, T.; Zhou, X.; Fan, B.; Ding, Q. Frost resistance of steel fiber reinforced micro-expansive concrete filled steel tube. *Appl. Mech. Mater.* **2012**, *204–208*, 3956–3960, doi:10.4028/www.scientific.net/AMM.204-208.3956.
76. Korhonen, Charles J Cortex, E.R.; Durning, T.A.; Jeknavorian, A.A. *Antifreeze Admixtures for Concrete - Special Report SP-97-26*; Hanover, NH, 1997;
77. Kivekäs, L.; Huovinen, S.; Leivo, M. *Concrete under arctic conditions*; VTT Technical Research Centre of Finland: Finland, 1985; Vol. 343; ISBN 951-38-2256-7.
78. Kivekas, L.; Kukko, H. STRENGTH DEVELOPMENT AND FROST RESISTANCE OF CONCRETE AT LOW TEMPERATURES. *Nord. Concr. Res.* **1983**, *2*, 137–148.
79. Wise, T.; Ramachandran, V.S.; Polomark, G.M. The effect of thiocyanates on the hydration of portland cement at low temperatures. *Thermochim. Acta* **1995**, *264*, 157–171, doi:10.1016/0040-6031(95)02323-T.
80. Brook, J.W.; Factor, D.F.; Kinney Frederick, D.; Sarkar, A.K. COLD WEATHER ADMIXTURE. *Concr. Int.* **1988**, *10*, 44–49.
81. Çullu, M.; Arslan, M. The effects of chemical attacks on physical and mechanical properties of concrete produced under cold weather conditions. *Constr. Build. Mater.* **2014**, *57*, 53–60, doi:10.1016/j.conbuildmat.2014.01.072.
82. Jiang, S.; Guan, X.; Dong, S.; Zhu, W. Application of C50 negative temperature concrete in bridge engineering. In Proceedings of the ICTE 2013 - Proceedings of the 4th International Conference on Transportation Engineering; American Society of Civil Engineers: Chengdu, China, 2013; pp. 3021–3026.
83. Nagrockienė, D.; Daugėla, A. Investigation into the properties of concrete modified with biomass combustion fly ash. *Constr. Build. Mater.* **2018**, *174*, 369–375, doi:10.1016/j.conbuildmat.2018.04.125.
84. Dong, S.; Feng, D.; Jiang, S.; Zhu, W. Effect of a new type antifreeze agent on the mechanical behavior of negative temperature concrete. In Proceedings of the ICTE 2013 - Proceedings of the 4th International Conference on Transportation Engineering; 2013; pp. 3027–3032.
85. Munteanu, C.; Georgescu, M. The influence of fly ash addition (of CET Govora origin)

- on some properties of concretes. *Univ. Politeh. Bucharest Sci. Bull. Ser. B - Chem. Mater. Sci.* **2013**, *75*, 43–52.
86. Feldman, R.F. Influence of Condensed Silica Fume and Sand/Cement Ratio on Pore Structure and Frost Resistance of Portland Cement Mortars. *Publ. SP - Am. Concr. Inst.* **1986**, *91*, 973–990.
 87. Karakurt, C.; Bayazit, Y. Freeze-thaw resistance of normal and high strength concretes produced with fly ash and silica fume. *Adv. Mater. Sci. Eng.* **2015**, *2015*, 8, doi:10.1155/2015/830984.
 88. Khan, M.I.; Siddique, R. Utilization of silica fume in concrete: Review of durability properties. *Resour. Conserv. Recycl.* **2011**, *57*, 30–35, doi:10.1016/j.resconrec.2011.09.016.
 89. Fediuk, R.; Timokhin, R.; Mochalov, A.; Otsokov, K.; Lashina, I. Performance properties of high-density impermeable cementitious paste. *J. Mater. Civ. Eng.* **2019**, *31*, doi:10.1061/(ASCE)MT.1943-5533.0002633.
 90. Chung, C.W.; Shon, C.S.; Kim, Y.S. Chloride ion diffusivity of fly ash and silica fume concretes exposed to freeze-thaw cycles. *Constr. Build. Mater.* **2010**, *24*, 1739–1745, doi:10.1016/j.conbuildmat.2010.02.015.
 91. Jang, Y. Il; Park, W.S.; Kim, S.W.; Yun, S.H.; Yun, H. Do; Khil, B.S.; Kim, D.G. Influence of cold weather on compressive strength in high performance with silica fume. *Key Eng. Mater.* **2015**, *627*, 445–448, doi:10.4028/www.scientific.net/KEM.627.445.
 92. Cwirzen, A.; Penttala, V. Aggregate-cement paste transition zone properties affecting the salt-frost damage of high-performance concretes. *Cem. Concr. Res.* **2005**, *35*, 671–679, doi:10.1016/j.cemconres.2004.06.009.
 93. Kjellsen, K.O.; Wallevik, O.H.; Fjällberg, L. Microstructure and microchemistry of the paste-aggregate interfacial transition zone of high-performance concrete. *Adv. Cem. Res.* **1998**, *10*, 30–40, doi:10.1680/adcr.1998.10.1.33.
 94. Toutanji, H.; Delatte, N.; Aggoun, S.; Duval, R.; Danson, A. Effect of supplementary cementitious materials on the compressive strength and durability of short-term cured concrete. *Cem. Concr. Res.* **2004**, *34*, 311–319, doi:10.1016/j.cemconres.2003.08.017.
 95. Yazici, H. The effect of silica fume and high-volume Class C fly ash on mechanical properties, chloride penetration and freeze-thaw resistance of self-compacting concrete. *Constr. Build. Mater.* **2008**, *22*, 456–462, doi:10.1016/j.conbuildmat.2007.01.002.
 96. Gebler, S.; Klieger, P. EFFECT OF FLY ASH ON THE AIR-VOID STABILITY OF CONCRETE. In Proceedings of the Publication SP - 9 - American Concrete Institute; 1983; pp. 103–120.
 97. Shon, C.S.; Abdigaliyev, A.; Bagitova, S.; Chung, C.W.; Kim, D. Determination of air-void system and modified frost resistance number for freeze-thaw resistance evaluation of ternary blended concrete made of ordinary Portland cement/silica fume/class F fly ash. *Cold Reg. Sci. Technol.* **2018**, *155*, 127–136, doi:10.1016/j.coldregions.2018.08.003.

98. Alkaysi, M.; El-Tawil, S.; Liu, Z.; Hansen, W. Effects of silica powder and cement type on durability of ultra high performance concrete (UHPC). *Cem. Concr. Compos.* **2016**, *66*, 47–56, doi:10.1016/j.cemconcomp.2015.11.005.
99. Liu, Z.; El-Tawil, S.; Hansen, W.; Wang, F. Effect of slag cement on the properties of ultra-high performance concrete. *Constr. Build. Mater.* **2018**, *190*, 830–837, doi:10.1016/j.conbuildmat.2018.09.173.
100. Tavasoli, S.; Nili, M.; Serpoosh, B. Effect of GGBS on the frost resistance of self-consolidating concrete. *Constr. Build. Mater.* **2018**, *165*, 717–722, doi:10.1016/j.conbuildmat.2018.01.027.
101. Shang, H.; Song, Y.; Ou, J. Behavior of air-entrained concrete after freeze-thaw cycles. *Acta Mech. Solida Sin.* **2009**, *22*, 261–266, doi:10.1016/S0894-9166(09)60273-1.
102. Raczkiwicz, W.; Grzmil, W.; Zapala-Slaweta, J. Impact of the air-entrained concrete with the blast-furnace slag cement on the intensity of reinforcement corrosion process. In Proceedings of the MATEC Web of Conferences - MATBUD'2018 – 8th Scientific-Technical Conference on Material Problems in Civil Engineering; 2018; Vol. 163, pp. 1–8.
103. Sahmaran, M.; Yildirim, G.; Erdem, T.K. Self-healing capability of cementitious composites incorporating different supplementary cementitious materials. *Cem. Concr. Compos.* **2013**, *35*, 89–101, doi:10.1016/j.cemconcomp.2012.08.013.
104. Strokova, V.V.; Botsman, L.N.; Ogurtsova, Y.N.; Nelubova, V.V. The efficiency of using antifreezing agents in monolithic construction. In Proceedings of the Proceedings of ECOS 2016: The 29th International Conference on Efficiency, Cost, Optimization, Simulation and Environmental Impact of Energy Systems; Portoroz, Slovenia, 2016; pp. 19–23.
105. Ratajczak, M.; Babiak, M.; Kulczewski, P.; Kosno, J. Diamidoamine Salt as the Admixture for Concrete Increasing the Resistance to the Freeze-Thaw Cycle. In Proceedings of the IOP Conference Series: Materials Science and Engineering; Yilmaz, I., Coisson, E., Segalini, A., Marschalko, M., Rybak, J., Decky, M., Drusa, M., Dabija, A.-M., Eds.; Institute of Physics Publishing: Prague, 2019; Vol. 471.
106. Shi, X.; Fay, L.; Peterson, M.M.; Berry, M.; Mooney, M. A FESEM/EDX investigation into how continuous deicer exposure affects the chemistry of Portland cement concrete. *Constr. Build. Mater.* **2011**, *25*, 957–966, doi:10.1016/j.conbuildmat.2010.06.086.
107. Jiang, L.; Niu, D.; Yuan, L.; Fei, Q. Durability of concrete under sulfate attack exposed to freeze-thaw cycles. *Cold Reg. Sci. Technol.* **2015**, *112*, 112–117, doi:10.1016/j.coldregions.2014.12.006.
108. Niu, D.; Jiang, L.; Fei, Q. Deterioration mechanism of sulfate attack on concrete under freeze-thaw cycles. *J. Wuhan Univ. Technol. Mater. Sci. Ed.* **2013**, *28*, 1172–1176, doi:10.1007/s11595-013-0839-6.
109. Mu, R.; Miao, C.; Liu, J.; Sun, W. Effect of NaCl and Na₂SO₄ solution on the frost resistance of concrete and its mechanism. *Kuei Suan Jen Hsueh Pao/ J. Chinese Ceram. Soc.* **2001**, *29*, 523–529.

110. Yamato, T.; Emoto, Y.; Soeda, M. STRENGTH AND FREEZING-AND-THAWING RESISTANCE OF CONCRETE INCORPORATING CONDENSED SILICA FUME. *Publ. SP - Am. Concr. Inst.* **1986**, *91*, 1095–1117.
111. Sabir, B.B. Mechanical properties and frost resistance of silica fume concrete. *Cem. Concr. Compos.* **1997**, *19*, 285–294, doi:10.1016/S0958-9465(97)00020-6.
112. Sobolev, K.G.; Soboleva, S.V. High-Performance Concrete Mixture Proportioning. *Spec. Publ.* **1998**, *179*, 421–438.
113. Mardani-Aghabaglou, A.; Inan Sezer, G.; Ramyar, K. Comparison of fly ash, silica fume and metakaolin from mechanical properties and durability performance of mortar mixtures view point. *Constr. Build. Mater.* **2014**, *70*, 17–25, doi:10.1016/j.conbuildmat.2014.07.089.
114. Cohen, M.D.; Yixia, Z.; Dolch, W.L. Non-air-entrained high-strength concrete - Is it frost resistant? *ACI Mater. J.* **1992**, *89*, 406–415, doi:10.14359/2582.
115. Turk, K.; Kina, C. Freeze-thaw resistance and sorptivity of self-compacting mortar with ternary blends. *Comput. Concr.* **2018**, *21*, 149–156, doi:10.12989/cac.2018.21.2.149.
116. Benli, A.; Turk, K.; Kina, C. Influence of silica fume and class F fly ash on mechanical and rheological properties and freeze-thaw durability of self-compacting mortars. *J. Cold Reg. Eng.* **2018**, *32*, doi:10.1061/(ASCE)CR.1943-5495.0000167.
117. Abbaszadeh, R.; Modarres, A. Freeze-thaw durability of non-air-entrained roller compacted concrete designed for pavement containing cement kiln dust. *Cold Reg. Sci. Technol.* **2017**, *141*, 16–27, doi:10.1016/j.coldregions.2017.05.007.
118. Duan, P.; Shui, Z.; Chen, W.; Shen, C. Enhancing microstructure and durability of concrete from ground granulated blast furnace slag and metakaolin as cement replacement materials. *J. Mater. Res. Technol.* **2013**, *2*, 52–59, doi:10.1016/j.jmrt.2013.03.010.
119. Zhang, L.; Glasser, F.P. Investigation of the microstructure and carbonation of CSA-based concretes removed from service. *Cem. Concr. Res.* **2005**, *35*, 2252–2260, doi:10.1016/j.cemconres.2004.08.007.
120. Yoon, H.N.; Seo, J.; Kim, S.; Lee, H.K.; Park, S. Hydration of calcium sulfoaluminate cement blended with blast-furnace slag. *Constr. Build. Mater.* **2021**, *268*, 1–16, doi:10.1016/j.conbuildmat.2020.121214.
121. Andac, O.; Glasser, F.P. Microstructure and microchemistry of calcium sulfoaluminate cement. *Mater. Res. Soc. Symp. - Proc.* **1994**, *370*, 135–142, doi:10.1557/proc-370-143.
122. Hargis, C.W. *Advances in Sustainable Cements*, UC Berkeley, 2013.
123. Winnefeld, F.; Martin, L.H.J.; Müller, C.J.; Lothenbach, B. Using gypsum to control hydration kinetics of CSA cements. *Constr. Build. Mater.* **2017**, *155*, 154–163, doi:10.1016/j.conbuildmat.2017.07.217.
124. Alzaza, A.; Ohenoja, K.; Isteri, V.; Hanein, T.; Geddes, D.; Poikelispää, M.; Illikainen, M. Blending eco-efficient calcium sulfoaluminate belite ferrite cement to enhance the

- physico-mechanical properties of Portland cement paste cured in refrigerated and natural winter conditions. *Cem. Concr. Compos.* **2022**, *129*, 1–15, doi:10.1016/j.cemconcomp.2022.104469.
125. Qin, L.; Gao, X.; Zhang, A. Potential application of Portland cement-calcium sulfoaluminate cement blends to avoid early age frost damage. *Constr. Build. Mater.* **2018**, *190*, 363–372, doi:10.1016/j.conbuildmat.2018.09.136.
 126. Pelletier, L.; Winnefeld, F.; Lothenbach, B. The ternary system Portland cement-calcium sulfoaluminate clinker-anhydrite: Hydration mechanism and mortar properties. *Cem. Concr. Compos.* **2010**, *32*, 497–507, doi:10.1016/j.cemconcomp.2010.03.010.
 127. Won, J.P.; Hwang, U.J.; Kim, C.K.; Lee, S.J. Mechanical performance of shotcrete made with a high-strength cement-based mineral accelerator. *Constr. Build. Mater.* **2013**, *49*, 175–183, doi:10.1016/j.conbuildmat.2013.08.014.
 128. Péra, J.; Ambroise, J.; Holard, E.; Beauvent, G. INFLUENCE OF THE TYPE OF CALCIUM SULFATE ON THE PROPERTIES OF CALCIUM SULFOALUMINATE CEMENT. In Proceedings of the 11th International Congress on the Chemistry of Cement.; 2003; pp. 1129–1135.
 129. Winnefeld, F.; Barlag, S. Calorimetric and thermogravimetric study on the influence of calcium sulfate on the hydration of ye'elimite. *J. Therm. Anal. Calorim.* **2010**, *101*, 949–957, doi:10.1007/s10973-009-0582-6.
 130. Pace, M.L.; Telesca, A.; Marroccoli, M.; Valenti, G.L. Use of industrial byproducts as alumina sources for the synthesis of calcium sulfoaluminate cements. *Environ. Sci. Technol.* **2011**, *45*, 6124–6128, doi:10.1021/es2005144.
 131. Afroughsabet, V.; Biolzi, L.; Monteiro, P.J.M.; Gastaldi, M.M. Investigation of the mechanical and durability properties of sustainable high performance concrete based on calcium sulfoaluminate cement. *J. Build. Eng.* **2021**, *43*, doi:10.1016/j.jobe.2021.102656.
 132. Li, P.; Gao, X.; Wang, K.; Tam, V.W.Y.; Li, W. Hydration mechanism and early frost resistance of calcium sulfoaluminate cement concrete. *Constr. Build. Mater.* **2020**, *239*, doi:10.1016/j.conbuildmat.2019.117862.
 133. Pacheco-Torgal, F.; Melchers, R.E.; Shi, X.; De Belie, N.; Van Tittelboom, K.; Sáez, A. *Eco-efficient Repair and Rehabilitation of Concrete Infrastructures*; Woodhead Publishing, 2018; ISBN 9780081021811.
 134. Kothari, A.; Tole, I.; Hedlund, H.; Ellison, T.; Cwirzen, A. Partial replacement of OPC with CSA cements – effects on hydration, fresh and hardened properties. *Adv. Cem. Res.* **2022**, 1–38, doi:10.1680/jadcr.22.00054.
 135. Álvarez-Pinazo, G.; Santacruz, I.; León-Reina, L.; Aranda, M.A.G.; De La Torre, A.G. Hydration reactions and mechanical strength developments of iron-rich sulfobelite eco-cements. *Ind. Eng. Chem. Res.* **2013**, *52*, 16606–16614, doi:10.1021/ie402484e.
 136. Huang, G.; Pudasainee, D.; Gupta, R.; Liu, W.V. Hydration reaction and strength development of calcium sulfoaluminate cement-based mortar cured at cold temperatures. *Constr. Build. Mater.* **2019**, *224*, 493–503,

doi:10.1016/j.conbuildmat.2019.07.085.

137. Le Saoût, G.; Lothenbach, B.; Hori, A.; Higuchi, T.; Winnefeld, F. Hydration of Portland cement with additions of calcium sulfoaluminates. *Cem. Concr. Res.* **2013**, *43*, 81–94, doi:10.1016/j.cemconres.2012.10.011.
138. Trauchessec, R.; Mechling, J.M.; Lecomte, A.; Roux, A.; Le Rolland, B. Hydration of ordinary Portland cement and calcium sulfoaluminate cement blends. *Cem. Concr. Compos.* **2015**, *56*, 106–114, doi:10.1016/j.cemconcomp.2014.11.005.
139. Telesca, A.; Marroccoli, M.; Pace, M.L.; Tomasulo, M.; Valenti, G.L.; Monteiro, P.J.M. A hydration study of various calcium sulfoaluminate cements. *Cem. Concr. Compos.* **2014**, *53*, 224–232, doi:10.1016/j.cemconcomp.2014.07.002.
140. Michel, M.; Georgin, J.F.; Ambroise, J.; Péra, J. The influence of gypsum ratio on the mechanical performance of slag cement accelerated by calcium sulfoaluminate cement. *Constr. Build. Mater.* **2011**, *25*, 1298–1304, doi:10.1016/j.conbuildmat.2010.09.015.
141. Tang, S.W.; Zhu, H.G.; Li, Z.J.; Chen, E.; Shao, H.Y. Hydration stage identification and phase transformation of calcium sulfoaluminate cement at early age. *Constr. Build. Mater.* **2015**, *75*, 11–18, doi:10.1016/j.conbuildmat.2014.11.006.
142. Bertola, F.; Gastaldi, D.; Canonico, F.; Paul, G. CSA and slag: Towards CSA composite binders. *Adv. Cem. Res.* **2019**, *31*, 147–158, doi:10.1680/jadcr.18.00105.
143. Gao, D.; Meng, Y.; Yang, L.; Tang, J.; Lv, M. Effect of ground granulated blast furnace slag on the properties of calcium sulfoaluminate cement. *Constr. Build. Mater.* **2019**, *227*, 1–9, doi:10.1016/j.conbuildmat.2019.08.046.
144. Zhang, Y.; Zhang, C.; Zhu, Y.; Cao, J.; Shao, X. An experimental study: various influence factors affecting interfacial shear performance of UHPC-NSC. *Constr. Build. Mater.* **2020**, *236*, 1–15, doi:10.1016/j.conbuildmat.2019.117480.
145. Brühwiler, E.; Denarié, E. Rehabilitation and strengthening of concrete structures using ultra-high performance fibre reinforced concrete. *Struct. Eng. Int. J. Int. Assoc. Bridg. Struct. Eng.* **2013**, *23*, 450–457, doi:10.2749/101686613X13627347100437.
146. Gadri, K.; Guettala, A. Evaluation of bond strength between sand concrete as new repair material and ordinary concrete substrate (The surface roughness effect). *Constr. Build. Mater.* **2017**, *157*, 1133–1144, doi:10.1016/j.conbuildmat.2017.09.183.
147. Hussein, H.H.; Walsh, K.K.; Sargand, S.M.; Steinberg, E.P. Interfacial properties of ultrahigh-performance concrete and high-strength concrete bridge connections. *J. Mater. Civ. Eng.* **2016**, *28*, doi:10.1061/(ASCE)MT.1943-5533.0001456.
148. Perez, F.; Bissonnette, B.; Gagné, R. Parameters affecting the debonding risk of bonded overlays used on reinforced concrete slab subjected to flexural loading. *Mater. Struct. Constr.* **2009**, *42*, 645–662, doi:10.1617/s11527-008-9410-x.
149. Beushausen, H. The influence of concrete substrate preparation on overlay bond strength. *Mag. Concr. Res.* **2010**, *62*, 845–852, doi:10.1680/macrc.2010.62.11.845.
150. Beushausen, H.; Höhlig, B.; Talotti, M. The influence of substrate moisture preparation on bond strength of concrete overlays and the microstructure of the OTZ.

- Cem. Concr. Res.* **2017**, *92*, 84–91, doi:10.1016/j.cemconres.2016.11.017.
151. Courard, L.; Piotrowski, T.; Garbacz, A. Near-to-surface properties affecting bond strength in concrete repair. *Cem. Concr. Compos.* **2014**, *46*, 73–80, doi:10.1016/j.cemconcomp.2013.11.005.
 152. Júlio, E.N.B.S.; Branco, F.A.B.; Silva, V.D. Concrete-to-concrete bond strength. Influence of the roughness of the substrate surface. *Constr. Build. Mater.* **2004**, *18*, 675–681, doi:10.1016/j.conbuildmat.2004.04.023.
 153. Jang, H.O.; Lee, H.S.; Cho, K.; Kim, J. Experimental study on shear performance of plain construction joints integrated with ultra-high performance concrete (UHPC). *Constr. Build. Mater.* **2017**, *152*, 16–23, doi:10.1016/j.conbuildmat.2017.06.156.
 154. Hong, S.G.; Kang, S.H. Effect of surface preparation and curing method on bond strength between UHPC and normal strength concrete. *IABSE Conf. Geneva 2015 Struct. Eng. Provid. Solut. to Glob. Challenges - Rep.* **2015**, *105*, 1–7, doi:10.2749/222137815818358925.
 155. Qian, J.; You, C.; Wang, Q.; Wang, H.; Jia, X. A method for assessing bond performance of cement-based repair materials. *Constr. Build. Mater.* **2014**, *68*, 307–313, doi:10.1016/j.conbuildmat.2014.06.048.
 156. Barros, J.A.O.; Cruz, J.M.S. STRENGTHENING A PRESTRESSED CONCRETE SLAB BY EPOXY-BONDED FRP COMPOSITES AND SFRC OVERLAYER Laminates of carbon fibre reinforced polymer (CFRP), layer of steel fibre reinforced concrete (SFRC) and the simultaneous use of CFRP laminates and SFRC overla. In Proceedings of the Proceedings of the seventh international conference on inspection appraisal repairs & maintenance of buildings & structures.; Nottingham Trent University, UK., 2001.
 157. Graybeal, B.A. *Material Property Characterization of Ultra-High Performance Concrete*; 2006; Vol. HRT-06-103;
 158. Haber, Z.B.; Munoz, J.F.; De la Varga, I.; Graybeal, B.A. Bond characterization of UHPC overlays for concrete bridge decks: Laboratory and field testing. *Constr. Build. Mater.* **2018**, *190*, 1056–1068, doi:10.1016/j.conbuildmat.2018.09.167.
 159. Yoo, D.Y.; Min, K.H.; Lee, J.H.; Yoon, Y.S. Shrinkage and cracking of restrained ultra-high-performance fiber-reinforced concrete slabs at early age. *Constr. Build. Mater.* **2014**, *73*, 357–365, doi:10.1016/j.conbuildmat.2014.09.097.
 160. Granger, S.; Loukili, A.; Pijaudier-Cabot, G.; Chanvillard, G. Experimental characterization of the self-healing of cracks in an ultra high performance cementitious material: Mechanical tests and acoustic emission analysis. *Cem. Concr. Res.* **2007**, *37*, 519–527, doi:10.1016/j.cemconres.2006.12.005.
 161. Richard, P.; Cheyrezy, M. Composition of reactive powder concretes. *Cem. Concr. Res.* **1995**, *25*, 1501–1511, doi:10.1016/0008-8846(95)00144-2.
 162. Park, J.J.; Kang, S.T.; Koh, K.T.; Kim, S.W.; Fehling, E. *Influence of the Ingredients on the Compressive Strength of UHPC as a Fundamental Study to Optimize the Mixing Proportion*; 2008; ISBN 9783899583762.
 163. Yu, R.; Spiesz, P.; Brouwers, H.J.H. Development of an eco-friendly Ultra-High

- Performance Concrete (UHPC) with efficient cement and mineral admixtures uses. *Cem. Concr. Compos.* **2015**, *55*, 383–394, doi:10.1016/j.cemconcomp.2014.09.024.
164. Li, W.; Huang, Z.; Cao, F.; Sun, Z.; Shah, S.P. Effects of nano-silica and nano-limestone on flowability and mechanical properties of ultra-high-performance concrete matrix. *Constr. Build. Mater.* **2015**, *95*, 366–374, doi:10.1016/j.conbuildmat.2015.05.137.
 165. Bentz, D.P.; Ardani, A.; Barrett, T.; Jones, S.Z.; Lootens, D.; Peltz, M.A.; Sato, T.; Stutzman, P.E.; Tanesi, J.; Weiss, W.J. Multi-scale investigation of the performance of limestone in concrete. *Constr. Build. Mater.* **2015**, *75*, 1–10, doi:10.1016/j.conbuildmat.2014.10.042.
 166. Camiletti, J.; Soliman, A.M.; Nehdi, M.L. Effects of nano- and micro-limestone addition on early-age properties of ultra-high-performance concrete. *Mater. Struct. Constr.* **2013**, *46*, 881–898, doi:10.1617/s11527-012-9940-0.
 167. Lothenbach, B.; Le Saout, G.; Gallucci, E.; Scrivener, K. Influence of limestone on the hydration of Portland cements. *Cem. Concr. Res.* **2008**, *38*, 848–860, doi:10.1016/j.cemconres.2008.01.002.
 168. Bédérina, M.; Khenfer, M.M.; Dheilly, R.M.; Quéneudec, M. Reuse of local sand: Effect of limestone filler proportion on the rheological and mechanical properties of different sand concretes. *Cem. Concr. Res.* **2005**, *35*, 1172–1179, doi:10.1016/j.cemconres.2004.07.006.
 169. Péra, J.; Husson, S.; Guilhot, B. Influence of finely ground limestone on cement hydration. *Cem. Concr. Compos.* **1999**, *21*, 99–105, doi:10.1016/S0958-9465(98)00020-1.
 170. Hewlett, P.C.; Liska, M. *Lea's chemistry of cement and concrete*; 2019; ISBN 9780081007730.
 171. Camiletti, J.; Soliman, A.M.; Nehdi, M.L. Effect of limestone addition on early-age properties of ultra high-performance concrete. *Proc. Inst. Civ. Eng. Constr. Mater.* **2014**, *167*, 65–78, doi:10.1680/coma.11.00064.
 172. Abbas, S.; Soliman, A.M.; Nehdi, M.L. Exploring mechanical and durability properties of ultra-high performance concrete incorporating various steel fiber lengths and dosages. *Constr. Build. Mater.* **2015**, *75*, 429–441, doi:10.1016/j.conbuildmat.2014.11.017.
 173. de Larrard, F.; Sedran, T. Optimization of ultra-high-performance concrete by the use of a packing model. *Cem. Concr. Res.* **1994**, *24*, 997–1009, doi:10.1016/0008-8846(94)90022-1.
 174. ASTM C191 - 19 - Standard test methods for Time of Setting of Hydraulic Cement by Vicat Needle. *ASTM Int.* **2019**.
 175. British Standards Institution BS EN 12350-8:2010 Testing fresh concrete Part 8: Self-compacting concrete - Slump-flow test. *Br. Stand.* **2010**.
 176. British Standards Institution BS EN 12390-3:2009 Testing hardened concrete Part 3: Compressive strength of test specimens. *Br. Stand.* **2009**.

177. BS1881-125 Testing concrete — Part 4: Determination of ultrasonic pulse velocity. *Br. Stand.* **2004**, doi:Construction Standard, CS1:2010.
178. Robins, P.J.; Austin, S.A. A unified failure envelope from the evaluation of concrete repair bond tests. *Mag. Concr. Res.* **1995**, *47*, 57–68, doi:10.1680/mac.1995.47.170.57.
179. ASTM C1583 Standard Test Method for Tensile Strength of Concrete Surfaces and the Bond Strength or Tensile Strength of Concrete Repair and Overlay Materials by Direct Tension (Pull-off Method). *ASTM Int.* **2013**, doi:10.1520/C1583_C1583M-13.
180. Schindelin, J.; Arganda-Carreras, I.; Frise, E.; Kaynig, V.; Longair, M.; Pietzsch, T.; Preibisch, S.; Rueden, C.; Saalfeld, S.; Schmid, B.; et al. Fiji: An open-source platform for biological-image analysis. *Nat. Methods* **2012**, 676–682.
181. Rossen, J.E.; Scrivener, K.L. Optimization of SEM-EDS to determine the C–A–S–H composition in matured cement paste samples. *Mater. Charact.* **2017**, *123*, 294–306, doi:10.1016/j.matchar.2016.11.041.
182. Rossen, J.E.; Lothenbach, B.; Scrivener, K.L. Composition of C-S-H in pastes with increasing levels of silica fume addition. *Cem. Concr. Res.* **2015**, *75*, 14–22, doi:10.1016/j.cemconres.2015.04.016.
183. Scrivener, K.L. Backscattered electron imaging of cementitious microstructures: Understanding and quantification. *Cem. Concr. Compos.* **2004**, *26*, 935–945, doi:10.1016/j.cemconcomp.2004.02.029.
184. Rueden, C.T.; Schindelin, J.; Hiner, M.C.; DeZonia, B.E.; Walter, A.E.; Arena, E.T.; Eliceiri, K.W. ImageJ2: ImageJ for the next generation of scientific image data. *BMC Bioinformatics* **2017**, *18*, doi:10.1186/s12859-017-1934-z.
185. Beyene, M.A.; Munoz, J.F.; Meininger, R.C.; Di Bella, C. Effect of internal curing as mitigation to minimize alkali-silica reaction damage. *ACI Struct. J.* **2017**, *114*, 417–428, doi:10.14359/51689562.
186. Soutsos, M.; Hatzitheodorou, A.; Kanavaris, F.; Kwasny, J. Effect of temperature on the strength development of mortar mixes with GGBS and fly ash. *Mag. Concr. Res.* **2017**, *69*, 787–801, doi:10.1680/jmacr.16.00268.
187. Zhang, G.; Yang, H.; Ju, C.; Yang, Y. Novel selection of environment-friendly cementitious materials for winter construction: Alkali-activated slag/Portland cement. *J. Clean. Prod.* **2020**, *258*, 1–11, doi:10.1016/j.jclepro.2020.120592.
188. Escalante, J.I.; Gómez, L.Y.; Johal, K.K.; Mendoza, G.; Mancha, H.; Méndez, J. Reactivity of blast-furnace slag in Portland cement blends hydrated under different conditions. *Cem. Concr. Res.* **2001**, *31*, 1403–1409, doi:10.1016/S0008-8846(01)00587-7.
189. Joseph, S.; Cizer, Ö. Hydration of Hybrid Cements at Low Temperatures: A Study on Portland Cement-Blast Furnace Slag—Na₂SO₄. *Materials (Basel)*. **2022**, *15*, doi:10.3390/ma15051914.
190. Han, F.; Liu, R.; Wang, D.; Yan, P. Characteristics of the hydration heat evolution of composite binder at different hydrating temperature. *Thermochim. Acta* **2014**, *586*, 52–57, doi:10.1016/j.tca.2014.04.010.

191. Bruno, F.; Belusko, M.; Liu, M.; Tay, N.H.S. 9 - Using solid-liquid phase change materials (PCMs) in thermal energy storage systems A2 - Cabeza, Luisa F. BT - Advances in Thermal Energy Storage Systems. In *Woodhead Publishing Series in Energy*; Woodhead Publishing, 2015; pp. 201–246 ISBN 978-1-78242-088-0.
192. Kaufmann, J. Experimental identification of damage mechanisms in cementitious porous materials on phase transition of pore solution under frost deicing salt attack. *EMPA Act.* **2000**, doi:10.5075/epfl-thesis-2037.
193. Lothenbach, B.; Winnefeld, F. Thermodynamic modelling of the hydration of Portland cement. *Cem. Concr. Res.* **2006**, *36*, 209–226, doi:10.1016/j.cemconres.2005.03.001.
194. Scherer, G.W. Crystallization in pores. *Cem. Concr. Res.* **1999**, *29*, 1347–1358, doi:10.1016/S0008-8846(99)00002-2.
195. Bager, D.H.; Sellevold, E.J. Ice formation in hardened cement paste, Part I - room temperature cured pastes with variable moisture contents. *Cem. Concr. Res.* **1986**, *16*, 709–720, doi:10.1016/0008-8846(86)90045-1.
196. Morishige, K.; Iwasaki, H. X-ray study of freezing and melting of water confined within SBA-15. *Langmuir* **2003**, *19*, 2808–2811, doi:10.1021/la0208474.
197. Schreiber, A.; Ketelsen, I.; Findenegg, G.H. Melting and freezing of water in ordered mesoporous silica materials. *Phys. Chem. Chem. Phys.* **2001**, 1185–1195, doi:10.1039/b010086m.
198. Sun, Z.; Scherer, G.W. Pore size and shape in mortar by thermoporometry. *Cem. Concr. Res.* **2010**, *40*, 740–751, doi:10.1016/j.cemconres.2009.11.011.
199. Li, W.; Yu, J.; Ma, S.; Hu, Y.; Ge, D.; Shen, X. The properties and hydration of Portland cement containing calcium sulfoaluminate cement. *Ceram. - Silikaty* **2018**, *62*, 364–373, doi:10.13168/cs.2018.0032.
200. Jansen, D.; Spies, A.; Neubauer, J.; Ectors, D.; Goetz-Neunhoeffler, F. Studies on the early hydration of two modifications of ye'elimite with gypsum. *Cem. Concr. Res.* **2017**, *91*, 106–116, doi:10.1016/j.cemconres.2016.11.009.
201. He, Z.; Yang, H.; Liu, M. Hydration mechanism of sulphoaluminate cement. *J. Wuhan Univ. Technol. Mater. Sci. Ed.* **2014**, *29*, 70–74, doi:10.1007/s11595-014-0869-8.
202. Burris, L.E.; Kurtis, K.E. Water-to-cement ratio of calcium sulfoaluminate belite cements: Hydration, setting time, and strength development. *Cement* **2022**, *8*, 1–13, doi:10.1016/j.cement.2022.100032.
203. Nocun-Wczelik, W.; Stok, A.; Konik, Z. Heat evolution in hydrating expansive cement systems. *J. Therm. Anal. Calorim.* **2010**, *101*, 527–532, doi:10.1007/s10973-010-0846-1.
204. BROWN, P.W.; LIBERMAN, L.O.; FROHNSDORFF, G. Kinetics of the Early Hydration of Tricalcium Aluminate in Solutions Containing Calcium Sulfate. *J. Am. Ceram. Soc.* **1984**, *67*, 793–795, doi:10.1111/j.1151-2916.1984.tb19702.x.
205. Liang, Z. Microstructure and performance of calcium sulfoaluminate cements, University of Aberdeen, 2000.

206. Ukrainczyk, N.; Franković Mihelj, N.; Šipušić, J. Calcium sulfoaluminate eco-cement from industrial waste. *Chem. Biochem. Eng. Q.* **2013**, *27*, 83–93.
207. Babu, P.N.; Kumar, K.S. Studies on Strength Characteristics of Concrete with “Sodium Nitrate” as an Admixture. *Int. J. Technol. Res. Eng.* **2016**, *4*, 449–456.
208. Alzaza, A.; Ohenoja, K.; Illikainen, M. Improved strength development and frost resistance of Portland cement ground-granulated blast furnace slag binary binder cured at 0 °C with the addition of calcium silicate hydrate seeds. *J. Build. Eng.* **2022**, *48*, 1–14, doi:10.1016/j.job.2021.103904.
209. Wang, F.; Kong, X.; Wang, D.; Wang, Q. The effects of nano-C-S-H with different polymer stabilizers on early cement hydration. *J. Am. Ceram. Soc.* **2019**, *102*, 5103–5116, doi:10.1111/jace.16425.
210. Belhadi, R.; Govin, A.; Grosseau, P. Hydration and rheology of sulfoaluminate cements (CSA) in presence of polycarboxylate superplasticizers (PCE) and citric acid. In Proceedings of the 15th International Congress on the Chemistry of Cement a success (ICCC 2019), the Research Institute of Binding Materials Prague; the Czech Cement Association; Brno University of Technology; Guarant International; HAL Open Science: Prague, Czech Republic, 2019.
211. Coppola, L.; Coffetti, D.; Crotti, E. Use of tartaric acid for the production of sustainable Portland-free CSA-based mortars. *Constr. Build. Mater.* **2018**, *171*, 243–249, doi:10.1016/j.conbuildmat.2018.03.137.
212. Živica, V. Properties of blended sulfoaluminate belite cement. *Constr. Build. Mater.* **2000**, *14*, 433–437, doi:10.1016/S0950-0618(00)00050-7.
213. Yeung, J.S.K.; Yam, M.C.H.; Wong, Y.L. 1-Year development trend of concrete compressive strength using Calcium Sulfoaluminate cement blended with OPC, PFA and GGBS. *Constr. Build. Mater.* **2019**, *198*, 527–536, doi:10.1016/j.conbuildmat.2018.11.182.
214. Kolani, B.; Buffo-Lacarrière, L.; Sellier, A.; Escadeillas, G.; Boutillon, L.; Linger, L. Hydration of slag-blended cements. *Cem. Concr. Compos.* **2012**, *34*, 1009–1018, doi:10.1016/j.cemconcomp.2012.05.007.
215. Jeong, Y.; Hargis, C.W.; Chun, S.C.; Moon, J. The effect of water and gypsum content on strätlingite formation in calcium sulfoaluminate-belite cement pastes. *Constr. Build. Mater.* **2018**, *166*, 712–722, doi:10.1016/j.conbuildmat.2018.01.153.
216. Klemm, A.J.; Klemm, P. Ice formation in pores in polymer modified concrete - I. The influence of the admixtures on the water to ice transition. *Build. Environ.* **1997**, *32*, 195–198, doi:10.1016/S0360-1323(96)00053-4.
217. Pruppacher, H.R. On the Growth of Ice in Aqueous Solutions Contained in Capillaries. *Zeitschrift für Naturforsch. - Sect. A J. Phys. Sci.* **1967**, *22a*, 895–901, doi:10.1515/zna-1967-0607.
218. Lencis, U.; Udris, A.; Korjakins, A. Frost influence on the ultrasonic pulse velocity in concrete at early phases of hydration process. *Case Stud. Constr. Mater.* **2021**, *15*, 1–8, doi:10.1016/j.cscm.2021.e00614.
219. Xu, L.; Wang, P.; Zhang, G. Formation of ettringite in Portland cement/calcium

- aluminate cement/calcium sulfate ternary system hydrates at lower temperatures. *Constr. Build. Mater.* **2012**, *31*, 347–352, doi:10.1016/j.conbuildmat.2011.12.078.
220. Çullu, M.; Arslan, M. The effects of antifreeze use on physical and mechanical properties of concrete produced in cold weather. *Compos. Part B Eng.* **2013**, *50*, 202–209, doi:10.1016/j.compositesb.2013.02.012.
 221. Kiernozycki, W.; Błyszko, J. The influence of temperature on the hydration rate of cements based on calorimetric measurements. *Materials (Basel)*. **2021**, *14*, 1–12, doi:10.3390/ma14113025.
 222. Whittaker, M.; Zajac, M.; Ben Haha, M.; Bullerjahn, F.; Black, L. The role of the alumina content of slag, plus the presence of additional sulfate on the hydration and microstructure of Portland cement-slag blends. *Cem. Concr. Res.* **2014**, *66*, 91–101, doi:10.1016/j.cemconres.2014.07.018.
 223. Moon, H.; Ramanathan, S.; Suraneni, P.; Shon, C.S.; Lee, C.J.; Chung, C.W. Revisiting the effect of slag in reducing heat of hydration in concrete in comparison to other supplementary cementitious materials. *Materials (Basel)*. **2018**, *11*, 1–17, doi:10.3390/ma11101847.
 224. Matschei, T.; Lothenbach, B.; Glasser, F.P. The AFm phase in Portland cement. *Cem. Concr. Res.* **2007**, *37*, 118–130, doi:10.1016/j.cemconres.2006.10.010.
 225. Powers, T.C.; Helmut, R.A. Theory of Volume Changes in Hardened Portland Cement Paste During Freezing. *Proc. Highw. Res. Board* **1953**, *32*, 285–297.
 226. Esping, O. Effect of limestone filler BET(H₂O)-area on the fresh and hardened properties of self-compacting concrete. *Cem. Concr. Res.* **2008**, *38*, 938–944, doi:10.1016/j.cemconres.2008.03.010.
 227. Bentz, D.P.; Sato, T.; De La Varga, I.; Weiss, W.J. Fine limestone additions to regulate setting in high volume fly ash mixtures. *Cem. Concr. Compos.* **2012**, *34*, 11–17, doi:10.1016/j.cemconcomp.2011.09.004.
 228. Kakali, G.; Tsivilis, S.; Aggeli, E.; Bati, M. Hydration products of C3A, C3S and Portland cement in the presence of CaCO₃. *Cem. Concr. Res.* **2000**, *30*, 1073–1077, doi:10.1016/S0008-8846(00)00292-1.
 229. Li, W.; Huang, Z.; Zu, T.; Shi, C.; Duan, W.H.; Shah, S.P. Influence of nanolimestone on the hydration, mechanical strength, and autogenous shrinkage of ultrahigh-performance concrete. *J. Mater. Civ. Eng.* **2016**, doi:10.1061/(ASCE)MT.1943-5533.0001327.
 230. Li, P.P.; Yu, Q.L.; Brouwers, H.J.H. Effect of coarse basalt aggregates on the properties of Ultra-high Performance Concrete (UHPC). *Constr. Build. Mater.* **2018**, *170*, 649–659, doi:10.1016/j.conbuildmat.2018.03.109.
 231. Li, P.P.; Brouwers, H.J.H.; Chen, W.; Yu, Q. Optimization and characterization of high-volume limestone powder in sustainable ultra-high performance concrete. *Constr. Build. Mater.* **2020**, *242*, 1–11, doi:10.1016/j.conbuildmat.2020.118112.
 232. Sobuz, H.R.; Visintin, P.; Mohamed Ali, M.S.; Singh, M.; Griffith, M.C.; Sheikh, A.H. Manufacturing ultra-high performance concrete utilising conventional materials and production methods. *Constr. Build. Mater.* **2016**, *111*, 251–261,

doi:10.1016/j.conbuildmat.2016.02.102.

233. Cwirzen, A.; Penttala, V.; Vornanen, C. Reactive powder based concretes: Mechanical properties, durability and hybrid use with OPC. *Cem. Concr. Res.* **2008**, *38*, 1217–1226, doi:10.1016/j.cemconres.2008.03.013.
234. Li, P.P.; Yu, Q.L.; Brouwers, H.J.H. Effect of coarse basalt aggregates on the properties of Ultra-high Performance Concrete (UHPC). *Constr. Build. Mater.* **2018**, *170*, 649–659, doi:10.1016/j.conbuildmat.2018.03.109.
235. Benachour, Y.; Davy, C.A.; Skoczylas, F.; Houari, H. Effect of a high calcite filler addition upon microstructural, mechanical, shrinkage and transport properties of a mortar. *Cem. Concr. Res.* **2008**, *38*, 727–736, doi:10.1016/j.cemconres.2008.02.007.
236. Lei, D.Y.; Guo, L.P.; Sun, W.; Liu, J.; Shu, X.; Guo, X.L. A new dispersing method on silica fume and its influence on the performance of cement-based materials. *Constr. Build. Mater.* **2016**, *115*, 716–726, doi:10.1016/j.conbuildmat.2016.04.023.
237. Kawashima, S.; Seo, J.W.T.; Corr, D.; Hersam, M.C.; Shah, S.P. Dispersion of CaCO₃ nanoparticles by sonication and surfactant treatment for application in fly ash-cement systems. *Mater. Struct. Constr.* **2014**, *47*, 1011–1023, doi:10.1617/s11527-013-0110-9.
238. Kumar, A.; Oey, T.; Kim, S.; Thomas, D.; Badran, S.; Li, J.; Fernandes, F.; Neithalath, N.; Sant, G. Simple methods to estimate the influence of limestone fillers on reaction and property evolution in cementitious materials. *Cem. Concr. Compos.* **2013**, *40*, 20–29, doi:10.1016/j.cemconcomp.2013.05.002.
239. Irish Standard Testing hardened concrete: Freeze-thaw resistance with de-icing salts - Scaling CEN/TS 12390-9:2016. *Irish Stand.* **2016**.
240. Lu, Z.; Feng, Z.; Yao, D.; Li, X.; Ji, H. Freeze-thaw resistance of Ultra-High performance concrete: Dependence on concrete composition. *Constr. Build. Mater.* **2021**, *293*, 1–10, doi:10.1016/j.conbuildmat.2021.123523.
241. Gu, C.P.; Ye, G.; Sun, W. Ultrahigh performance concrete-properties, applications and perspectives. *Sci. China Technol. Sci.* **2015**, *58*, 587–599, doi:10.1007/s11431-015-5769-4.
242. Wang, D.; Shi, C.; Wu, Z.; Xiao, J.; Huang, Z.; Fang, Z. A review on ultra high performance concrete: Part II. Hydration, microstructure and properties. *Constr. Build. Mater.* **2015**, *96*, 368–377, doi:10.1016/j.conbuildmat.2015.08.095.
243. Gu, C.; Sun, W.; Guo, L.; Wang, Q.; Liu, J.; Yang, Y.; Shi, T. Investigation of Microstructural Damage in Ultrahigh-Performance Concrete under Freezing-Thawing Action. *Adv. Mater. Sci. Eng.* **2018**, *9*, doi:10.1155/2018/3701682.
244. Peng, Y.; Zhang, J.; Liu, J.; Ke, J.; Wang, F. Properties and microstructure of reactive powder concrete having a high content of phosphorous slag powder and silica fume. *Constr. Build. Mater.* **2015**, *101*, 482–487, doi:10.1016/j.conbuildmat.2015.10.046.
245. Muller, A.C.A.; Scrivener, K.L.; Skibsted, J.; Gajewicz, A.M.; McDonald, P.J. Influence of silica fume on the microstructure of cement pastes: New insights from ¹H NMR relaxometry. *Cem. Concr. Res.* **2015**, *74*, 116–125, doi:10.1016/j.cemconres.2015.04.005.

246. Lee, M.G.; Wang, Y.C.; Chiu, C. Te A preliminary study of reactive powder concrete as a new repair material. *Constr. Build. Mater.* **2007**, *21*, 182–189, doi:10.1016/j.conbuildmat.2005.06.024.
247. Aaleti, S.; Sritharan, S. Quantifying Bonding Characteristics between UHPC and Normal-Strength Concrete for Bridge Deck Application. *J. Bridg. Eng.* **2019**, *24*, doi:10.1061/(ASCE)BE.1943-5592.0001404.
248. Bissonnette, B.; Vaysburd, A.M.; Fay, K.F. von *Best Practices for Preparing Concrete Surfaces Prior to Repairs and Overlays - No MERL 12-17*; 2012;
249. Santos, P.M.D.; Júlio, E.N.B.S.; Silva, V.D. Correlation between concrete-to-concrete bond strength and the roughness of the substrate surface. *Constr. Build. Mater.* **2007**, *21*, 1688–1695, doi:10.1016/j.conbuildmat.2006.05.044.
250. Zhu, Y.; Zhang, Y.; Hussein, H.H.; Chen, G. Flexural strengthening of reinforced concrete beams or slabs using ultra-high performance concrete (UHPC): A state of the art review. *Eng. Struct.* **2020**, *205*, doi:10.1016/j.engstruct.2019.110035.
251. Momayez, A.; Ehsani, M.R.; Ramezani-pour, A.A.; Rajaie, H. Comparison of methods for evaluating bond strength between concrete substrate and repair materials. *Cem. Concr. Res.* **2005**, *35*, 748–757, doi:10.1016/j.cemconres.2004.05.027.
252. Tayeh, B.A.; Abu Bakar, B.H.; Megat Johari, M.A.; Zeyad, A.M. Microstructural analysis of the adhesion mechanism between old concrete substrate and UHPFC. *J. Adhes. Sci. Technol.* **2014**, *28*, 1846–1864, doi:10.1080/01694243.2014.925386.
253. Tayeh, B.A.; Abu Bakar, B.H.; Megat Johari, M.A.; Zeyad, A.M. The role of silica fume in the adhesion of concrete restoration systems. *Adv. Mater. Res.* **2013**, *626*, 265–269, doi:10.4028/www.scientific.net/AMR.626.265.
254. Vivekanandam, K.; Patnaikuni, I. Transition zone in high performance concrete during hydration. *Cem. Concr. Res.* **1997**, *27*, 817–823, doi:10.1016/S0008-8846(97)00079-3.
255. Goldman, A.; Bentur, A. The influence of microfillers on enhancement of concrete strength. *Cem. Concr. Res.* **1993**, *23*, 962–972, doi:10.1016/0008-8846(93)90050-J.
256. Sprinkel, M.M.; Ozyildirim, C. *Evaluation of High Performance Concrete Overlays Placed on Route 60 over Lynhaven Inlet in Virginia*; Virginia Transportation Research Council, Charlottesville, 2000;
257. Carbonell Muñoz, M.A.; Harris, D.K.; Ahlborn, T.M.; Froster, D.C. Bond performance between ultrahigh-performance concrete and normal-strength concrete. *J. Mater. Civ. Eng.* **2014**, *26*, doi:10.1061/(ASCE)MT.1943-5533.0000890.
258. De la Varga, I.; Muñoz, J.F.; Bentz, D.P.; Spragg, R.P.; Stutzman, P.E.; Graybeal, B.A. Grout-concrete interface bond performance: Effect of interface moisture on the tensile bond strength and grout microstructure. *Constr. Build. Mater.* **2018**, *170*, 747–756, doi:10.1016/j.conbuildmat.2018.03.076.
259. Santos, P.M.D.; Julio, E.N.B.S. Factors affecting bond between new and old concrete. *ACI Mater. J.* **2011**, *108*, 449–456, doi:10.14359/51683118.
260. Chorinsky, E.G. REPAIR OF CONCRETE FLOORS WITH POLYMER MODIFIED

CEMENT MORTARS. *Adhes. between Polym. Concr. / Adh sion entre polym res B t.* **1986**, 230–234, doi:10.1007/978-1-4899-3454-3_25.

261. Yuting, Z. Effect of Surface Moisture Condition on Bond Strength Between New and Old Concrete. *Bull. 159* **1992**.
262. Valikhani, A.; Jahromi, A.J.; Mantawy, I.M.; Azizinamini, A. Experimental evaluation of concrete-to-UHPC bond strength with correlation to surface roughness for repair application. *Constr. Build. Mater.* **2020**, *238*, doi:10.1016/j.conbuildmat.2019.117753.
263. Scrivener, K.L.; Crumbie, A.K.; Laugesen, P. The interfacial transition zone (ITZ) between cement paste and aggregate in concrete. *Interface Sci.* **2004**, *12*, 411–421, doi:10.1023/B:INTS.0000042339.92990.4c.

Department of Civil, Environmental and Natural Resources Engineering
Division of BOB

ISSN 1402-1544

ISBN 978-91-8048-540-1 (print)

ISBN 978-91-8048-541-8 (pdf)

Luleå University of Technology 2024